Spring 3-6-2014

Processing Submillisecond Timing Differences in a Model Electrosensory System

Ariel Maia Lyons-Warren
Washington University in St. Louis

WASHINGTON UNIVERSITY IN ST. LOUIS

Division of Biology & Biomedical Sciences

Neurosciences

Dissertation Examination Committee:

Bruce A. Carlson, Chair
Dennis L. Barbour
Erik D. Herzog
James E. Huettner
Timothy E. Hullar
Steven Mennerick
Ralf Wessel

Processing Submillisecond Timing Differences in a Model Electrosensory System

by

Ariel Maia Lyons-Warren

A dissertation presented to the
Graduate School of Arts and Sciences
of Washington University in
partial fulfillment of the
requirements for the degree
of Doctor of Philosophy

May 2014

St. Louis, Missouri

TABLE OF CONTENTS

LIST OF FIGURES

Chapter 1

Chapter 2

Chapter 3

Chapter 4

LIST OF ABBREVIATIONS

BW_{10}: Bandwidth

BF: Best Frequency

EL: Exterolateral Nucleus

ELa: Anterior Exterolateral Nucleus

ELp: Posterior Exterolateral Nucleus

EOD: Electric Organ Discharge

EODC: Electric Organ Discharge Command

FSL: First Spike Latency

IC: Inferior Colliculus

ID: Inner diameter

ILD: Interaural level differences

ITD: Interaural timing differences

KO: Knollenorgan

MS-222: Tricaine methanesulfonate

nELL: Electrosensory Lateral Line Lobe

OD: Outer diameter

SC: Superior Colliculus

TLL: Time Locked Latency

Equations

Threshold Intensity (I_t)

Tuning curve asymptote (a)

Resistance of the Membrane (R_m)

Series Capacitance of Knollenorgans (C_s)

Voltage drop across the Membrane (V_m)

Synaptic Conductance (g_s)

Time constant of the conductance (τ_s)

Stimulus Duration (d)

Tuning curve time constant, Tau (τ)

Capacitance of the Membrane (C_m)

Resistance of the Skin (R_s)

Voltage drop across the Skin (V_s)

Maximum Conductance (g_{max})

Reversal Potential (V_r)

ACKNOWLEDGMENTS

Washington University in St. Louis is a supportive, encouraging, and stimulating place to train. Due to the amazingly collaborative nature of this institution, I have been mentored by too many faculty members, each taking hours out of their day to talk with me about my science, to name them individually. However, I would like to especially recognize one of my first science mentors, Tammy Hershey, whose continued support over the past decade has empowered successes in all areas of my life, and my first graduate school mentor, Bob Heuckeroth, whose contagious enthusiasm for science of all varieties pulled me from the beaches of the Mediterranean back into academia.

Over the past four years I have had the honor and privilege to be guided by some of the finest electrophysiologists at Washington University in St. Louis. Thank you to the members of my thesis committee for being willing to venture into the world of electric fish, especially to Steven Mennerick who allowed the fish and me to invade his lab. In addition to the formal guidance from my committee, the members of the Carlson and Mennerick labs have been a constant source of support and encouragement. Special thanks to Christa Baker for always listening and to Tsunehiko Kohashi for teaching me the importance of a chocolate and coffee break during a long experiment day. On the medical campus, thank you to Devon Crawford for doing everything first so I could learn how and to Julian Meeks for essential technical guidance. I am indebted to my classmates from both the medical and graduate schools for challenging me intellectually while helping me to not take graduate school so seriously. Thank you also to the administrative staff who made sure I did not have to worry about anything except my

science. In deference to the philosophy portion of my degree, I have chosen to include a relevant quote from E.D. Adrian's 1928 book The Basis of Sensation at the beginning of each chapter. Thank you to the Archives and Rare Books Department for accommodating an amateur historian with a deadline. Most importantly, thank you to my mentor, Bruce Carlson, who – if nothing else – has taught me to slow down and think.

The work in this thesis was supported financially by an international cadre of funding agencies. Thank you to the National Science Foundation (NSF), National Institutes of Health (NIH), the German Academic Exchange Service, the Uehara Memorial Foundation, and the Japan Society for the Promotion of Science. Specifically, this work was supported by NSF funding to Bruce Carlson (IOS-1050701 and IOS-081839) and NIH funding to Steven Mennerick (NS54174) and myself (F30DC0111907).

Lastly, I would like to thank my family and friends for tolerating my erratic lab schedule and intense medical school study schedule - and resultant tardiness from each - while listening to me talk about nothing but fish. I am indebted to you for your constant reminders to take care of myself, and when I failed to heed this advice, your willingness to come to my aid. I could not have accomplished the body of work that follows without the support of all these individuals.

ABSTRACT OF THE DISSERTATION

Processing Submillisecond Timing Differences in a Model Electrosensory System

by

Ariel Maia Lyons-Warren

Doctor of Philosophy in Biology & Biomedical Sciences

Neurosciences

Washington University in St. Louis, 2014

Professor Bruce A. Carlson, Chairperson

Perception of sensory cues requires peripheral encoding followed by extraction of behaviorally relevant signal components by central neurons. Some sensory systems can detect temporal information with submillisecond accuracy, despite these signals occurring faster than the approximately 1 ms timescale of neuronal firing. In sound localization, the best studied example of this phenomenon, there are at least two distinct mechanisms for detecting submillisecond timing differences, indicating that multiple solutions to this fundamental problem exist. I investigated mechanisms for processing submillisecond timing differences by studying electrosensory processing in a time coding expert, mormyrid weakly electric fish, which can detect submillisecond differences in the duration of electric signals.

First, I measured responses of peripheral receptors to stimuli of different durations. I found that each unit responded preferentially to longer stimuli, but with response thresholds that varied among units within the behaviorally relevant range of durations.

This variability establishes a population code operating at near threshold intensities in which the number and identity of responding receptors represents duration. At higher stimulus intensities all units respond independent of duration, rendering the population code obsolete. Importantly, peripheral receptors respond either to the start or end of a signal. Thus, stimulus duration is also represented by a temporal code, as a difference in spike times between receptors.

Next, I investigated the central mechanism for detection of submillisecond spike time differences by recording from time comparator neurons (Small Cells) in the midbrain. Recording from Small Cells is challenging because their somas are small and relatively inaccessible. I therefore designed a novel method using retrograde labeling to directly visualize and record from Small Cells in *vivo*. I showed that patterns of duration tuning vary among Small Cells due to a combination of blanking inhibition corresponding to one edge of a stimulus and variably delayed excitation corresponding to one or both edges of a stimulus. Other circuits that detect submillisecond timing differences rely either on precisely-timed inhibition or delay-line coincidence detection. I demonstrate a novel mechanism by which mormyrids combine delay-line coincidence detection with precisely-timed blanking inhibition to establish diverse patterns of duration tuning among a population of time comparators.

Chapter 1

Introduction and thesis objectives

It turns out that the messages from our sense organs are all made up of a common vocabulary of the simplest kind.

-E.D. Adrian, 1928

SENSORY PROCESSING

Sensory processing involves the encoding of a sensory event by peripheral receptors followed by the decoding and recoding of stimulus features by central neurons. Peripheral receptors are specific to the type of sensory information being encoded (Müller, 1840). For example, hair cells encode auditory stimuli by responding to changes in air pressure caused by sound waves. Similarly, photoreceptors are specific to visual information, mechanoreceptors are activated by touch, and electroreceptors respond to changes in electrical charge (Gardner and Martin, 2000). Although each receptor type uses distinct mechanics to detect a sensory signal, information from all modalities is subsequently represented using a common vocabulary – a pattern of action potentials (Adrian, 1928). Most commonly, neural circuits represent information either in the rate or timing of action potentials (Ainsworth et al., 2012). To be maximally efficient, however, the same chains of neurons can encode different features using different codes (Panzeri et al., 2010). Importantly, neural codes are not unique to sensory systems. Disruptions to both sensory and non-sensory circuits may share a common origin. For example, autism patients exhibit a high prevalence of sensory processing disorders that can affect any of the five major senses in addition to the behavioral and learning deficits associated with the disease (Tomchek and Dunn, 2007). Thus, a basic understanding of sensory coding is important for a general understanding of how nervous systems encode information (Ferster and Spruston, 1995).

Temporal coding, the representation of information within the specific timing patterns of neural activity (Theunissen and Miller, 1995), is particularly well adapted for encoding time parameters of a sensory signal such as start time, frequency or duration (Grothe and Klump, 2000). Importantly, these temporal features are critical components of natural sound sources and can occur on a range of timescales (Figure 1) (Mauk and Buonomano, 2004; Singh and Theunissen, 2003). Processing information on a submillisecond timescale represents an especially interesting computational challenge because such short intervals are below the resolution of a single action potential (Carr, 1993).

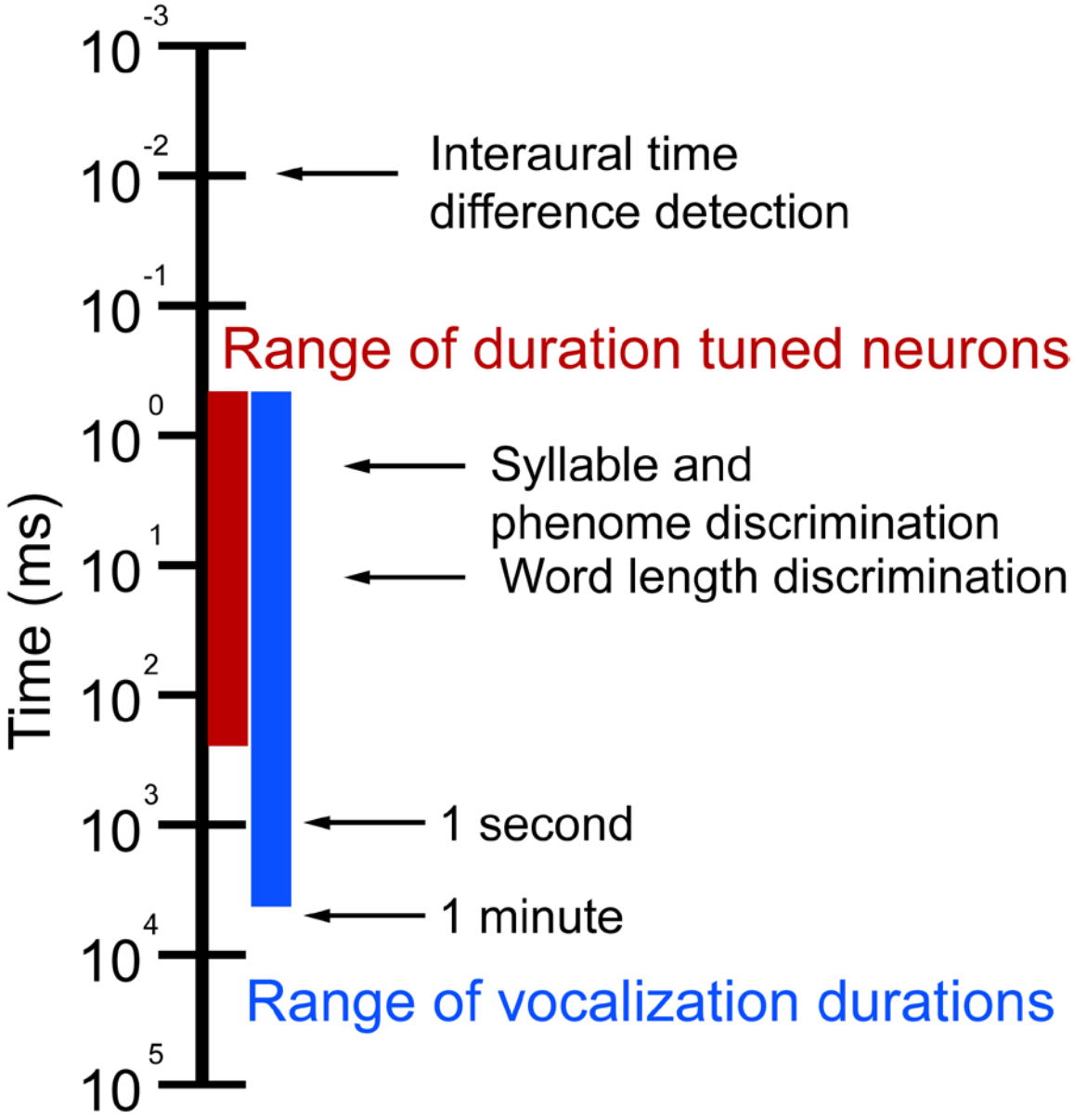

FIG 1: Timescale of behaviorally relevant temporal features of sound, adapted from Mauk and Buonomano 2004. Birds and mammals can detect interaural time differences on the order of 10^{-2} ms. Duration tuned neurons have been demonstrated in 13 species with best durations ranging from 0.5 to 300 ms (red) (Sayegh et al., 2011). In the same group of species, vocalization durations (blue) range from 0.5 to 1,600 ms (Sayegh et al., 2011). Humans can discriminate syllable and phenome differences in the 1-10 ms range (Kato et al., 2003; Kawai and Carrell, 2012) and can discriminate word length in the 10-100 ms range (van Wieringen and Pols, 1994).

MECHANISMS FOR PROCESSING SMALL TIMING DIFFERENCES

Mechanisms for processing submillisecond spike timing differences have been extensively studied in sound localization. One sensory cue utilized for sound localization by many animals is the comparison of interaural time differences (ITD), which are the differences in the time sound arrives at each ear. Jeffress (1948) proposed a now canonical model for how nervous systems can process submillisecond spike time differences (Figure 2). In the Jeffress model, axon lengths vary resulting in different conduction times, or delay-lines, for each input. Time comparator neurons detect coincident arrival of inputs by firing maximally when the two signals arrive simultaneously. Simultaneous arrival only occurs if the axonal delay is equivalent to the difference in ITD (Ashida and Carr, 2011; Jeffress, 1948). This mechanism results in a labeled-line code, in which the firing of each time comparator neuron corresponds to a particular ITD, which in turn represents a location in space. Anatomical evidence for the Jeffress model has been demonstrated in barn owls (Carr and Konishi, 1990) and alligators (Carr et al., 2009). However, evidence for this model in mammals is more controversial (McAlpine and Grothe, 2003). Putative delay-lines were shown in cats (Smith et al., 1993), but have not been demonstrated in any other mammal. Further, glycinergic inhibition in mammals has been shown to convert spike time differences into a rate code for azimuthal sound localization (Grothe et al., 2010).

The mechanisms for encoding short durations in auditory stimuli are similar to those utilized in sound localization (Sayegh et al., 2011). Duration tuned neurons have

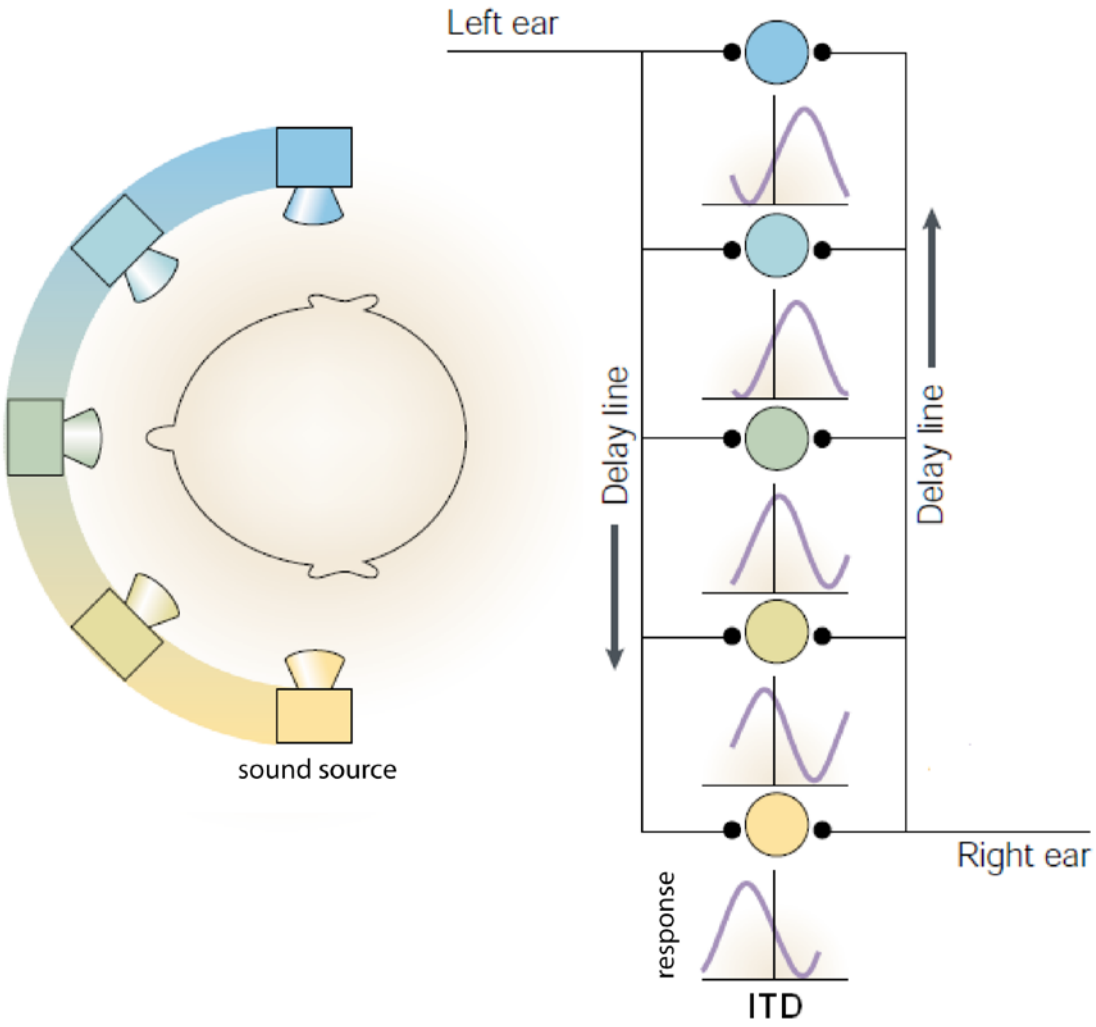

FIG 2: Jeffress model for sound localization, adapted from Grothe 2003. The relative location of a sound source determines the time sound arrives at each ear. The interaural time differences (ITD) are encoded in the spike timing differences of the primary afferents from each ear. Signals travel through a systematic projection of increasing axon lengths which serve as delay lines. The longer axons result in greater conduction times, compensating for ITD. Time comparator neurons (circles) receive one input from each ear. Each cell fires maximally only when the two inputs arrive simultaneously (ITD vs. response curves). Thus, each cell selectively responds to a specific ITD.

been demonstrated in the auditory system of bats (Fuzessery and Hall, 1999), frogs (Gooler and Feng, 1992), guinea pigs (Wang et al., 2006), rats (Pérez-González et al., 2006), mice (Brand et al., 2000), cats (He et al., 1997), and chinchillas (Chen, 1998). Three models have been proposed to explain the selectivity of these neurons (Aubie et al., 2009). The first model parallels the Jeffress model. Time comparator neurons respond to stimuli of specific durations by detecting coincident arrival of excitatory inputs corresponding to the start and end of the signal. The second model similarly relies on coincidence detection, but instead of a second excitatory input, time comparator neurons detect excitation that is coincident with rebound from sustained inhibition. The third model is an anti-coincidence detection model in which an inhibitory post synaptic potential is prolonged for the duration of the stimulus. Excitatory inputs to each cell are variably delayed. A response is elicited only if the delay to that particular cell is greater than the stimulus duration, allowing the inhibition to end before the excitation arrives. In the second and third models, the timing of both inputs corresponds to the start of the stimulus. Notably, each of these three models shares some features with the Jeffress model.

Duration tuned neurons have also been demonstrated in electrosensory processing in mormyrid weakly electric fish (Amagai, 1998). Friedman and Hopkins proposed that duration tuning arises through delay-line anti-coincidence detection of submillisecond spike time differences (Friedman and Hopkins, 1998; Xu-Friedman and Hopkins, 1999). This mechanism serves as a critical link between sound localization and duration tuning because it employs both delay-line coincidence detection similar to mechanisms for

sound localization and start-inhibition with stop-excitation similar to mechanisms for duration tuning. These shared features make electrosensory processing in mormyrids an interesting model for investigating how submillisecond spike timing differences are processed.

WEAKLY ELECTRIC FISH AS A MODEL SYSTEM

Weakly electric fish are an ideal model system for studying mechanisms of temporal coding in sensory processing (Fortune et al., 2006; Zakon, 2003). Mormyrid weakly electric fish, specifically, can detect 2 μsec differences in stimulus duration, making them time coding experts (Paintner and Kramer, 2003). In Africa, these fish live sympatrically with species that produce similar communication signals (Gallant et al., 2011) varying slightly in duration between species (Hopkins, 1981) and sexes (Arnegard et al., 2006; Feulner et al., 2009). Thus, just as temporal patterns are important in communication cues for birds and frogs (Chi and Margoliash, 2001; Edwards et al., 2002); detection of submillisecond differences in stimulus duration is behaviorally relevant for these fish.

The electric communication signal emitted by weakly electric fish is called an electric organ discharge (EOD) (Hopkins, 1974). EODs are processed in a dedicated, isolated, relatively simple neural circuit (Figure 3) making experimental studies less technically demanding. This circuit begins with peripheral receptors called knollenorgans. The number of knollenorgans increases with increasing body size (Harder, 1968). For example, there are approximately 166 knollenorgans on a 6.5 cm *B.*

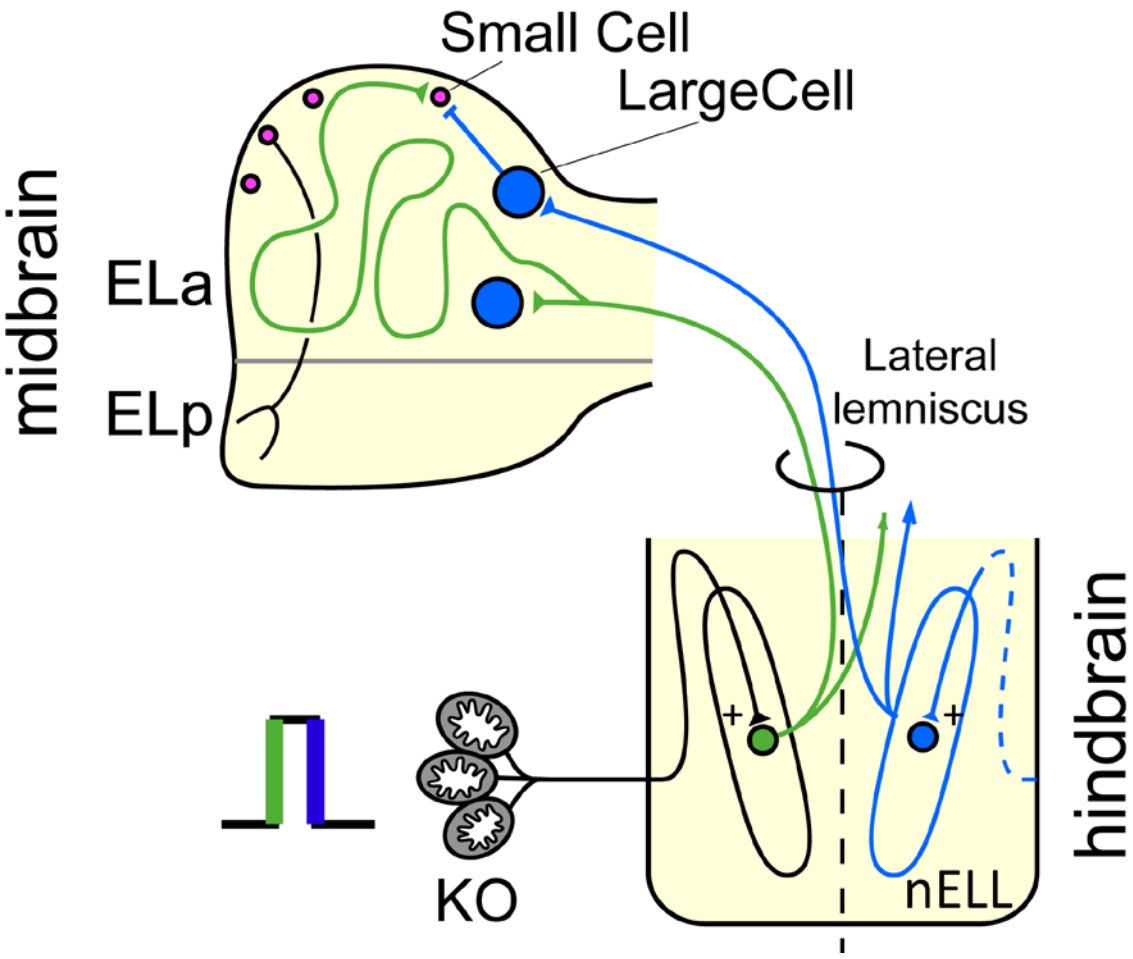

FIG 3: Mormyrid electrosensory circuit, adapted from Friedman and Hopkins 1998 and Xu-Friedman and Hopkins 1999. Peripheral receptors called knollenorgans (KO) spike in response to positive changes in electrical charge. These signals are relayed through the hindbrain nucleus of the electrosensory lateral line (nELL). 55% of nELL axons project contralaterally, 35% project ipsilaterally, and the remaining 10% project bilaterally. These axons project via the lateral lemniscus to the anterior portion of the exterolateral nucleus (ELa). In ELa, nELL axons synapse on inhibitory interneurons (Large Cells). Notably, as nELL axons synapse on small, adendritic projection cells (Small Cells) they wind for 0-7 mm within ELa. Small Cells project to the adjacent posterior portion of the exterolateral nucleus (ELp).

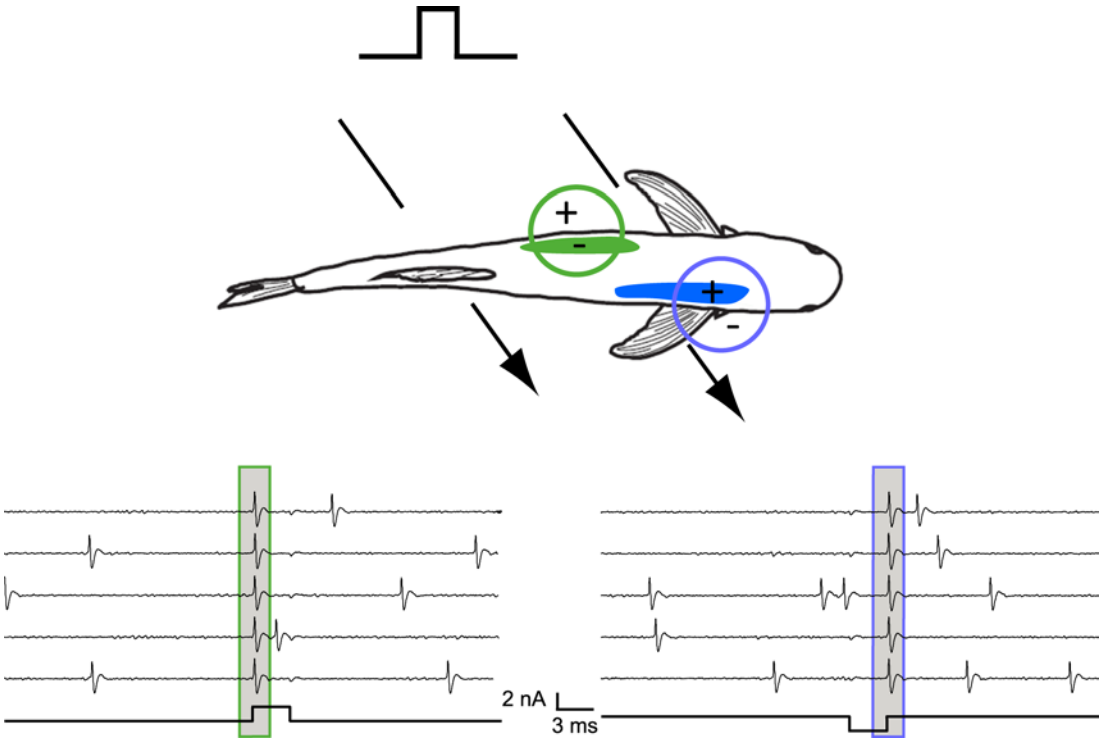

FIG 4: Knollenorgans respond selectively to positive changes in electrical charge, adapted from Lyons-Warren et al. 2012. Knollenorgans (KO) spike when the outside of the skin is positive relative to the inside of the body (top, green). For an externally generated, monophasic positive electrical stimulus, KOs on the same side of the body as the source (green) will spike at the beginning. In contrast, KOs on the opposite side (blue) will perceive the opposite polarity and will spike at the end (Hopkins and Bass, 1981). 5 representative traces from the same KO in response to a 2 nA, 3 ms square pulse (bottom) showing a time-locked spike to the upward edge of a monophasic positive (left) and negative (right) stimulus.

brachyistius (Carlson et al., 2011) and up to almost 1000 on a 12.2 cm *G. petersii* (Harder, 1968). Knollenorgans respond to positive, but not negative, changes in electrical charge by generating an action potential (Figure 4) (Bennett, 1965; Hopkins and Bass, 1981). Thus, different knollenorgans will respond to different components of a sensory signal depending upon their body location. Spike timing differences between receptors in different receptive fields correspond to the duration of the signal. Each knollenorgan primary afferent projects to the nucleus of the electrosensory lateral line (nELL) located in the hindbrain and creates 1-4 boutons on each soma that it contacts. Further, each knollenorgan afferent synapses onto 3-11 different nELL somas. In turn, each nELL soma will receive inputs from 1-4 knollenorgans (Bell and Grant, 1989). Thus there is both convergence and divergence in the hindbrain.

nELL cells send their axons to the exterolateral nucleus in the midbrain (EL). Interestingly, sensory information is usually represented contralaterally, as for touch sensation (Gardner and Martin, 2000), or divided evenly to both hemispheres as in vision (Wurtz and Kandel, 2000). In contrast, electrosensory axons from nELL send twice as many fibers to the contralateral midbrain as to the ipsilateral midbrain (Szabo et al., 1983). In addition, 10% of fibers project bilaterally (Friedman and Hopkins, 1998; Szabo et al., 1983). Upon entering ELa, nELL axons synapse almost immediately on large, GABAergic interneurons called Large Cells. In contrast, nELL axons wind circuitously for 0-7 mm in ELa while synapsing on 33-72 small, adendritic cells called Small Cells (Friedman and Hopkins, 1998; Mugnaini and Maler, 1987). Small Cells also receive GABAergic inhibitory input from Large Cells in the form of a calyceal synapse

(Friedman and Hopkins, 1998; Mugnaini and Maler, 1987). Small Cells therefore receive delayed excitation which varies from cell to cell and inhibition corresponding to separate edges of a stimulus. Friedman and Hopkins proposed that Small Cells act as time comparator neurons, similar to the role of MSO neurons in sound localization. However, the Friedman-Hopkins model proposed delay-line *anti*-coincidence detection in which Small Cells only respond if excitatory and inhibitory inputs arrive separately (Figure 5) (Xu-Friedman and Hopkins, 1999).

Small Cells represent the only output from ELa to the adjacent ELp. In ELp, there are neurons that are both band-pass and long-pass tuned to stimulus duration (Amagai, 1998) as well as neurons that respond to other stimulus features such as inter-pulse interval (Carlson, 2009; George et al., 2011). Thus, it is clear that feature extraction occurs after Small Cells, but that Small Cells serve a critical computational function in processing electrosensory information. Unfortunately, Small Cells are technically challenging to investigate. Not only are they very small, but ELa is filled with myelin due to the large number of nELL axons. Further, the inhibitory calyceal synapses from Large Cells engulf the Small Cell somas, making them even less accessible. Despite almost a decade of effort, only 2 putative Small Cell recordings, each lasting only a few seconds, have been reported (Friedman and Hopkins, 1998)

One of the interesting features of electrosensory processing in morymrids is the presence of an inhibitory calyceal synapse (Friedman and Hopkins, 1998; George et al., 2011; Mugnaini and Maler, 1987). Synapse morphology directly relates to synapse function (Atwood and Karunanithi, 2002; Xu-Friedman and Regehr, 2004). The Calyx of

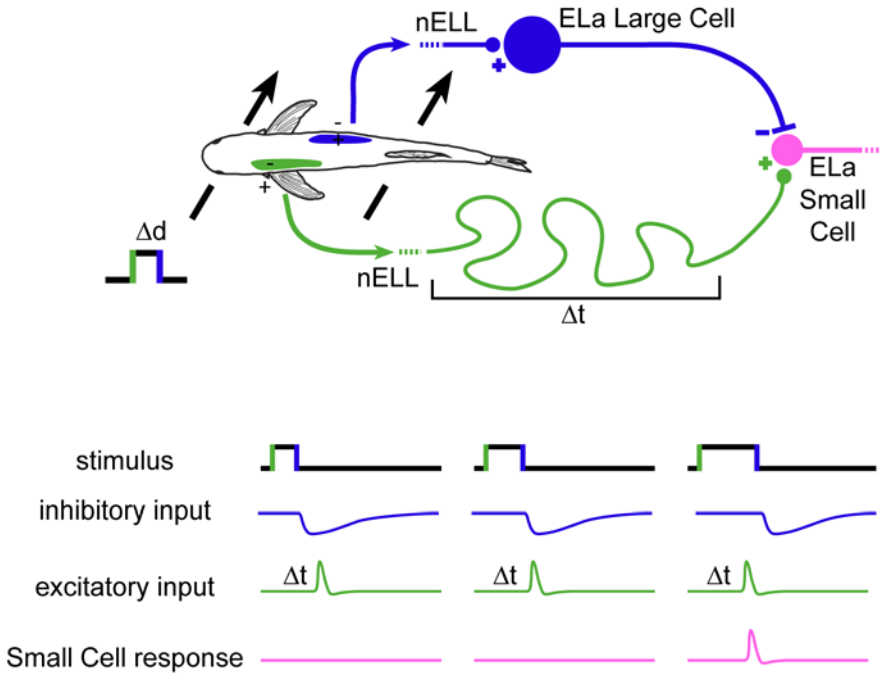

FIG 5: Friedman-Hopkins model for detecting submillisecond spike time differences, adapted from Friedman and Hopkins 1998. Peripheral receptors spike in response to the start or end of a square pulse. The resultant spike time differences encode stimulus duration. Each Small Cell (pink) receives delayed excitation (green) corresponding to one stimulus edge and inhibition (blue) corresponding to the opposite edge. At short durations, inhibition and excitation arrive at the Small Cell simultaneously, and no response occurs. However, at long durations, inhibition arrives after excitation, and the Small Cell is able to spike. The specific minimum duration at which a Small Cell first responds depends on the excitatory delay (Δt).

Held, the best studied calyceal synapse, is described as a large, morphologically complex terminal with hundreds of active zones (Spirou et al., 2008). The unique structure of the calyx imparts a heterogeneous release probability resulting in nearly fail safe transmission with each pre-synaptic depolarization (Nicol and Walmsley, 2002). Calyceal synapses have also been described for cerebellar mossy fibers, visual thalamocortical cells, and retinogeniculate cells. In all these cases they contribute to reliable, temporally precise transmission (Borst, 2010). A possible inhibitory calyx was reported in the ventral cochlear nucleus of rats (Köpf-Maier, 1979). However, the functional implications of an inhibitory calyx have not been reported.

THESIS OBJECTIVES

I was interested in understanding how an electrosensory circuit codes for stimulus duration as a model of general mechanisms for process submillisecond spike time differences. Thus, the overall goal of this thesis is to identify mechanisms used by mormyrid weakly electric fish to process submillisecond differences in the duration of electric signals. To address this question, I look at the encoding of stimulus duration by peripheral receptors called knollenorgans as well as population responses to stimulus duration in two midbrain nuclei, the anterior and posterior portions of the nucleus exterolateralis, ELa and ELp respectively. Further, I directly measure the responses to changes in stimulus duration by individual time comparator neurons in ELa called Small Cells. To acquire these measurements, I develop a novel method using retrograde dye transport to selectively label Small Cell axons. Once visible, axons can be targeted with

a recording electrode and specific, single unit responses can be recorded. I characterize how Small Cells respond to stimuli of varying duration under control conditions and then use complex stimuli and pharmacological approaches to separate the excitatory and inhibitory inputs underlying duration tuning. In contrast to the model proposed by Friedman and Hopkins, my results suggest multiple excitatory inputs to Small Cells. I therefore provide indirect evidence to show that multiple excitatory inputs to each Small Cell would be feasible.

REFERENCES

Adrian, E. D. (1928). The basis of sensations. New York: W.W. Norton & Co.

Ainsworth, M., Lee, S., Cunningham, M. O., Traub, R. D., Kopell, N. J. and Whittington, Miles A. (2012). Rates and rhythms: A synergistic view of frequency and temporal coding in neuronal networks. Neuron **75**, 572-583.

Amagai, S. (1998). Time coding in the midbrain of mormyrid electric fish. II. Stimulus selectivity in the nucleus exterolateralis pars posterior. J Comp Physiol A Neuroethol Sens Neural Behav Physiol. **182**, 131-143.

Arnegard, M. E., Jackson, B. S. and Hopkins, C. D. (2006). Time-domain signal divergence and discrimination without receptor modification in sympatric morphs of electric fishes. J Exp Biol. **209**, 2182-2198.

Ashida, G. and Carr, C. E. (2011). Sound localization: Jeffress and beyond. Curr Opin Neurobiol. **21**, 745-751.

Atwood, H. L. and Karunanithi, S. (2002). Diversification of synaptic strength: Presynaptic elements. Nat Rev Neurosci. **3**, 497-516.

Aubie, B., Becker, S. and Faure, P. A. (2009). Computational models of millisecond level duration tuning in neural circuits. J Neurosci. **29**, 9255-9270.

Bell, C. C. and Grant, K. (1989). Corollary discharge inhibition and preservation of temporal information in a sensory nucleus of mormyrid electric fish. J Neurosci. **9**, 1029-1044.

Bennett, M. V. L. (1965). Electroreceptors in mormyrids. In Cold Spring Harb Symp Quant Biol. vol. **30**, pp. 245-262.

Borst, J. G. G. (2010). The low synaptic release probability in vivo. Trends Neurosci. **33**, 259-266.

Brand, A., Urban, R. and Grothe, B. (2000). Duration tuning in the mouse auditory midbrain. J Neurophysiol **84**, 1790-1799.

Carlson, B. A. (2009). Temporal-pattern recognition by single neurons in a sensory pathway devoted to social communication behavior. J Neurosci. **29**, 9417-9428.

Carlson, B.A., Hasan, S.M., Hollmann, M., Miller, D.B., Harmon, L.J. and Arnegard, M.E. (2011). Brain evolution triggers increased diversification of electric fishes. Science **332**, 583-586.

Carr, C. E. (1993). Processing of temporal information in the brain. Annu Rev Neurosci. **16**, 223-243.

Carr, C. E. and Konishi, M. (1990). A circuit for detection of interaural time differences in the brain stem of the barn owl. J Neurosci. **10**, 3227-3246.

Carr, C. E., Soares, D., Smolders, J. and Simon, J. Z. (2009). Detection of interaural time differences in the alligator. J Neurosci. **29**, 7978-7990.

Chen, G.-D. (1998). Effects of stimulus duration on responses of neurons in the chinchilla inferior colliculus. Hear Res. **122**, 142-150.

Chi, Z. and Margoliash, D. (2001). Temporal Precision and Temporal Drift in Brain and Behavior of Zebra Finch Song. Neuron **32**, 899-910.

Edwards, C. J., Alder, T. B. and Rose, G. J. (2002). Auditory midbrain neurons that count. Nat Neurosci. **5**, 934-936.

Ferster, D. and Spruston, N. (1995). Cracking the neuronal code. Science **270**, 756-757.

Feulner, P. G. D., Plath, M., Engelmann, J., Kirschbaum, F. and Tiedemann, R. (2009). Electrifying love: electric fish use species-specific discharge for mate recognition. Biol Lett. **5**, 225-228.

Fortune, E., Rose, G. and Kawasaki, M. (2006). Encoding and processing biologically relevant temporal information in electrosensory systems. J Comp Physiol A Neuroethol Sens Neural Behav Physiol. **192**, 625-635.

Friedman, M. A. and Hopkins, C. D. (1998). Neural substrates for species recognition in the time-coding electrosensory pathway of mormyrid electric fish. J Neurosci. **18**, 1171-1185.

Fuzessery, Z. M. and Hall, J. C. (1999). Sound duration selectivity in the pallid bat inferior colliculus. Hear Res. **137**, 137-154.

Gallant, J., Arnegard, M., Sullivan, J., Carlson, B. and Hopkins, C. (2011). Signal variation and its morphological correlates in *Paramormyrops kingsleyae* provide insight into the evolution of electrogenic signal diversity in mormyrid electric fish. J Comp Physiol A Neuroethol Sens Neural Behav Physiol. **197**, 799-817.

Gardner, E. P. and Martin, J. H. (2000). Coding of sensory information. In Principles of Neural Science, vol. 1 eds. E. R. Kandel J. H. Schwartz and T. M. Jessell, pp. 430-450. New York: McGraw-Hill.

George, A. A., Lyons-Warren, A. M., Ma, X. and Carlson, B. A. (2011). A diversity of synaptic filters are created by temporal summation of excitation and inhibition. J Neurosci. **31**, 14721-14734.

Gooler, D. M. and Feng, A. S. (1992). Temporal coding in the frog auditory midbrain: the influence of duration and rise-fall time on the processing of complex amplitude-modulated stimuli. J Neurophysiol **67**, 1-22.

Grothe, B. (2003). New roles for synaptic inhibition in sound localization. Nat Rev Neurosci **4**, 540-550.

Grothe, B. and Klump, G. M. (2000). Temporal processing in sensory systems. Curr Opin Neurobiol. **10**, 467-473.

Grothe, B., Pecka, M. and McAlpine, D. (2010). Mechanisms of sound localization in mammals. Physiol Rev **90**, 983-1012.

Harder, W. (1968). The interrelations between electroreceptors, electric organ, lateral-line organ, and nervous system in Mormyridae (Teleostei, pisces). Zeitschrift für vergleichende Physiologie **59**, 272-318.

He, J., Hashikawa, T., Ojima, H. and Kinouchi, Y. (1997). Temporal integration and duration tuning in the dorsal zone of cat auditory cortex. J Neurosci **17**, 2615-2625.

Hopkins, C. D. (1974). Electric communication in fish. Am Sci. **62**, 426-37.

Hopkins, C. D. (1981). On the diversity of electrical signals in a community of mormyrid electric fish in West Africa. Amer. Zool. **21**, 211-222.

Hopkins, C. D. and Bass, A. H. (1981). Temporal coding of species recognition signals in an electric fish. Science **212**, 85-87.

Jeffress, L. A. (1948). A place theory of sound localization. J Comp Physiol Psychol. **41**, 35-39.

Kato, H., Tsuzaki, M. and Sagisaka, Y. (2003). Functional differences between vowel onsets and offsets in temporal perception of speech: Local-change detection and speaking-rate discrimination. J. Acoust. Soc. Am. **113**, 3379-3389.

Kawai, N. and Carrell, T. (2012). Discrimination of differences in digitally manipulated phoneme length during speech. Percept Mot Skills. **114**, 189-203.

Köpf-Maier, P. (1979). A new type of synapse in the ventral cochlear nucleus. Cell Tissue Res. **198**, 373-380.

Lyons-Warren, A. M., Hollmann, M. and Carlson, B. A. (2012). Sensory receptor diversity establishes a peripheral population code for stimulus duration at low intensities. J Exp Biol. **215**, 2586-600.

Mauk, M. D. and Buonomano, D. V. (2004). The neural basis of temporal processing. Annu Rev Neurosci. **27**, 307-340.

McAlpine, D. and Grothe, B. (2003). Sound localization and delay lines - do mammals fit the model? Trends Neurosci. **26**, 347-350.

Mugnaini, E. and Maler, L. (1987). Cytology and immunocytochemistry of the nucleus extrolateralis anterior of the mormyrid brain: possible role of GABAergic synapses in temporal analysis. Anat Embryol (Berl). **176**, 313-36.

Müller, J. (1840). Handbuch der physiologie des menschen für Vorlesunge. Coblenz: J. Hölscher.

Nicol, M. J. and Walmsley, B. (2002). Ultrastructural basis of synaptic transmission between endbulbs of Held and bushy cells in the rat cochlear nucleus. J Physiol **539**, 713-723.

Paintner, S. and Kramer, B. (2003). Electrosensory basis for individual recognition in a weakly electric, mormyrid fish, Pollimyrus adspersus (Günther, 1866). Behav Ecol Sociobiol. **55**, 197-208.

Panzeri, S., Brunel, N., Logothetis, N. K. and Kayser, C. (2010). Sensory neural codes using multiplexed temporal scales. Trends Neurosci. **33**, 111-120.

Pérez-González, D., Malmierca, M. S., Moore, J. M., Hernández, O. and Covey, E. (2006). Duration selective neurons in the inferior colliculus of the rat: Topographic distribution and relation of duration sensitivity to other response properties. J Neurophysiol **95**, 823-836.

Sayegh, R., Aubie, B. and Faure, P. (2011). Duration tuning in the auditory midbrain of echolocating and non-echolocating vertebrates. J Comp Physiol A Neuroethol Sens Neural Behav Physiol. **197**, 571-583.

Singh, N. C. and Theunissen, F. E. (2003). Modulation spectra of natural sounds and ethological theories of auditory processing. J. Acoust. Soc. Am. **114**, 3394-3411.

Smith, P., Joris, P. and Yin, T. (1993). Projections of physiologically characterized spherical bushy cell axons from the cochlear nucleus of the cat: evidence for delay lines to the medial superior olive. J Comp Neurol **331**, 245-60.

Spirou, G. A., Chirila, F. V., von Gersdorff, H. and Manis, P. B. (2008). Heterogeneous Ca^{2+} influx along the adult calyx of held: A structural and computational study. Neuroscience **154**, 171-185.

Szabo, T., Ravaille, M., Libouban, S. and Enger, P. S. (1983). The mormyrid rhombencephalon: I. Light and EM investigations on the structure and

connections of the lateral line lobe nucleus with HRP labeling. Brain Res. **266**, 1-19.

Theunissen, F. and Miller, J. (1995). Temporal encoding in nervous systems: a rigorous definition. J Comput Neurosci. **2**, 149-62.

Tomchek, S. D. and Dunn, W. (2007). Sensory processing in children with and without Autism: A comparative study using the short sensory profile. Am J Occup Ther **61**, 190-200.

van Wieringen, A. and Pols, L. C. W. (1994). Frequency and duration discrimination of short first-formant speechlike transitions. J. Acoust. Soc. Am. **95**, 502-511.

Wang, J., van Wijhe, R., Chen, Z. and Yin, S. (2006). Is duration tuning a transient process in the inferior colliculus of guinea pigs? Brain Res. **1114**, 63-74.

Wurtz, R. H. and Kandel, E. R. (2000). Central Visual Pathways. In Principles of Neural Science, vol. 1 eds. E. R. Kandel J. H. Schwartz and T. M. Jessell, pp. 523-547. New York: McGraw-Hill.

Xu-Friedman, M. A. and Hopkins, C. D. (1999). Central mechanisms of temporal analysis in the knollenorgan pathway of mormyrid electric fish. J Exp Biol. **202**, 1311-1318.

Xu-Friedman, M. A. and Regehr, W. G. (2004). Structural contributions to short-term synaptic plasticity. Physiol Rev **84**, 69-85.

Zakon, H. H. (2003). Insight into the mechanisms of neuronal processing from electric fish. Curr Opin Neurobiol. **13**, 744-750.

Chapter 2

Sensory receptor diversity establishes a peripheral population code for stimulus duration at low intensities

But a stimulus will rarely excite only one end organ and the central nervous system will take account of the number of sensory fibers in action as well as of the discharge in each fibre.

-E.D. Adrian, 1928

This chapter contains a previously published manuscript:

A.M. Lyons-Warren, M. Hollmann, and B.A. Carlson (2012). Sensory receptor diversity establishes a peripheral population code for stimulus duration at low intensities. *J Exp. Biol*. 215: 2586-2600.

Author contributions for the above citation:

A.L-W performed all experiments except those relating to figure 7C-E which were done by M.H. A.L-W. analyzed all data with guidance from B.A.C. Modeling was done by B.A.C. All authors contributed to conceptualization and discussion of the experiments. The manuscript was written by A.L-W and B.A.C.

ABSTRACT

Peripheral filtering is a fundamental mechanism for establishing frequency tuning in sensory systems. By contrast, detection of temporal features, such as duration, is generally thought to result from temporal coding in the periphery, followed by an analysis of peripheral response times within the central nervous system. We investigated how peripheral filtering properties affect the coding of stimulus duration in the electrosensory system of mormyrid fishes using behavioral and electrophysiological measures of duration tuning. We recorded from individual knollenorgans, the electrosensory receptors that mediate communication, and found correlated variation in frequency tuning and duration tuning, as predicted by a simple circuit model. In response to relatively high intensity stimuli, knollenorgans responded reliably with fixed latency spikes, consistent with a temporal code for stimulus duration. At near threshold intensities, however, both the reliability and temporal precision of responses decreased. Evoked potential recordings from the midbrain, as well as behavioral responses to electrosensory stimulation, revealed changes in sensitivity across the range of durations associated with the greatest variability in receptor sensitivity. Further, this range overlapped with the natural range of variation in species-specific communication signals, suggesting that peripheral duration tuning affects the coding of behaviorally-relevant stimuli. We measured knollenorgan, midbrain and behavioral responses to natural communication signals and found that each of them were duration-dependent. We conclude that at relatively low intensities for which temporal coding is ineffective, diversity among sensory receptors establishes a population code, in which duration is reflected in the population of responding knollenorgans.

INTRODUCTION

Sensory processing involves the detection of multiple stimulus features in what can generally be considered a two-step process: peripheral filtering followed by central computation. For example, in auditory systems frequency tuning is first established by peripheral filtering, whereas tuning to temporal features of sounds such as interaural time differences (Köppl, 2009), duration (Aubie et al., 2009), and interval (Edwards et al., 2007; Edwards et al., 2008) are thought to arise from central computations. Similarly, peripheral electroreceptors in weakly electric fish are frequency tuned (Hopkins, 1976; Hopkins, 1981), whereas tuning to temporal features is generally thought to arise within central electrosensory pathways (Fortune et al., 2006). However, these central computations are based on peripheral responses, which can vary in relation to frequency tuning as well as other variables. Good examples include the need to resolve phase ambiguity when trying to localize sounds using interaural time differences by integrating across frequency channels (Peña and Konishi, 2000), and the detection of 'phantom' phase differences due to amplitude-dependent latency shifts in weakly electric fishes (Carlson and Kawasaki, 2006; Carlson and Kawasaki, 2007). In the current study, we directly addressed how diversity among peripheral electrosensory receptors affects the coding of temporal information in the African mormyrid electric fish *Brienomyrus brachyistius*.

The electrosensory systems of weakly electric fishes are excellent model systems for studying temporal processing by sensory systems (Fortune et al., 2006; Rose, 2004; Sawtell et al., 2005; Zakon, 2003). Mormyrids emit a pulse-type electric organ discharge

(EOD) for use in communication (Carlson, 2006) and active electrolocation (von der Emde, 1999). The EOD waveform is species-specific (Hopkins, 1981). Temporal features of the EOD, particularly duration, play an important role in species recognition and mate choice (Arnegard et al., 2006; Feulner et al., 2009; Hopkins and Bass, 1981; Machnik and Kramer, 2008). In *B. brachyistius*, the EOD is composed of three phases: an initial, head-negative P0 of relatively small amplitude, followed by a head-positive P1, and finally a head-negative P2 (Carlson et al., 2000).

Electric communication in mormyrids is mediated by a dedicated electrosensory pathway (Bell and Grant, 1989; Xu-Friedman and Hopkins, 1999). Electroreceptors called knollenorgans (KO) respond to outside-positive changes in electrical potential with a fixed latency spike (Bennett, 1965; Hopkins and Bass, 1981). Primary afferent fibers synapse in the hindbrain nucleus of the electrosensory lateral line lobe (nELL) (Bell and Grant, 1989). From the nELL, bilateral projections are sent to a midbrain region, the anterior exterolateral nucleus (ELa), which projects ipsilaterally to the adjacent posterior exterolateral nucleus (ELp) (Carlson, 2009; Friedman and Hopkins, 1998; Szabo et al., 1983).

Hopkins and Bass (1981) proposed a temporal code for EOD duration, in which different KOs respond to either the start or end of an EOD, due to differences in stimulus polarity on opposite sides of the body. Duration information would then be extracted by comparing spike latency differences within the central KO pathway, most likely within ELa (Mugnaini and Maler, 1987; Friedman and Hopkins, 1998). However, KOs are not simply edge detectors. They are broadly tuned to frequencies that roughly correspond to

the power spectrum of the species-specific EOD (Hopkins, 1981). Notably, frequency tuning differs among KOs (Arnegard et al., 2006), revealing that the peripheral coding of electrosensory stimuli varies across the population of receptors. In the current study, we asked how the diversity of KOs influences the peripheral coding of stimulus duration.

MATERIALS AND METHODS

Study Species

We used individuals of both sexes of the weakly electric mormyrid fish *Brienomyrus brachyistius* (Gill, 1862). Individuals ranged from 5.3-17.0 cm in standard length. Fish were purchased from commercial distributors and housed in community aquariums at a temperature of 26-28 ºC and conductivity of 200-400 µS/cm, with a 12:12 hour light:dark cycle. Fish were fed live black worms four times per week. All procedures were in accordance with guidelines established by the National Institutes of Health (NIH) and were approved by the Animal Care and Use Committee at Washington University in St. Louis.

Knollenorgan Recording

We anesthetized fish in 300 mg/l tricaine methanesulfonate (MS-222) (Sigma-Aldrich, St. Louis MO, USA). We then immobilized and electrically silenced fish with 20-100 µl of 0.3 mg/ml gallamine triethiodide (Sigma-Aldrich). Once immobilized, the fish were submerged in a 12.5 x 20 x 45 cm chamber filled with freshwater, and placed on a platform with lateral supports. Aerated freshwater was gravity fed to the fish

through a pipette tip placed into the mouth. Fish generally recovered from anesthesia within 15 minutes of freshwater respiration. We forged electrodes from borosilicate capillary glass (OD=1mm/ID=0.5mm; A-M Systems, Inc., Everett Washington, USA) using a Bunsen burner to bend the last 1 cm to a 30° angle and to polish the tip. Tip inner diameter was 0.5 mm. Mean and s.e.m. resistance for 5 representative electrodes was 0.4 ± 0.1 MΩ. The electrode was filled with tank water, connected to the headstage of a DC amplifier (A-M Systems model 1600), and then placed over, but not touching, individual knollenorgans (KO). Electrical activity was amplified 10x, digitized at 195.3 kHz (Tucker-Davis Model RP2.1, Tucker Davis Technologies, Alachua Florida, USA), and saved to disk using custom-made software (Matlab 7.4, Mathworks, Natick Massachusetts, USA).

Constant-current stimuli were delivered by the amplifier through the electrode using bridge balance to minimize artifact (Arnegard et al., 2006). Stimuli were generated in Matlab. Sinusoidal stimuli ranged from 0.1 to 30 kHz and consisted of 90 ms bursts with 5 ms cosine-squared on and off ramps. Monophasic positive and negative square-pulse stimuli ranged from 0.01 to 5 ms. Natural and manipulated EOD waveforms were generated in Matlab using previously recorded waveforms. Stimuli were digital-to-analog converted (Tucker-Davis model RP2.1) and then attenuated (Tucker-Davis model PA5) prior to delivery. Threshold intensity was defined as the minimum stimulus intensity required to elicit an increased response relative to an equal duration reference window. Reference and response windows were 90 ms for sine waves and 20 ms for square pulses and natural waveforms. Due to the difference in window duration, necessary to accurately

accommodate the different stimulus types, and the desire to quantify the time-locked edge response to square pulses, we used slightly different response criteria for the different types of stimuli. For sine wave stimuli, a positive response constituted at least 1 more spike per repetition in the response window relative to the reference window across 15 repetitions. For square pulse and natural waveform stimuli, spikes from 25 repetitions were binned into 200 ms bins and a response was positive if the highest bin in the response window was greater than the highest bin in the reference window.

For frequency tuning curves, we determined the best frequency (BF, frequency with the lowest threshold) and the bandwidth, measured as the difference between upper and lower frequencies with thresholds 10 dB above the threshold at the BF (BW_{10}), based on logarithmic extrapolation between adjacent data points. We fit duration tuning curves to the equation:

$$I_t = \frac{a}{1 - e^{\left(-\frac{d}{\tau}\right)}} \quad (1)$$

where I_t is the threshold intensity, d is stimulus duration, and a and τ are the asymptote and time constant, respectively, of the exponential decrease in threshold as a function of duration. Duration tuning curves using monophasic square pulses are equivalent to the strength-duration curves historically used to study neuronal excitability (Neumann and Nachmansohn, 1975).

To investigate the effect of stimulus intensity on KO response latency and frequency we tested 6 square pulse durations (0.01, 0.05, 0.1, 0.5, 1, and 3ms) across a range of intensities, from below threshold to above saturation. This range was

approximately 20dB, but varied for each unit and duration. We calculated relative probability of response by subtracting the number of spikes in a 3 ms reference window immediately before the stimulus from the number of spikes in the 3 ms response window starting with the stimulus, and dividing by the number of repetitions (100). We calculated the first spike latency by identifying the time of the first spike within a 3 ms response window from the start of the stimulus for each repetition and then taking the mean of these times. Repetitions with no spike in the 3 ms window were excluded from the first spike latency calculation. From these first spike latencies, we calculated s.d. as a measure of variability in first spike latency (i.e. jitter).

Modeling

To investigate the relationship between frequency and duration tuning, we modeled KOs using a simple electrical circuit (Bennett, 1965; Bennett, 1971). We started with a leaky integrate-and-fire neuron modeled as a resistance (R_m) and capacitance (C_m) in parallel (Gabbiani and Koch, 1998). To this we added a series capacitance (C_s) to represent the contributions of the epithelial plug that covers the sensory cells, the layers of epithelial cells in the wall of the receptor canal, and the apical surface of the receptor cells (Szabo, 1965; Harder, 1968b; Zakon, 1986). We also added a parallel resistance to represent skin resistance (R_s), resulting in voltage drops across the skin (V_s) and across the receptor (V_m) (Fig. 3A, inset).

In response to current, C_s will act as a high-pass filter of V_m whereas C_m will act as a low-pass filter of V_m. The total current, I, will be divided equally between R_s and C_s.

Following Ohm's law, the resulting voltage changes across R_s and C_s are described in equation 2:

$$I = \frac{(V_s + V_m)}{R_s} + C_s\left(\frac{dV_s}{dt}\right) \quad (2)$$

First, the term representing the current across R_s is moved using algebraic rearrangement. All current passing through C_s will then be divided across R_m and C_m. Thus, that term in the equation can be further broken down, again following Ohm's law as shown in equation 3:

$$I - \frac{(V_s + V_m)}{R_s} = \frac{V_m}{R_m} + C_m\left(\frac{dV_m}{dt}\right) \quad (3)$$

Further algebraic rearrangement yields the following difference equations:

$$\left(\frac{dV_s}{dt}\right) = \left(\frac{1}{C_s}\right)\left[I - \frac{V_s}{R_s} - \frac{V_m}{R_s}\right] \quad (4)$$

$$\left(\frac{dV_m}{dt}\right) = \left(\frac{1}{C_m}\right)\left[I - \frac{V_s}{R_s} - \frac{V_m}{R_s} - \frac{V_m}{R_m}\right] \quad (5)$$

We varied C_s and C_m from 0.005 to 1 nF and R_s and R_m from 1 to 10 MΩ and measured the input current required for V_m to reach an arbitrary voltage threshold (1 mV) as a function of sine-wave frequency and square-pulse duration (same stimuli used for KO recordings). The goal of this modeling was to assess the nature of the relationship between frequency tuning and duration tuning, and then determine whether a similar relationship was found for actual KOs.

Midbrain Evoked Potential Recording

To measure evoked field potentials in ELa and ELp, we prepared fish for surgery by anesthetizing them in 300 mg/l MS-222 and then immobilizing them with 100-300 µl of a 3 mg/ml solution of gallamine triethiodide. Fish were then moved to a recording chamber and submerged, except for a small region of the dorsal surface of the head. 0.4% lidocaine was used as a local anesthetic and general anesthesia was maintained throughout the surgery by respirating fish with 100 mg/l MS-222. After removing the skin and securing a post to the skull, an area of bone was removed to expose ELa and ELp as described previously (Carlson, 2009). Once the surgery was complete, we switched respiration to aerated fresh water to bring the fish out of general anesthesia. We used a pair of electrodes placed next to the caudal peduncle to monitor the EOD command. This signal was amplified 1000x on a differential A-C amplifier (A-M Systems model 1700) and sent to a window discriminator (World Precision Instruments SYS-121, World Precision Instruments, Inc., Sarasota Florida, USA) to detect EOD command times. The EOD command triggers inhibition of the KO pathway in nELL (Bell and Grant, 1989). Therefore, any repetition in which the fish emitted a command 2 to 5 ms before the stimulus was ignored.

Recording electrodes (OD=1.2mm/ID=0.68 mm; A-M Systems model 62700) were pulled on a Flaming/Brown micropipette puller (Sutter Instrument Company model P-97, Novato CA, USA), broken to a tip diameter of 10-15 µm and filled with 3M NaCl (resistance <100 kΩ). Evoked potentials from ELa and ELp were amplified 1000x and band-pass-filtered from 0.1 Hz to 5 kHz with a differential AC Amplifier (A-M Systems

model 1700), digitized at 97.6 kHz (Tucker-Davis model RX8), averaged and saved to disk using a custom Matlab program. Evoked field potentials were identified based on their characteristic shape and timing (Amagai, 1998; Carlson, 2009; Szabo et al., 1979).

We delivered transverse electrosensory stimuli using electrodes located on the sides of the tank. Square pulses were generated by an isolated square pulse generator (A-M Systems model 2100) and attenuated before delivery (Hewlett Packard 350D, Hewlett Packard Company, Palo Alto, California, USA). Natural and manipulated EOD waveforms were generated in Matlab, delivered by a signal processor (Tucker-Davis model RX8), attenuated (Tucker-Davis model PA5), and then isolated from ground (A-M Systems model 2200). Stimulus intensities are reported in mV/cm as measured at the location where fish were placed, in the absence of a fish. To measure evoked potential thresholds, we presented a single stimulus at a range of intensities and recorded the mean potential in response to 20 repetitions for natural/manipulated EODs or 40 repetitions for square pulses. We scored trials as responses when the mean potential exceeded three s.d. above or below the baseline mean. Three s.d. was chosen to encompass all of the variation observed during the 50 ms baseline pre-stimulus recording period. We adjusted stimulus intensity in 1dB steps until we identified the least intense signal that yielded a response. This stimulus intensity was considered threshold. To measure the magnitude of responses to isointensity stimulation, we calculated the total area of the response. The area of the response was calculated using the sum of all points in the evoked potential (after subtracting the baseline mean) rather than the peak potential to capture differences in both duration and amplitude in a single measure. Importantly, this measure of total

response area is not affected by the stimulus artifact because the upward- and downward-going edges give rise to symmetrical positive and negative areas, respectively, which cancel each other out. Responses were then normalized to the largest response across all durations tested within that particular brain nucleus within a given fish to account for variation in the amplitude and duration of evoked potentials in ELa and ELp, as well as to control for differences in evoked potential responses due to fish size or electrode placement. Normalizing the values in this way allowed us to directly compare differences in response magnitude with respect to variation in stimulus duration.

Behavioral Playback

Fish were isolated in a 20 l aquarium and confined to a PVC enclosure (20 x 3.5 x 3.5 cm) using netted end-caps (see Carlson et al., 2011). Uniform electric stimuli were presented to the fish using two 7.6 cm chlorided silver wires running along the inside of the side walls of the enclosure, with recording electrodes on each end of the enclosure. Square pulse stimuli were generated by an isolated square pulse stimulator (A-M Systems model 2100) followed by attenuation (Hewlett Packard 350D). We chose both monophasic and biphasic square pulses because behavioral responses to monophasic square pulses could be influenced by responses from ampullary receptors to the D.C. components of this signal (Bennett, 1965; Zakon, 1986). Natural and manipulated EOD waveforms were generated using a custom Matlab program, delivered at 97.6 kHz (Tucker-Davis model RX8), attenuated (Tucker-Davis model PA5), and then isolated from ground (A-M Systems model 2200). Stimulus intensities are reported in mV/cm as

measured from the center of the recording chamber in the absence of a fish. Recorded signals were amplified 100x and band-pass-filtered from 0.1 Hz to 20 kHz with a differential AC amplifier (A-M Systems model 1700). Recordings were digitized at 97.6 kHz (Tucker-Davis model RX8) and custom Matlab software was used to mark EOD times of occurrence relative to stimulus times.

EOD rates were estimated by convolving EOD times with a 300 ms Gaussian filter (Carlson and Hopkins, 2004; Szücs, 1998) and averaging responses to 20 repetitions of the stimulus (inter-stimulus intervals were 20 s). To minimize habituation, fish were allowed one minute of rest between each trial. To determine behavioral thresholds, we calculated a baseline mean and s.d. during the 5 s preceding a stimulus. We defined responses to stimuli as recordings in which the mean EOD rate exceeded two s.d. above the baseline mean within 500 ms after stimulus presentation. We adjusted stimulus intensity in 1dB steps until we identified the least intense signal that yielded a response. This stimulus intensity was considered threshold. The discharge rate of mormyrids can be highly variable (Carlson, 2002). Therefore, to avoid false positive responses, trials were repeated if the trace exceeded 2 s.d. during the baseline period before the stimulus; to avoid false negative responses, trials were repeated if the s.d. was greater than 1.5 EODs/s.

To measure isointensity responses, 15 or 20 stimulus repetitions were presented at 20 second intervals. For square pulses, each trial was repeated three times and then averaged. From the average of all trials, we defined the duration of the response as the time from when the EOD rate first crossed 2 s.d. above the baseline mean until it recrossed

this line. We then calculated the response as the area under this curve. If the EOD rate did not recross the two s.d. line, the duration was calculated using the time of the minimum EOD rate between the start of the response and the end of the recording as the endpoint.

RESULTS

Knollenorgans are Diverse in their Frequency and Duration Tuning

We recorded knollenorgan (KO) spiking responses to constant frequency sine waves (Fig. 1A,B). Stimuli above threshold elicit an increased number of spikes relative to the prestimulus period (Fig. 1A) whereas stimuli below threshold do not (Fig. 1B). Consistent with previous reports (Arnegard et al., 2006; Hopkins, 1981), all KOs were band-pass tuned, with best frequencies (BF) ranging from 0.35 to 4 kHz and bandwidths at 10 dB above threshold (BW_{10}) ranging from 0.30 to 9.69 kHz (Fig. 1C; Table 1). The range of peak power frequencies for *B. brachyistius* EODs is 0.58 to 6.22 kHz (Fig. 1C; Carlson et al., 2000).

FIG 1

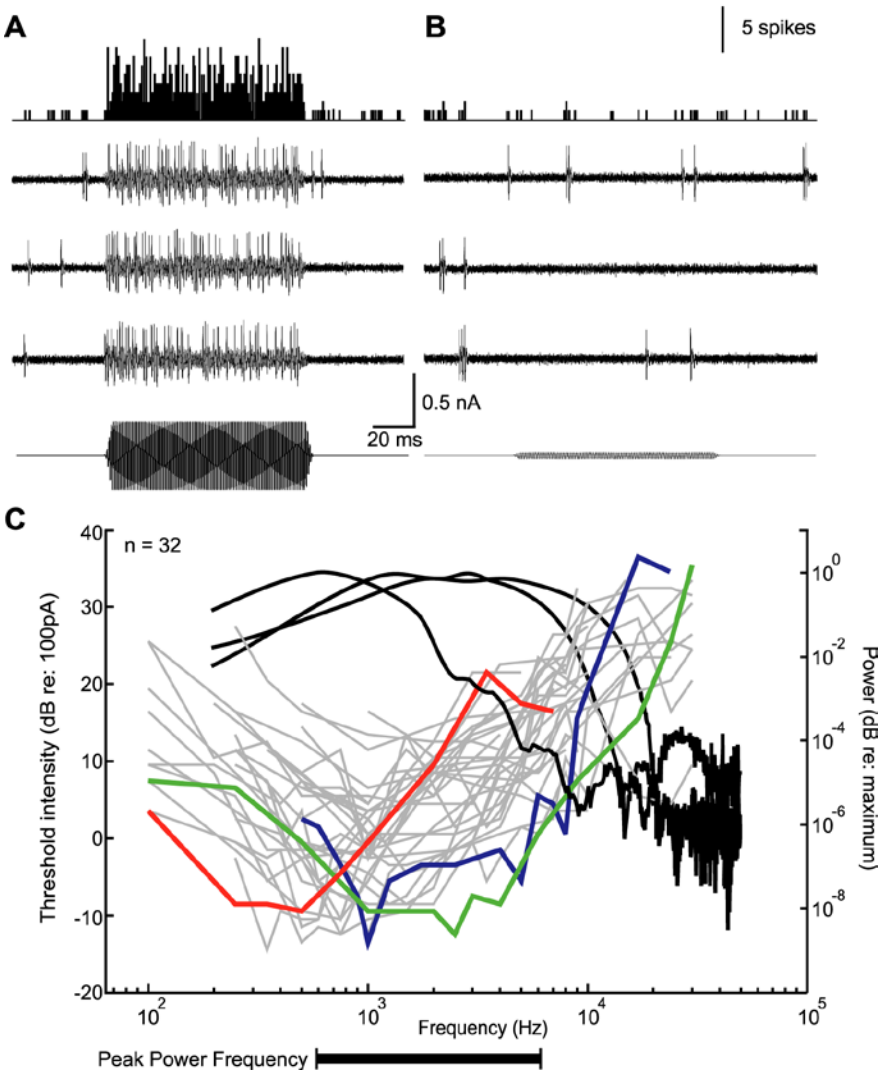

FIG 1: The frequency tuning of knollenorgan electroreceptors varies across units. (A) Spike time histogram (top) and three selected traces from 15 repetitions of a 90 ms, 1 kHz, 0.63 nA stimulus with 5 ms on and off ramps showing increased spike rate during the stimulus. (B) Spike time histogram (top) and three selected traces from 15 repetitions of a 90 ms, 1 kHz, 0.06 nA stimulus with 5 ms on and off ramps illustrating a subthreshold response from the same unit. (C) Threshold frequency tuning curves from 32 different knollenorgans illustrating variability in frequency tuning across units. Three example units, each from a different fish, are highlighted in red, blue and green, whereas all other units are shown in grey. The fast Fourier transforms of the three sample EODs illustrated in figure 2 are shown in black (sampling rate = 100 kHz). The range of peak power frequencies (PPF) for *B. brachyistius* EODs are shown below the threshold tuning curves (Carlson et al., 2000).

Fish ID	BF (Hz)	BW_{10} (Hz)	*a* (nA)	τ (ms)
BB0254	1000	4275	--	--
	1000	2609	0.3957	0.0885
	1500	2167	0.2707	0.2029
	2500	5842	0.7318	0.1111
BB0292	1000	3522	0.2225	0.2039
	1750	4825	0.4291	0.0742
BB0293	1500	7280	0.6803	0.0661
	--	--	0.3687	0.1161
BB0295	1000	539	--	--
	4000	8826	0.9603	0.0917
BB0296	1000	4817	--	--
	1000	632	0.1003	0.4876
	1000	9685	0.8469	0.6502
BB0297	500	946	0.0268	2.7843
	875	3310	0.0114	4.2978
	1000	6918	--	--
BB0298	500	300	--	--
	1000	1719	--	--
	1500	3330	0.3654	0.1272
BB0300	1000	1375	0.3014	0.1039
	--	--	0.3297	0.0909
BB0301	500	710	0.0947	0.5968
	1500	2788	0.3993	0.1587
	--	--	0.3209	0.1684
BB0302	350	1041	--	--
	1250	2677	0.2603	0.1284
BB0303	1200	1630	0.2010	0.5622
BB0304	350	445	0.1214	0.5215
	1000	972	0.1929	0.3230
BB0308	750	494	0.4167	0.1263
BB0376	750	1845	0.0887	0.2056
	750	1027	0.1073	0.4198
	1375	7036	0.2568	0.1509
	2500	4657	0.1415	0.1554
	3500	6897	0.2271	0.0321
	--	--	0.0331	2.0717

Table 1: Summary table illustrating knollenorgan diversity across and within fish. Frequency tuning is indicated by best frequency (BF) and bandwidth (BW_{10}). Duration tuning is summarized by *a* and τ values as described in methods.

We also recorded KO spiking responses to monophasic square pulses. Consistent with previous reports (Bennett, 1965; Hopkins and Bass, 1981), KOs generated a relatively fixed-latency spike in response to outside-positive-going edges of both positive and negative monophasic stimuli (Fig. 2A). This response is only observed when stimulus intensities are above threshold (Fig. 2B). All of the KOs were long-pass tuned for both stimulus polarities, with thresholds decreasing as duration increased (Fig. 2C). However, the shapes of these curves varied across units. We used an exponential fit to quantify variation in duration tuning (see 'Materials and Methods'). Values for a, which describes the asymptote of the fit, ranged from 0.01 to 0.96 nA and values for τ, which describes the time constant of the fit, ranged from 0.07 to 4.30 ms (Table 1). Total EOD durations in *B. brachyistius* range from 0.39 to 2.37 ms (Fig. 2C; Carlson et al., 2000). For each KO, threshold range was calculated as the difference between the minimum and maximum thresholds over a given range of stimulus durations. Across the natural range of total EOD durations, the thresholds of individual KOs showed little variation (mean range of thresholds ± s.d for stimulus durations between 0.39 and 2.37 ms = 0.14 ± 0.13 nA). However, the EODs of *B. brachyistius* consist of three distinct phases ranging in duration from 0.06 to 1.0 ms (Fig. 2C; Carlson et al., 2000). These three phases are roughly similar to three monophasic square pulses in series. Therefore, EOD phase durations represent the behaviorally-relevant range of stimulus durations when interpreting responses to monophasic square pulses. Across this range of durations, individual KO thresholds had four times the range of thresholds observed for the range of total EOD durations and eight times as much variation in the s.d. across units

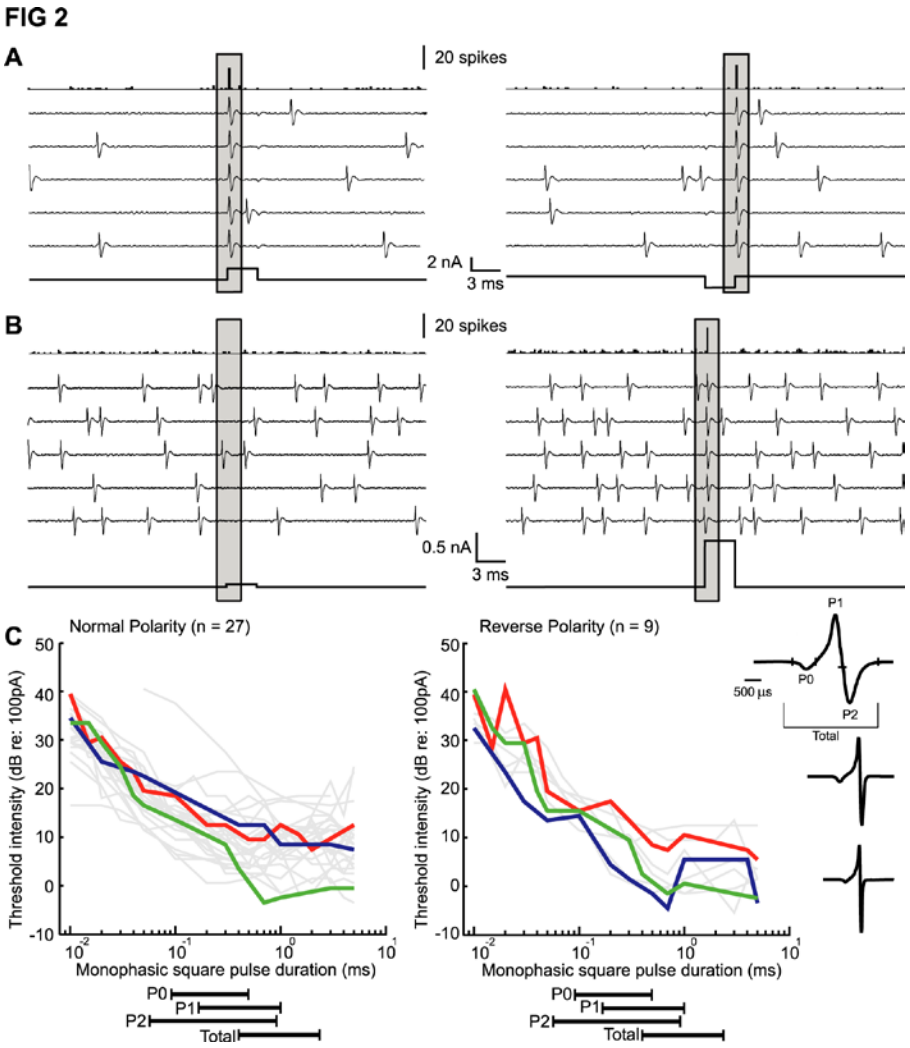

FIG 2: The duration tuning of knollenorgan electroreceptors varies across units. (A) Spike time histograms (top) and 5 selected traces from 25 repetitions of a 2 nA, 3 ms square pulse showing a time-locked spike to the upward edge of both monophasic positive (left) and negative (right) stimuli from the same unit. (B) Spike time histograms (top) and 5 selected traces from 25 repetitions of a 0.08 nA (left) and 0.8 nA (right), 3 ms square pulse illustrating the difference between a subthreshold (left) and suprathreshold (right) response from a second unit. (C) Threshold tuning curves in response to normal (left) and reverse (right) polarity square pulses illustrate the diversity of duration tuning across units. Tuning curves from three units, each from a different fish, are highlighted in red, blue and green, whereas all other units are shown in grey. For each unit, the tuning curves in response to positive and negative polarity stimuli are shown in the same color. Three sample EODs are included as insets (sampling rate = 100 kHz), and the three distinct phases (P0, P1, and P2) are illustrated in the topmost EOD. The range of durations for each phase of the EOD (P0, P1 and P2) and the total EOD duration of *B. brachyistius* are shown below (Carlson et al., 2000).

(mean range of thresholds ± s.d for stimulus durations between 0.06 and 1.0 ms = 0.61 ± 1.10 nA). This difference was statistically significant (Paired t-test, $t_{34} = 2.49$, $p < 0.02$). Importantly, the diversity in KO tuning was not simply due to diversity among fish, since different KOs from the same fish also varied in their tuning (Table 1; Fig. 3B).

Simple Models Reveal a Link between Frequency and Duration Tuning

To ask if variation in duration tuning relates to variation in frequency tuning, we generated a simple electrical circuit model of KOs (Fig. 3A, inset, see 'Materials and Methods'). We adjusted both the capacitance and resistance values in this circuit to ask how changes in passive filtering properties affect frequency and duration tuning. First, with series resistance (R_s) and membrane resistance (R_m) held constant at 5 MΩ, increasing series capacitance (C_s) decreased the BF (Spearman rank R = -0.84, $p < 1e^{-6}$) and the BW_{10} of frequency tuning curves (Spearman rank R = -0.78, $p < 1e^{-6}$) of model KOs (Fig. 3A). Increasing C_s also increased τ of the duration tuning curve (Spearman rank R = 0.79, $p < 1e^{-6}$) but did not have a significant effect on a (Spearman rank R = -0.30, p = 0.09). Increasing membrane capacitance (C_m) decreased both BF and BW_{10} of model KOs (Spearman rank R = -0.88, $p < 1e^{-6}$, and R = -0.93, $p < 1e^{-6}$, respectively) while increasing both a and τ (Spearman rank R = 0.49, $p<0.005$, and R = 0.96, $p < 1e^{-6}$, respectively) of the duration tuning curve (Fig. 3A). With C_s and C_m held constant at 0.5 nF, increasing R_s non-significantly decreased BF and significantly decreased BW_{10} (Spearman rank R = -0.433, p = 0.24, and R = -0.84, $p < 0.005$, respectively) of model

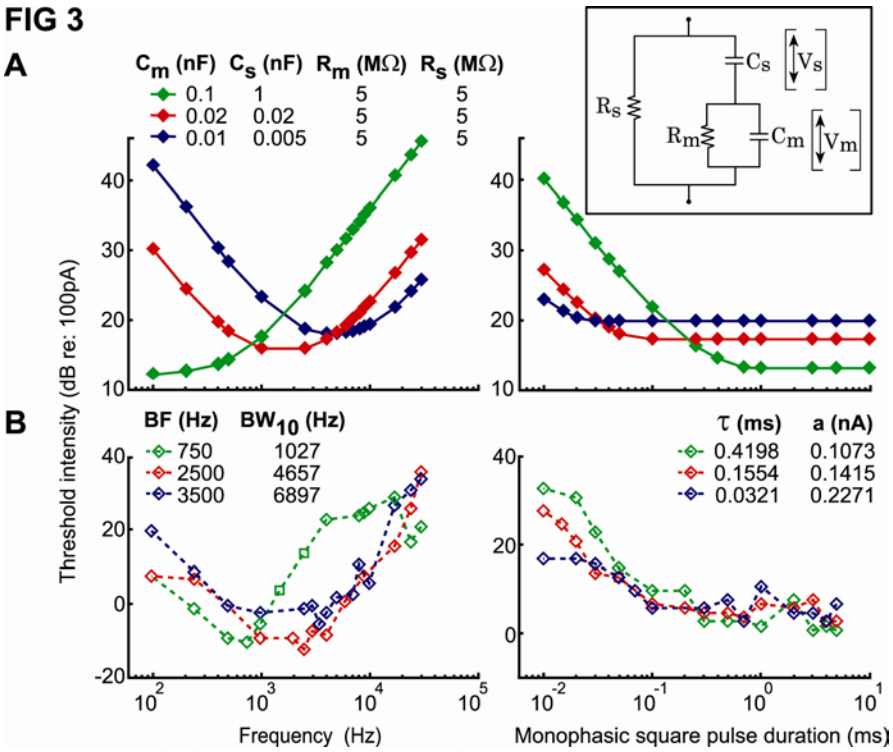

FIG 3: Modeling the knollenorgan receptor as a simple electrical circuit. (A) Frequency (left) and duration (right) tuning curves generated from 3 model neurons with resistance values set to 5 MΩ and variable capacitance values. as indicated. Inset shows the electrical circuit model of knollenorgan receptors, which consists of a skin resistance (R_s), membrane resistance (R_m), membrane capacitance (C_m), and series capacitance (C_s). Corresponding voltage drops (V_s) and (V_m) across the two capacitors are shown with arrows. (B) Frequency (left) and duration (right) tuning curves from 3 different knollenorgans recorded from a single fish with measured values for best frequency (BF), bandwidth (BW_{10}), duration tuning curve time constant (τ) and duration tuning curve asymptote (a).

KOs while decreasing a and increasing τ of the duration tuning curve (Spearman rank R = -0.84, $p < 0.005$, and R = 0.84, $p < 0.005$, respectively) (Fig. 3A). Increasing R_m did not lead to any significant changes in BF, BW_{10}, a or τ (Spearman rank R = -0.43, p = 0.24, R = -0.47, p = 0.20, R = -0.47, p = 0.2, R = 0.47, p = 0.2, respectively).

As a result of these effects, there was a strong negative correlation between BF and τ among our model KOs (Spearman rank R = -0.90, $p < 1e^{-6}$), as well as between BW_{10} and τ (Spearman rank R = -0.99, $p < 1e^{-10}$). Neither BF nor BW_{10} were significantly correlated with a (Spearman rank R = -0.18, $p > 0.3$, and R = -0.22, $p > 0.2$, respectively). The three sample tuning curves shown in Fig. 3A illustrate the relationship between frequency and duration tuning of model KOs, but it is important to realize that these particular combinations of capacitance and resistance do not necessarily represent a unique solution for those particular tuning curves. Similar correlations between frequency and duration tuning were observed among different KOs recorded from a single fish (Fig. 3B). Indeed, across all KOs, BF was negatively correlated with τ (Spearman rank R = -0.67, $p < 1e^{-3}$), and BW_{10} was likewise negatively correlated with τ (Spearman rank R = -0.46, $p < 0.03$).

Stronger Signals Create Tighter Responses

The accuracy of temporal coding depends on the precision of time-locked responses to stimuli. However, temporal precision in sensory systems is generally intensity-dependent. Therefore, we investigated how stimulus intensity affected the timing of KO responses. Decreasing stimulus intensity led to a consistent increase in

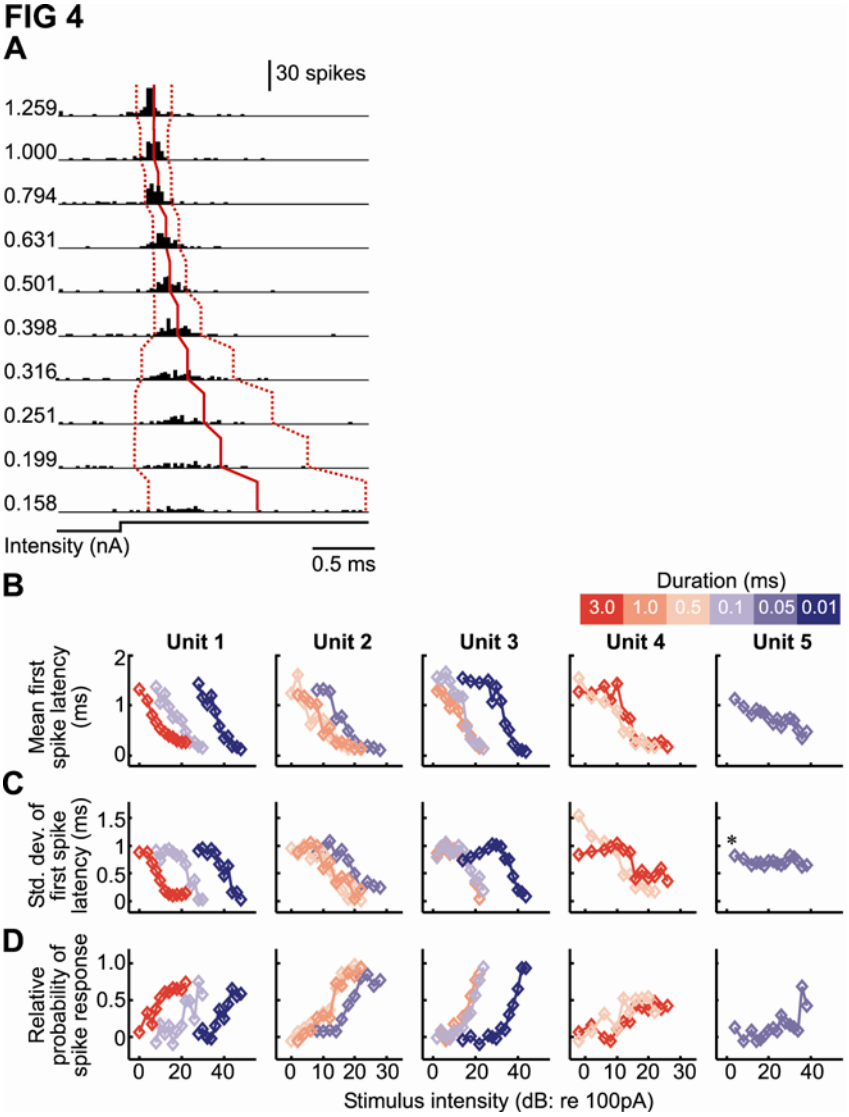

FIG 4: Knollenorgan spike latency and variability is stimulus intensity-dependent. (A) Spike time histograms from a single knollenorgan in response to 100 repetitions of a 3 ms monophasic positive square pulse stimulus presented at intensities ranging from 0.158 nA to 1.259 nA. Mean and s.d. of first spike latencies are shown as solid and dashed red lines, respectively. Responses to six different durations tested twice each across 5 units for a total of 12 experiments are shown in B-D. (B) Mean first spike latency decreases with increasing stimulus intensity (Spearman rank R = -1 to -0.85, $p < 0.05$). (C) Standard deviation (s.d.) of first spike latency decreases with increasing stimulus intensity (Spearman rank R = -0.92 to -0.62, $p < 0.05$; *indicates that the correlation between the response measure and stimulus intensity was not significant. (D) Relative probability of spike response, calculated as number of spikes per stimulus relative to pre-stimulus baseline activity (see 'Materials and Methods'), increases with increasing stimulus intensity (Spearman rank R = 0.6 to 0.97, $p < 0.05$).

response latency (i.e. amplitude-dependent latency shift), as well as an increase in the variability of response times (i.e. jitter; Fig. 4A). This effect was consistent across 5 units tested with a range of stimulus durations (Fig. 4B-D). Mean first spike latency decreased significantly with increasing stimulus intensity in all cases (range of Spearman rank $R = -1$ to -0.85, $p < 0.05$) (Fig. 4B). First spike latency s.d. also decreased significantly with increasing stimulus intensity in 11 of the 12 cases (range of Spearman rank $R = -0.92$ to -0.62, $p < 0.05$) (Fig. 4C). Finally, relative response probability increased significantly with increasing stimulus intensity in all cases (range of Spearman rank $R = 0.60$ to 0.97, $p < 0.05$) (Fig. 4D). Therefore, the temporal precision needed for accurately coding stimulus duration into spike latency differences was greatest at relatively high intensities.

Midbrain Responses Reflect the Peripheral Coding of Duration

We next asked how the diversity of duration coding by KOs influenced electrosensory responses within the central KO pathway. We recorded evoked field potentials in ELa and ELp in response to monophasic and biphasic square pulses presented at an intensity of 3.7 mV/cm and varying in total duration from 0.01 ms to 20 ms. Normalized responses, measured as the total area of the evoked potential, increased with increasing duration for both monophasic (Fig. 5A, top) and biphasic square pulses (Fig. 5B, top). Using a repeated-measures ANOVA we found a significant increase in response with increasing duration for monophasic ($F_{13, 143} = 51.8$, $p < 1e^{-6}$) and biphasic ($F_{13,117} = 34.7$, $p < 1e^{-6}$) pulses. In comparing isointensity tuning curves for ELa and ELp,

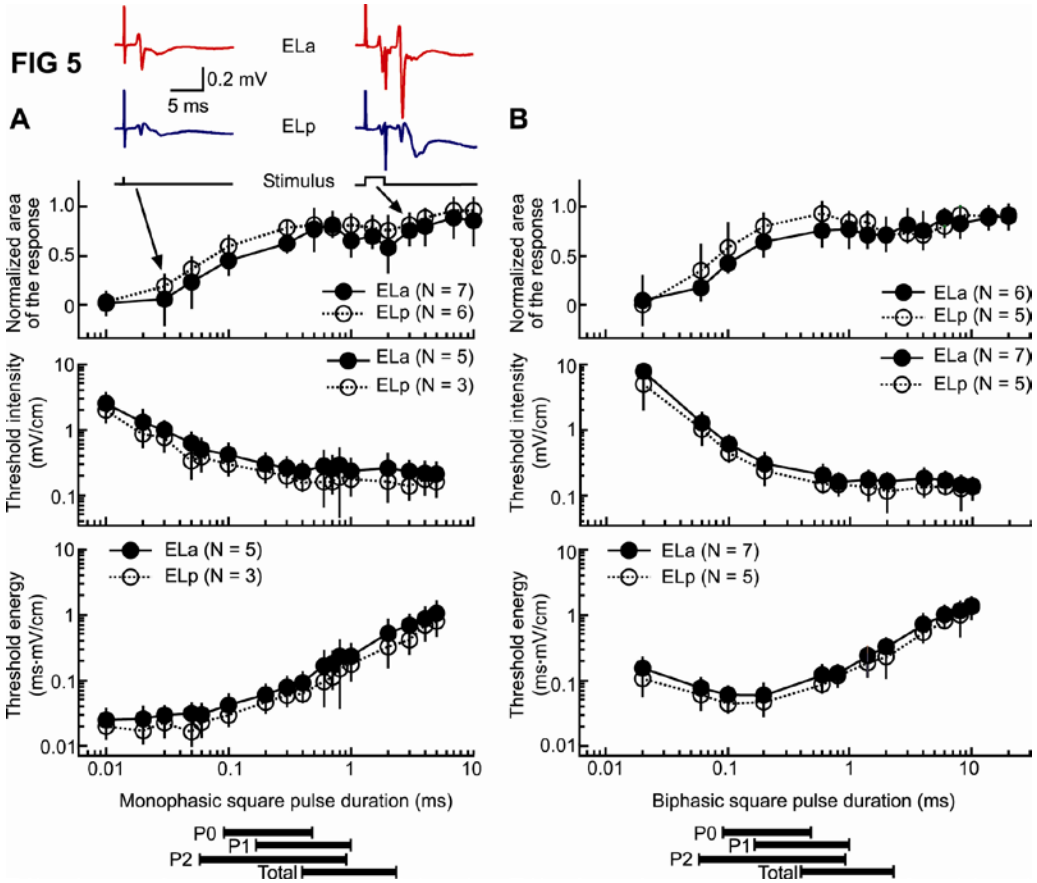

FIG 5: Duration tuning of evoked potentials in the exterolateral nucleus (EL) of the midbrain reveals changes in sensitivity across the range of natural EOD durations. Mean isointensity tuning curves in response to monophasic (A, top) and biphasic (B, top) square pulses of varying durations in both the anterior (solid) and posterior (dashed) subdivisions of EL (ELa and ELp, respectively). Example evoked potential responses from ELa (red) and ELp (blue) at two different stimulus durations (arrows) are shown. Each region has a unique, characteristic response shape. Therefore, responses were normalized to the largest response across all durations tested for the same nucleus in the same fish. Normalized responses increase with increasing stimulus duration for both monophasic ($F_{13,\ 143} = 51.8$, $p < 1e^{-6}$) and biphasic ($F_{13,117} = 34.7$, $p < 1e^{-6}$) pulses. Isointensity tuning curves were generated with a stimulus intensity of 3.7 mV/cm, and all response magnitudes were normalized to the largest response for each fish. Threshold intensity tuning curves in response to monophasic (A, middle) and biphasic (B, middle) square pulses of varying durations in both brain regions decrease with increasing stimulus duration for both monophasic ($F_{16,96} = 27.0$, $p < 1e^{-6}$) and biphasic ($F_{11,99} = 37.6$, $p < 1e^{-6}$) pulses. Threshold energy tuning curves in response to monophasic (A, bottom) and biphasic (B, bottom) square pulses of varying durations in both brain regions increase with increasing stimulus duration (for both monophasic ($F_{16,96} = 23.3$, $p < 1e^{-6}$) and biphasic ($F_{11,99} = 57.1$, $p < 1e^{-6}$) stimuli. Values shown are the mean ± s.d. across fish. The range of durations for each phase of the EOD (P0, P1 and P2) and the total EOD duration of *B. brachyistius* are shown below (Carlson et al., 2000).

there was no significant interaction effect between recording location and stimulus duration for monophasic ($F_{13,143}$= 0.6 p > 0.84) or biphasic ($F_{13,117}$ = 1.2, p > 0.27) stimuli, indicating no difference in the isointensity duration tuning curves of evoked potential responses of the two midbrain regions.

We also measured threshold stimulus intensities for evoked field potentials in ELa and ELp in response to monophasic and biphasic square pulses with total durations ranging from 0.01 to 20 ms. For both monophasic (Fig. 5A, middle) and biphasic (Fig. 5B, middle) square pulses we found greater sensitivity to longer pulse durations in both ELa and ELp (repeated-measures ANOVA, monophasic $F_{16,96}$ = 27.0, p < $1e^{-6}$, biphasic $F_{11,99}$ = 37.6, p < $1e^{-6}$). There was no significant interaction effect between recording location and stimulus duration for either monophasic ($F_{16,96}$ = 0.5, p > 0.95) or biphasic ($F_{11,99}$ = 0.7, p > 0.75) stimuli, indicating no difference in the threshold duration tuning curves of evoked potential responses of the two midbrain regions. Importantly, the range of durations over which ELa and ELp showed the greatest change in both isointensity response and threshold intensity directly corresponded to the range of durations over which KOs exhibited the greatest variation in threshold (compare Fig. 5A,B with Fig. 2C). This suggests that the long-pass tuning observed in ELa and ELp was due to the progressive recruitment of additional KOs with increasing stimulus duration.

To ensure that long-pass tuning was consistent across a range of intensities, we measured the magnitude of evoked potentials in response to intensities ranging from 0.11 to 35.4 mV/cm. In ELa, we observed long-pass tuning at all intensities ≥1.1 mV/cm, and these curves did not saturate even at the longest durations and intensities tested (Fig. S1A). In

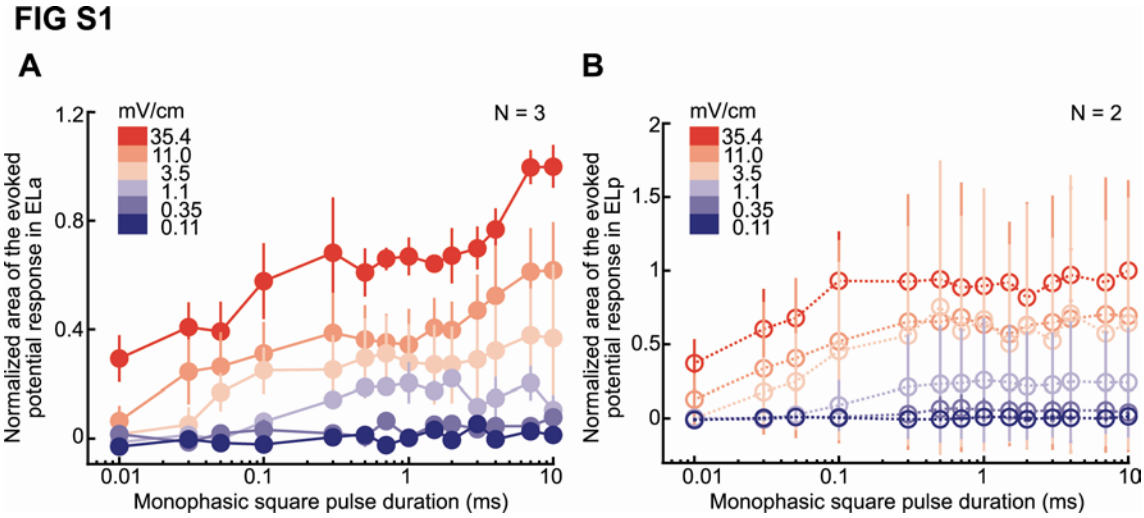

FIG S1: Knollenorgan population response measured in the exterolateral nucleus (EL) of the midbrain. Isointensity tuning curves for monophasic square pulses presented at a range of intensities (0.11 to 35.4 mV/cm) in ELa (A) and ELp (B) all show long-pass tuning. All response magnitudes were normalized to the largest response for each fish. Values shown are mean ± s.d. for the normalized values across fish.

ELp, we also observed long-pass tuning at all intensities ≥1.1 mV/cm, although the curve saturated at ~0.1 ms at the higher intensities tested (Fig. S1B).

Increasing the duration of a square pulse increases the total energy of the stimulus. To determine whether the observed long-pass tuning was due solely to the effects of increasing stimulus energy, we determined the threshold energy (threshold intensity multiplied by duration) as a function of duration. If changes in energy fully accounted for the observed long-pass tuning, then we would expect threshold energy to be the same for all durations; however, threshold energy increased with duration for both monophasic ($F_{16,96} = 23.3$, $p < 1e^{-6}$) (Fig. 5A, bottom) and biphasic ($F_{11,99} = 57.1$, $p < 1e^{-6}$) (Fig. 5B, bottom) stimuli.

Behavioral Responses Reflect the Peripheral Coding of Duration

Next, we asked how the diversity of duration coding by KOs impacted behavioral responses to electrosensory stimulation. To assess this, we used the 'novelty response', which is an increase in the rate of EOD emission in response to presentation of a novel stimulus (Carlson et al., 2011; Post and von der Emde, 1999). We presented monophasic and biphasic square pulses ranging in duration from 0.01 to 10 ms at an intensity of 145 mV/cm. We measured EOD frequency over time by convolving EOD times of occurrence with a 300 ms-wide Gaussian function (Carlson and Hopkins, 2004) and averaging across repetitions. The magnitude of the novelty response was calculated as the area under the response curve (Fig. 6A, see 'Materials and Methods'). The magnitude of the fish's response increased with stimulus duration for both monophasic

FIG 6

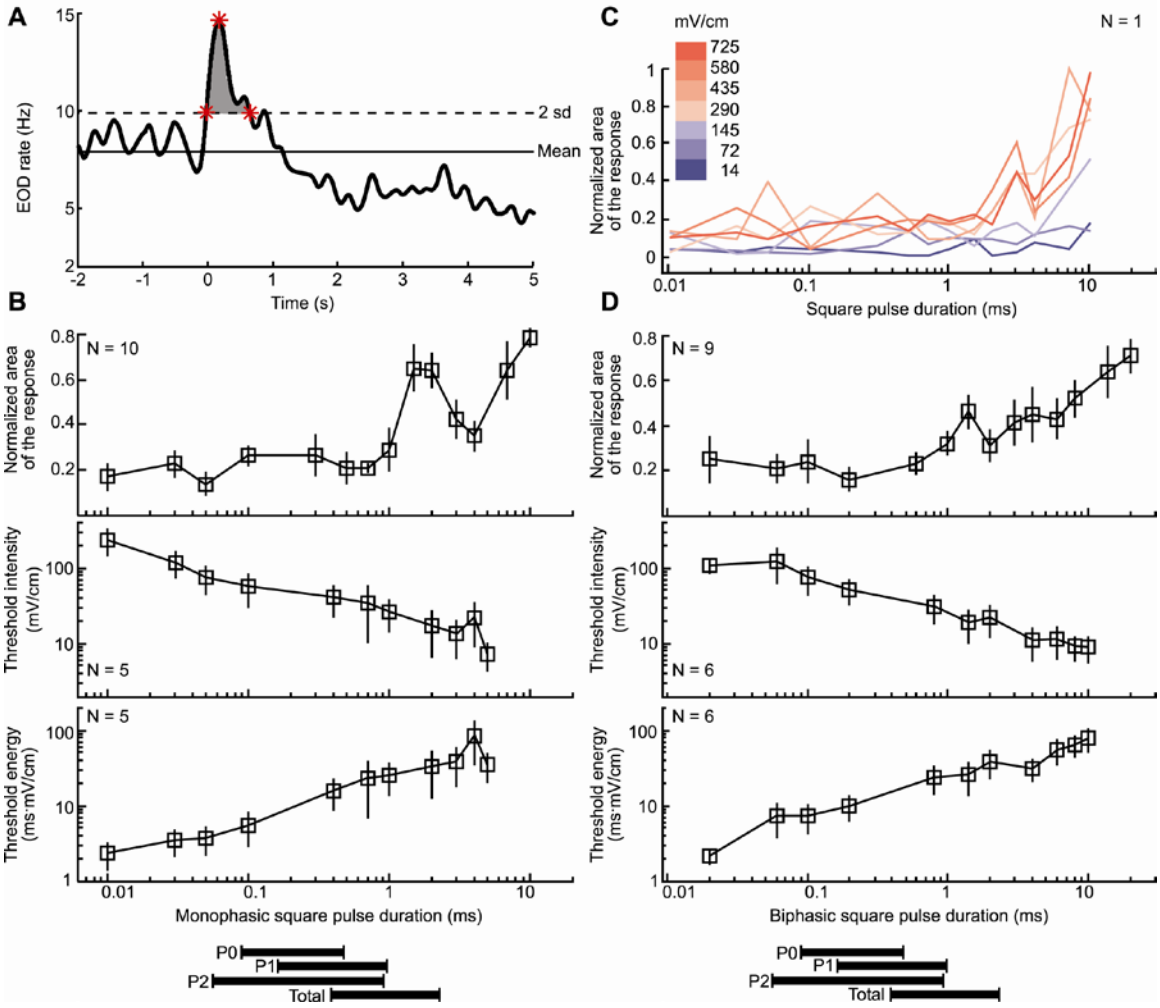

FIG 6: Duration tuning of behavioral novelty responses reveals changes in sensitivity across the range of natural EOD durations. (A) Example of increased EOD rate (novelty response) in response to a biphasic square pulse delivered at time = 0 s. Isointensity responses were calculated using the area under the curve above the 2 s.d. line as shown in gray. (B) Normalized response ($F_{13,117} = 6.9$, $p < 1e^{-6}$; top), threshold intensity ($F_{10,40} = 4.8$, $p < 1e^{-3}$; middle) and threshold energy ($F_{10,40} = 2.5$, $p < 0.021$; bottom) tuning curves for novelty responses to monophasic square pulses of varying durations. (C) Isointensity tuning curves for monophasic square pulses presented at a range of intensities (14 to 725 mV/cm) all show long-pass tuning. (D) Normalized response ($F_{13,104} = 3.2$, $p < 1e^{-3}$; top), threshold intensity ($F_{10,50} = 4.8$, $p < 1e^{-4}$; middle) and threshold energy ($F_{10,50} = 4.9$, $p < 1e^{-4}$; bottom) tuning curves for novelty responses to biphasic square pulses of varying durations. Values shown are mean ± s.d.. The range of durations for each phase of the EOD (P0, P1 and P2) and the total EOD duration of *B. brachyistius* are shown below (Carlson et al., 2000).

(repeated-measures ANOVA, $F_{13,117} = 6.9$, $p < 1e^{-6}$; Fig. 6B, top) and biphasic ($F_{13,104} = 3.2$, $p < 1e^{-3}$; Fig. 6D, top) stimuli. The threshold intensity necessary to elicit a novelty response decreased with stimulus duration for both monophasic ($F_{10,40} = 4.8$, $p < 1e^{-3}$; Fig. 6B, middle) and biphasic ($F_{10,50} = 4.8$, $p < 1e^{-4}$; Fig. 6D, middle) stimuli. Finally, we tested if stimulus energy was the sole source of long-pass tuning by plotting threshold energy against stimulus duration. As with evoked potentials in ELa and ELp, threshold energy increased with increasing stimulus duration for both monophasic ($F_{10,40} = 2.5$, $p < 0.021$; Fig. 6B, bottom) and biphasic ($F_{10,50} = 4.9$, $p < 1e^{-4}$; Fig. 6D, bottom) stimuli. To determine whether stimulus intensity impacted the shape of the isointensity tuning curve, we measured the magnitude of the responses of one fish for 0.01 to 10 ms monophasic pulses presented at 7 intensities ranging from 14 to 725 mV/cm and observed long-pass tuning at each intensity (Fig. 6C).

The Peripheral Coding of Duration Affects Detection of Natural Stimulus Waveforms

Finally, we asked how the coding of duration by KOs affected the detection of behaviorally-relevant stimuli by measuring KO threshold intensities to natural EOD waveforms of 10 different mormyrid species. We also measured thresholds to *B. brachyistius* EODs subjected to three different temporal manipulations: cutting the duration in half, doubling the duration, and time-reversing the EOD.

KOs respond to the rising edge of a natural waveform with a fixed-latency spike (Fig. 7A), just as they do to square pulses (Fig. 2A,B). KO threshold intensity varied in response to different species' EODs (repeated-measures ANOVA, $F_{11,88}=10.5$, $p < 1e^{-6}$,

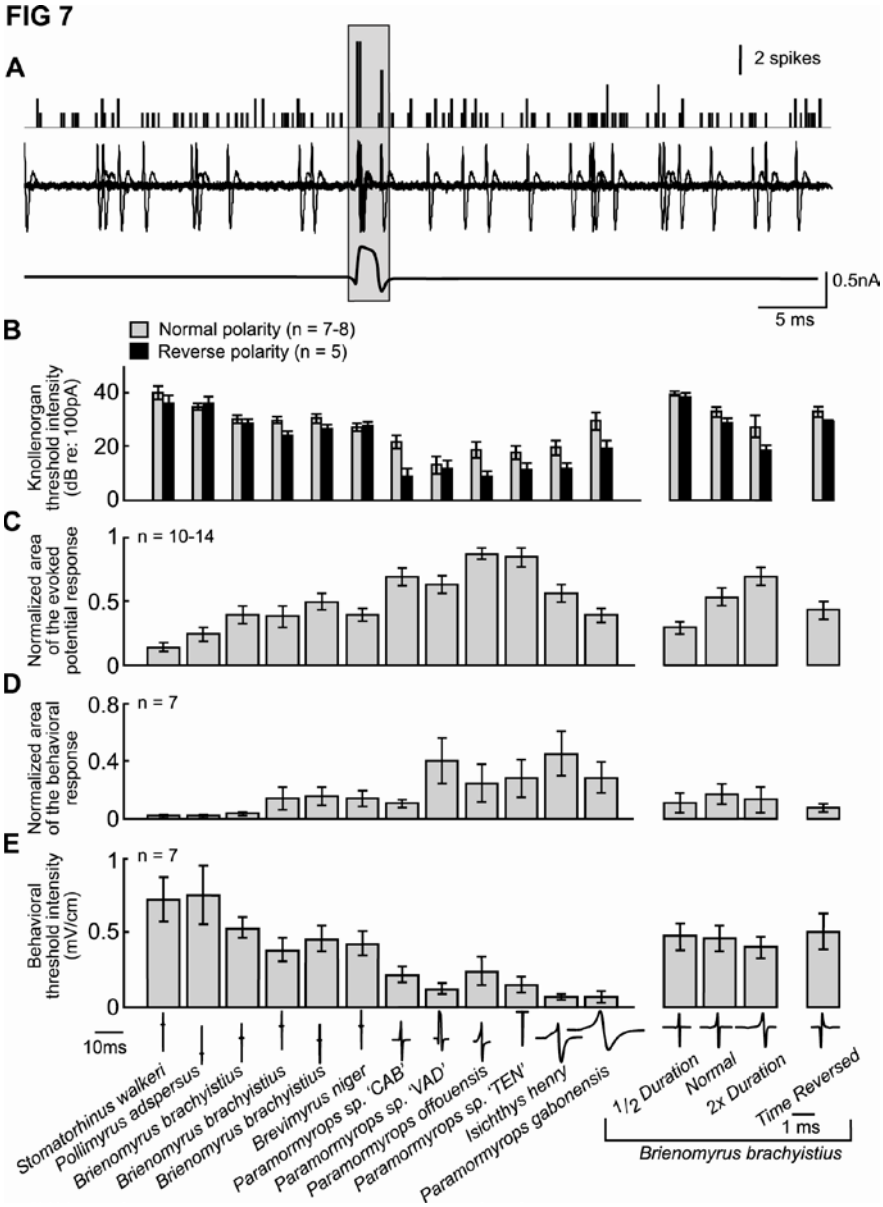

FIG 7: Sensitivity to natural and manipulated EOD waveforms is duration-dependent. (A) Spike time histogram (top) and 5 superimposed selected traces from 25 repetitions of a *Paramormyops vadamans* EOD presented at 0.63 nA showing a time-locked knollenorgan spike to the upward edge. (B) Knollenorgan response thresholds to EOD waveforms from 10 different species vary significantly, (left) as well as manipulated versions of *B. brachyistius* EODs (right). (C) Normalized ELp mean evoked potential responses to the same waveforms from (B). Normalized behavioral (D) and threshold (E) responses to the same waveforms from (B). Waveforms and genus and species names are shown below each column of data, which are arranged in order of decreasing peak power frequency. 3-letter cheironyms refer to undescribed species of *Paramormyrops* recently discovered in Gabon, Africa (Arnegard et al., 2005; Arnegard and Hopkins, 2003; Carlson et al., 2011; Sullivan et al., 2002). Values shown are mean ± s.e.m.

Fig. 7B, left), but there was no difference in threshold between normal and reversed polarities ($F_{1,8} = 2.2$, $p > 0.1$). The peak power frequencies (PPF) of EODs negatively correlate with duration (Hopkins, 1981). We therefore used PPF to quantify species differences in EOD waveforms, and found that KO thresholds decreased significantly with decreasing PPF (Spearman rank $R = 0.62$, $p < 0.05$). We presented waveforms recorded from three different *B. brachyistius* individuals and found average thresholds of 3.34 ± 0.84, 3.50 ± 0.70, and 3.10 ± 0.34 nA for normal polarity stimuli and 2.26 ± 0.48, 2.87 ± 0.62, and 1.96 ± 0.39 nA for reverse polarity stimuli. The thresholds for the three waveforms were not significantly different from each other ($F_{2,20} = 1.8$, $p > 0.1$), nor were the thresholds of normal vs. reversed polarity stimuli ($F_{1,10} = 2.3$, $p > 0.1$).

Artificial manipulation of the duration of a *B. brachyistius* EOD caused a significant change in KO threshold (repeated-measures ANOVA, $F_{2,22} = 22.0$, $p < 1e^{-5}$), with lower thresholds for elongated EODs and higher thresholds for shortened EODs. There was no difference between normal and reverse polarity stimuli ($F_{1,11} = 0.63$, $p > 0.4$). For the time-reversed EOD, neither the normal ($t_6 = 0.59$, $p > 0.5$) nor reverse polarity ($t_4 = -0.02$, $p > 0.95$) thresholds were significantly different from the natural EOD (Fig. 7B, right).

The magnitude of evoked potentials in ELp also differed significantly in response to different species' EODs (repeated-measures ANOVA, $F_{11,66} = 11.3$, $p < 1e^{-6}$) (Fig. 7C, left). Evoked potentials increased significantly in magnitude with decreasing PPF (Spearman rank $R = -0.61$, $p < 0.05$). Artificial manipulation of the duration of a *B. brachyistius* EOD significantly changed the magnitude of evoked potential responses

($F_{2,22}$=11.0, $p < 1e^{-3}$), with larger responses to elongated EODs and weaker responses to shortened EODs. Unlike at the periphery, the time-reversed waveform evoked a significantly smaller response ($t_{12} = -2.3$, $p < 0.05$) (Fig. 7C, right).

Finally, behavioral measures of sensitivity also showed duration-dependence. Normalized behavioral responses did not differ significantly in response to different species' EODs, although there was a clear trend (repeated-measures ANOVA, $F_{11,55} = 1.8$, $p < 0.1$), and behavioral thresholds did differ significantly in response to different species' EODs ($F_{11,66} = 7.4$, $p < 1e^{-6}$). Further, normalized behavioral responses increased significantly with decreasing PPF (Spearman rank R = -0.88, $p < 0.05$) (Fig. 7D, left), and behavioral thresholds decreased significantly with decreasing PPF (Spearman rank R = 0.94, $p < 0.05$) (Fig. 7E, left). Neither behavioral threshold ($F_{2,12} = 0.3$, $p > 0.7$) nor normalized behavioral responses ($F_{2,12} = 0.2$, $p > 0.8$) differed significantly in response to artificial manipulation of EOD duration. Similarly, the time reversed waveform was not significantly different from the original waveform for either normalized behavioral responses ($t_6 = 1.4$, $p>0.2$) or behavioral thresholds ($t_6 = 0.3$, $p>0.7$) (Fig. 7D,E, right).

DISCUSSION

We asked how variation among peripheral sensory receptors impacts the coding of stimulus duration. We found that knollenorgan (KO) electroreceptors exhibit long-pass duration tuning that varies among units (Fig. 2C). The diversity in duration tuning correlates with variation in frequency tuning, as predicted by a simple circuit model of

KOs (Fig. 3). Population responses in two midbrain nuclei that process electrosensory communication signals are also long-pass tuned to duration (Fig. 5), as are behavioral novelty responses (Fig. 6). Importantly, both midbrain and behavioral thresholds varied most dramatically across the same range of durations for which KO receptors exhibited the greatest diversity in tuning. This window of stimulus durations corresponds to the range of durations observed for different phases of conspecific EODs (Carlson et al., 2000). In relating natural EODs to monophasic square pulses, we propose that the range of EOD phase durations, not the range of total EOD durations, represents the behaviorally-relevant range of stimulus durations. The triphasic EOD of *B. brachyistius* is roughly similar to three monophasic square pulses in series. KO receptors respond to either rising or falling edges, which occur at the start or end of each phase of a natural EOD and at the start or end of a monophasic square pulse. Indeed, responses to natural waveforms from a variety of species that vary widely in EOD duration demonstrate duration-dependent differences in sensitivity, confirming the relevance of peripheral duration tuning to the detection and discrimination of natural signals (Fig. 7).

Peripheral Diversity Creates a Population Code for Duration

Multiple observations on the response properties of KOs (Bennett, 1965; Bell, 1990; Zakon, 1986) led Hopkins and Bass (1981) to propose a temporal coding model for species recognition, in which EOD duration is coded by spike timing differences between KOs on opposite sides of the body (Fig. 8). Several lines of evidence suggest that these spike timing differences are compared within the anterior exterolateral nucleus (ELa) to

establish single-neuron tuning to stimulus duration (Amagai, 1998; Amagai et al., 1998; Friedman and Hopkins, 1998; Carr and Friedman, 1999; Mugnaini and Maler, 1987; Xu-Friedman and Hopkins, 1999). However, as stimulus intensity decreased, we found significant decreases in KO response probability and significant increases in response latency and jitter (Fig. 4), revealing that the temporal coding of stimulus duration is less effective at near-threshold intensities. Sound intensity similarly affects the accuracy of temporal coding for sound localization (Nishino et al., 2008). Population averaging of peripheral responses through anatomical convergence is one mechanism for reducing temporal jitter in auditory and electrosensory systems (Carr and Friedman, 1999). Our data suggest another solution to this problem: a population code allows fish to obtain information about stimulus duration at intensities too low for a temporal code to reliably signal duration. Using our particular behavioral measure (the novelty response), threshold detection levels for natural EOD waveforms ranged from 0.06 to 0.74 mV/cm (Fig. 7E). Work in other mormyrid species based on more sensitive measures of signal detection have revealed a minimum threshold for detection of communication signals as low as 1-10 μV/cm (Moller and Bauer, 1973; Moller et al., 1989). Paintner and Kramer (2003) demonstrated that the minimum intensity for trained mormyrids to discriminate a 2 μs difference in waveform ranged from 4.9 μV/cm to 123 μV/cm. Using evoked potential responses in ELa and ELp as a readout of the KO population response, we found that threshold intensities to monophasic square pulses ranged from 140 μV/cm to 2.54 mV/cm (Fig. 5A). Therefore, stimulus intensities greater than 2.5 mV/cm are necessary for all KOs to respond reliably and this value is well above the minimum

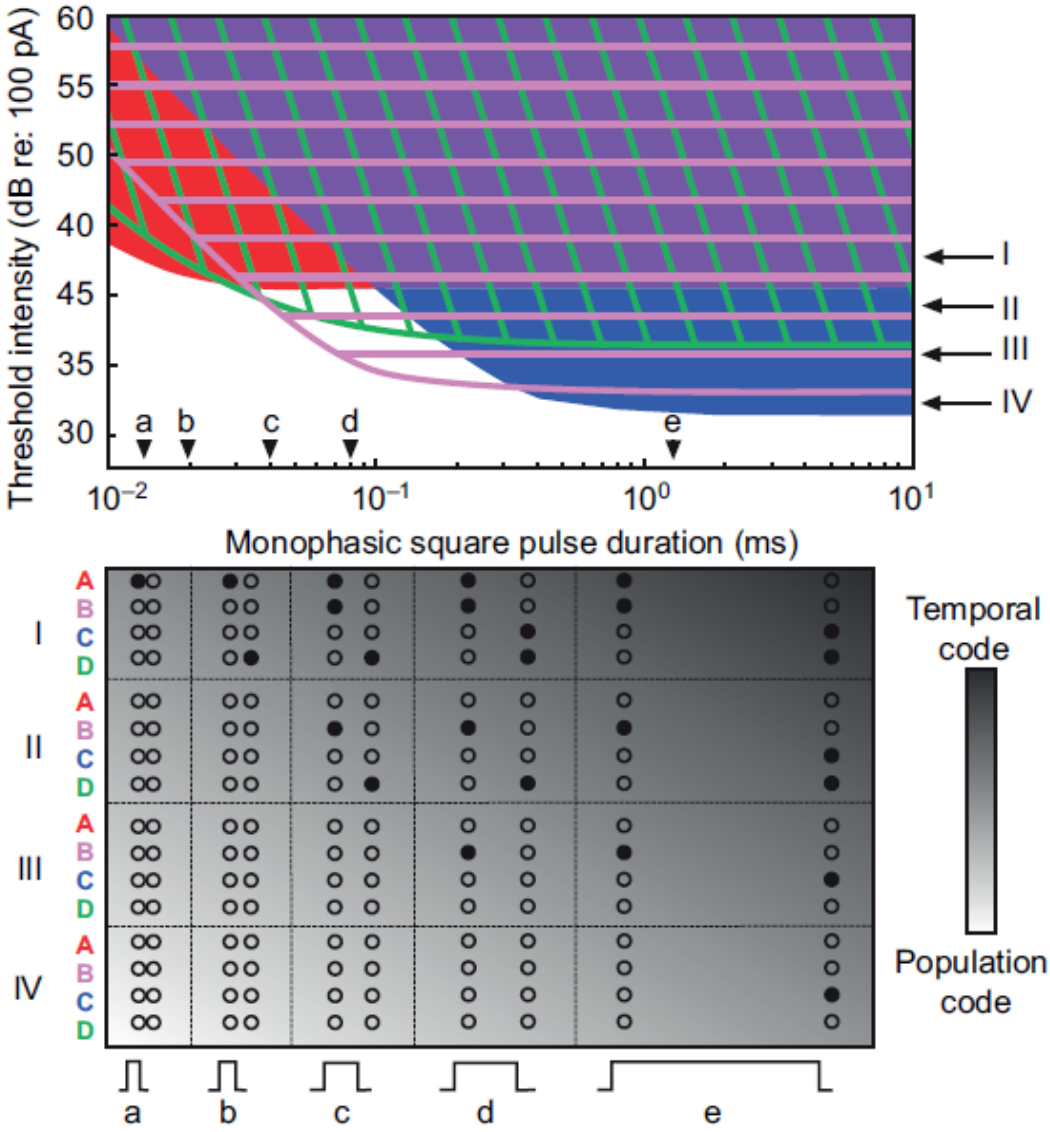

FIG 8: Conceptual model of duration tuning utilizing a temporal code at high intensities and a population code at low intensities. Duration tuning curves (top) from four model knollenorgans with shading to indicate response properties. The colors (unit A= red, unit B = pink, unit C = blue, unit D = green) indicate the duration and intensity combinations that will elicit a suprathreshold response from that unit. Spiking patterns (bottom) of the same four model knollenorgans at four intensities (arrows) and five durations (arrow heads) with shading to indicate the relative contribution of the temporal code and the population code. Filled circles indicate a response, open circles indicate a lack of response. At high intensities and long durations, spike timing differences between units responding to the start of the square pulse (A, B) and units responding to the end of the pulse (C,D) provide a precise temporal code for duration. In contrast, shorter and weaker stimuli are characterized by a population code in which duration is represented by the pattern of responses across all knollenorgans (filled circles).

intensity for accurate signal discrimination. Even restricting the range of durations to the behaviorally-relevant phase durations of 0.06 to 1 ms, we found that threshold intensities ranged from 176 μV/cm to 508 μV/cm (Fig. 5A). Therefore, mormyrids can discriminate species-specific EODs at intensities that are too weak for the temporal code to work effectively.

Each KO studied exhibited long-pass tuning (Fig. 2C), as expected due to membrane capacitance, which acts as a low-pass filter of input current for all neurons. Interestingly, however, long-pass tuning characteristics differed among KOs, both between and within fish, over the range of behaviorally-relevant durations corresponding to the range of EOD phase durations (Figs. 2C, 3B; Table 1). Therefore, at near-threshold intensities, increasing stimulus duration across the behaviorally-relevant range leads to the recruitment of an increasing number of KOs (Fig. 8). As increases in both stimulus intensity and duration will lead to the recruitment of more KOs (Fig. 8), there is some ambiguity to a simple population code based solely on the number of responding receptors. Importantly, we found that the shape of each KO's tuning curve differs (Figs. 2C, 3B; table 1), meaning that different combinations of stimulus duration and intensity will result in unique patterns of population-level responses (Fig. 8).

Two Codes for Stimulus Duration, One Circuit

Together, these observations suggest two distinct mechanisms for the peripheral coding of stimulus duration (Fig. 8). At relatively high stimulus intensities (i.e. >1 nA; see Fig. 2C), all KOs are above threshold across the behaviorally-relevant range of

durations, so a temporal code based on spike latency differences would allow for reliable coding of stimulus duration. However, at near-threshold intensities (i.e. 0.1-1 nA; see Fig. 2C) for which a temporal code is less effective, increasing stimulus duration leads to the recruitment of an increasing number of KOs, suggesting a population code for stimulus duration. Although it is unclear how a given amount of current injected directly into a receptor organ corresponds to the amount of current that would result from a natural electric field, the two will scale linearly. Thus, our results make it clear that there is a 10-fold range of stimulus intensities just above threshold over which stimulus duration is represented by both the number and identity of responding KOs (Fig. 2C).

Based on anatomical evidence, Friedman and Hopkins (1998) proposed a delay-line anti-coincidence detection model for the recoding of peripheral spike latency differences. According to this model, small cells in ELa receive delayed excitation from one receptive field, and inhibition from local interneurons (Mugnaini and Maler, 1987; George et al., 2011) corresponding to a different receptive field. As a result, small cells only respond when a stimulus is long enough such that onset-triggered delayed excitation arrives before offset-triggered inhibition, resulting in long-pass tuning to stimulus duration. Differences in excitatory delay would establish variation in the minimum stimulus duration needed to elicit a response across the population of small cells. As a result, increases in stimulus duration would increase small cell recruitment, thereby recoding the peripheral temporal code into a population code for duration (Xu-Friedman and Hopkins, 1999).

By identifying a potential mechanism for converting a temporal code into a population code, the Friedman-Hopkins model reveals how the peripheral code for stimulus duration at high stimulus intensities can be converted into the same type of code we found to operate at low intensities, potentially establishing a single common population code among small cells for all intensities. Evoked potentials in both ELa and ELp scale with stimulus duration across a wide range of intensities (Fig. S1), consistent with a small cell population code for stimulus duration. However, multiple different intensity/duration combinations elicit the same evoked potential response (Fig. S1). As evoked potentials reflect the summed activity of populations of neurons, this overlap indicates that a population code based simply on the number of active small cells would not unambiguously code for stimulus duration. As with the population coding of stimulus duration by KO receptors, we propose that stimulus duration may be represented by unique spatial patterns of responsive small cells. This type of population-coding scheme could also allow for the coding of other behaviorally-relevant attributes of EODs, such as intensity, orientation, and polarity. Neurons in ELp exhibit tuning to all of these stimulus attributes (Amagai, 1998), as well as to the interpulse intervals between EODs (Carlson, 2009), so this information is clearly encoded in the output of small cells.

If a population code can be used to obtain information about stimulus duration, then why would there also be a temporal code, which is associated with anatomical features that are presumably energetically expensive such as large cells, thick axons, and heavy myelination (Carr and Friedman, 1999)? It is likely that a “start-stop” peripheral code provides for greater temporal precision, whereas a peripheral population code would

still provide some information about duration at low intensities that do not allow for this level of precision. Further, a key aspect of a temporal code for stimulus duration is that it greatly extends the dynamic range of the system. A population code for duration is intensity-dependent: above a certain intensity, the system will saturate (all receptors will respond to all durations) and information about stimulus duration cannot be encoded into changes in the population of responding receptors. By contrast, a "start-stop" temporal code never saturates (Bennett, 1965; Hopkins and Bass, 1981).

Differences in Passive and Active Membrane Properties May Explain Peripheral Variation

Previous studies have shown that KOs are band-pass tuned to frequencies close to the peak power frequencies of conspecific EODs (Arnegard et al., 2006; Bass and Hopkins, 1984; Hopkins, 1981). We confirmed this (Fig. 1C), finding variation in the range of best frequencies and bandwidths both between and within fish (Fig. 3B; Table 1). Variability in frequency tuning among the population of receptors is indicative of physiological differences that should also affect duration tuning. Indeed, we found that the duration- and frequency-tuning characteristics of KOs were correlated in the same way as simple models in which we systematically varied membrane and series capacitances and resistances (Fig. 3). Thus, differences in capacitance or resistance between units could account for the observed covariation in frequency- and duration-tuning. Ampullary receptors could potentially contribute to behavioral responses because they respond to the D.C. components of monophasic square pulses (Bennett, 1965; Zakon,

1986). However, biphasic pulses do not have a D.C. component, and behavioral responses to monophasic and biphasic square pulses were similar (Fig. 6). Further, ELa and ELp do not receive input from the ampullary system (Bell and Szabo, 1986), and the responses of these nuclei were consistent with the behavioral results (Figs. 5, 6).

Variation in capacitive or resistive properties could result from differences in electroreceptor organ morphology (Zakon, 1986). KOs are tuberous electroreceptors composed of a canal leading to a sensory chamber typically containing 1-10 sensory cells, each 40-50 μm in diameter (Bennett, 1965; Szabo, 1965; Harder, 1968b; Zakon, 1986). The canal is lined by a wall composed of numerous layers of flattened epithelial cells and it is filled with a plug of loosely packed epithelial cells (Szabo, 1965). The epithelial plug, which is not present in low-frequency ampullary electroreceptors, establishes a series capacitance (Fig. 3A, inset) that acts as a high-pass filter of current through the organ (Zakon, 1986). Differences in the number of cells within the epithelial plug or in their morphology could establish variation in series capacitance. The canal walls of tuberous electroreceptors may also contribute to the series capacitance of receptors (Zakon, 1986). Tuberous receptors in gymnotiforms have more layers of flattened epithelial cells in the canal wall than ampullary receptors, suggesting that differences in tuning between the two receptor types relates to differences in the capacitive contribution of the canal wall (Bennett, 1971). Indeed, the maximum number of layers within the capsular wall of tuberous organs varies from 10 to 60 across 9 different species of gymnotiform fishes, and this variation correlates with receptor frequency tuning (Lissmann and Mullinger, 1968; Zakon, 1986). There is even extensive variation in

tuberous organ morphology within species: among tuberous receptors of the gymnotiform *Hypopomus*, the number of layers of flattened epithelial cells varies from 10 to 50, causing the wall thickness to vary from 2 to 5 μm (Szamier and Wachtel, 1970). In mormyrids, Harder (1968b) reported that the thickness of the electroreceptor epidermis varies throughout the body. The sensory cells themselves could also serve as a source of variation in capacitance. The apical surface of the receptor cells is thought to contribute to series capacitance whereas the basal surface is thought to affect membrane excitability as a 'typical' parallel capacitance (Bennett, 1965; Bennett, 1971). The diameter of individual sensory cells within a KO only varies from 40 to 50 μm, but these cells are covered with branching microvilli that increase the surface area of each cell approximately 40-fold (Derbin and Szabo, 1968). Similarly, variation in the number of sensory cells per KO could also impact the capacitive properties of the receptor organ. The number of sensory cells per KO does indeed vary among the KOs within a single fish (Harder, 1968a). Like capacitance, resistance will be impacted by morphological features such as skin thickness, pore diameter and epithelial wall thickness.

Finally, studies of the axon initial segment have demonstrated that properties of voltage-gated ion channels such as location, distribution, and inactivation kinetics play a pivotal role in the shape and timing of a spiking response, which contributes to electrical frequency tuning (Clark et al., 2009). This basic mechanism can also play a role in peripheral sensory tuning. For example, the amplitude of the current through mechanotransducer channels and the speed of adaptation covary with the best frequency of hair cells in the turtle cochlea, suggesting a role for variation in ion channel properties

in generating frequency tuning (Ricci et al., 2003). Thus, there are multiple morphological and physiological features that could establish differences in sensory filtering across KOs, and thereby explain the observed covariation in frequency and duration tuning.

Implications for Behavior

Pulse-type mormyrid electric fish use EODs for species recognition and mate choice (Arnegard et al., 2006; Feulner et al., 2009; Hopkins and Bass, 1981; Machnik and Kramer, 2008). In *B. brachyistius*, males have longer EODs than females, and EOD duration correlates with relative dominance status among males (Carlson et al., 2000). Thus, long-pass filtering in the KO electrosensory system establishes a basic mechanism for distinguishing behaviorally-relevant variation in conspecific EOD duration. However, there is extensive overlap in EOD duration among sympatric species (Arnegard et al., 2010; Carlson et al., 2011; Hopkins, 1981), suggesting the need to precisely distinguish small differences in duration. Further, EODs are individually-distinctive (Friedman and Hopkins, 1996), and there is evidence that some species of mormyrids can use this information to discriminate between individuals (Graff and Kramer, 1992). Behavioral positioning during aggressive interactions maximizes the signal intensity experienced by receivers (Arnegard et al., 2006), possibly to maximize the discrimination of small temporal differences between waveforms. Precise temporal coding provides a robust mechanism for distinguishing slight variation in stimulus duration during overt

behavioral interactions, whereas population coding provides a rough measure of stimulus duration at low intensities, when signaling fish are at a distance.

We tested natural EOD waveforms from 10 species as well as conspecific EOD waveforms subjected to temporal manipulations, and determined that the long-pass tuning we observed had clear effects on the detection of these behaviorally-relevant stimuli (Fig. 7). Interestingly, for all measures tested, fish were more sensitive to heterospecific EODs of longer duration than conspecific EODs. This does not imply that the fish prefer heterospecific EODs that are longer in duration than conspecific EODs, only that they are more detectable at a given intensity. Our behavioral experiments provided a measure of signal detection, not preference, such as would be important in mate choice or intraspecific competition. Indeed, previous work has revealed clear behavioral preferences for conspecific EODs in several species (Arnegard et al., 2006; Feulner et al., 2009; Hopkins and Bass, 1981; Machnik and Kramer, 2008). Further, the early stages in the sensory pathway that we recorded from likely have less selectivity for specific waveforms compared to higher sensory regions. Thus, increases in either EOD amplitude or duration can increase the effective range of electric communication, but not necessarily increase signal preference in specific behavioral contexts. Further, we found that threshold energy increased with increasing stimulus duration, likely due to the AC-coupling of KOs. This suggests that greater energy is required to produce an equally detectable pulse of longer duration, which may place a limit on evolutionary increases in EOD duration. Thus, it will be interesting to determine how species diversity in EOD duration relates to diversity in EOD amplitude and energy, which will require carefully

calibrated measurements in the field. It is possible that the evolution of increased EOD duration is compensated for by decreasing EOD amplitude. Alternatively, variation in EOD duration may relate to diversity in the rates of EOD production, or to species differences in population density that place different selective pressures on signal range. It will also be interesting to relate variation in EOD duration, amplitude, and energy to differences in KO physiology across species. The frequency tuning of KOs varies across species (Bass & Hopkins, 1984; Hopkins, 1981), suggesting that duration tuning will likely vary as well.

Relevance to Other Sensory Systems

The use of multiple coding strategies is common in sensory systems (Lawhern et al., 2011). However, these distinct computations are often implemented in parallel sensory pathways that are specialized to extract information about different stimulus features (Carlson and Kawasaki, 2006; Nishino and Ohmori, 2009; Livingstone and Hubel, 1988; Sullivan and Konishi, 1984; Young, 1998). We demonstrate two distinct coding mechanisms in the sensory periphery operating at different ranges of intensities. Our findings are novel in revealing that both codes operate within the same circuit to extract information about the same stimulus feature, but work most effectively at different ranges of intensity. A combination of distinct coding schemes operating at different intensities may be used in other sensory systems as well.

We further demonstrate significant variability in peripheral tuning. Neural heterogeneity can increase the amount of information encoded in the activity of a

population of central sensory neurons (Chelaru and Dragoi, 2008; Marsat and Maler, 2010). On the other hand, redundancy, which exists at multiple stages of neural processing, can increase prediction accuracy and decrease ambiguity (Barlow, 1972; Barlow, 2001). Our results reveal that heterogeneity among peripheral sensory receptors allows for information processing through population coding. Heterogeneity in the frequency tuning of peripheral receptors may also be important for other temporal codes, such as the detection of interaural time differences (ITD) in sound localization (Carr and Friedman, 1999). Indeed, monoaural inputs to ITD detector neurons in barn owls vary in their spectrotemporal filtering properties, and this filtering has strong effects on ITD tuning (Fischer et al., 2011). Thus, the effects of spectrotemporal filtering at the periphery should be considered for a wide range of temporal codes.

Finally, our results reveal a basic mechanism by which sensory systems can determine stimulus duration even at low intensities, when the temporal precision of peripheral responses is severely degraded. Duration tuning in auditory systems is important for functions as varied as echolocation, acoustic communication, conspecific recognition, and appreciation of music (Covey and Casseday, 1999). Duration tuned neurons have been identified in the central auditory systems of echolocating bats as well as nonecholocating animals including frogs, rats, mice, guinea pigs, chinchillas, and cats (Sayegh et al., 2011). In mouse auditory midbrain, duration tuning is strongly dependent on other stimulus features, including intensity (Brand et al., 2000). We have demonstrated an intensity-dependent change in the peripheral code for duration. When

analyzing central mechanisms for temporal processing, the diversity of peripheral responses and the importance of stimulus intensity should therefore be considered.

ACKNOWLEDGMENTS

We thank Arielle Grossman and Chelsea Casareale for help with behavior experiments and knollenorgan recordings, respectively. We thank Dan Moran and Baranidharan Raman for help with modeling. We thank Jim Huettner for input on earlier versions of the manuscript. This research was supported by the National Science Foundation [IOS-0818390]; the National Institute on Deafness and Other Communication Disorders [F30-DC011197]; and the German Academic Exchange Service.

REFERENCES

Amagai, S. (1998). Time coding in the midbrain of mormyrid electric fish. II. Stimulus selectivity in the nucleus exterolateralis pars posterior. J Comp Physiol A Neuroethol Sens Neural Behav Physiol. **182**, 131-143.

Amagai, S., Friedman, M. A. and Hopkins, C. D. (1998). Time coding in the midbrain of mormyrid electric fish. I. Physiology and anatomy of cells in the nucleus exterolateralis pars anterior. J Comp Physiol A Neuroethol Sens Neural Behav Physiol.**182**, 115-130.

Arnegard, M. E., Bogdanowicz, S. M. and Hopkins, C. D. (2005). Multiple cases of striking genetic similarity between alternate electric fish signal morphs in sympatry. Evolution. **59**, 324-343.

Arnegard, M. E. and Hopkins, C. D. (2003). Electric signal variation among seven blunt-snouted *Brienomyrus* species (Teleostei: Mormyridae) from a riverine species flock in Gabon, Central Africa. Environ. Biol. Fishes. **67**, 321-339.

Arnegard, M. E., Jackson, B. S. and Hopkins, C. D. (2006). Time-domain signal divergence and discrimination without receptor modification in sympatric morphs of electric fishes. J Exp Biol. **209**, 2182-2198.

Arnegard, M. E., McIntyre, P. B., Harmon, L. J., Zelditch, M. L., Crampton, W. G., Davis, J. K., Sullivan, J. P., Lavoué, S. and Hopkins, C. D. (2010). Sexual signal evolution outpaces ecological divergence during electric fish species radiation. Am Nat. **176**, 335-356.

Aubie, B., Becker, S. and Faure, P. A. (2009). Computational models of millisecond level duration tuning in neural circuits. J Neurosci. **29**, 9255-9270.

Barlow, H. B. (1972). Single units and sensation: a neuron doctrine for perceptual psychology? Perception **1**, 371-394.

Barlow, H. B. (2001). Redundancy reduction revisited. Network: Comput. Neural Syst. **12**, 241-253.

Bass, A. H. and Hopkins, C. D. (1984). Shifts in frequency tuning of electroreceptors in androgen-treated mormyrid fish. J Comp Physiol A Neuroethol Sens Neural Behav Physiol.**155**, 713-724.

Bell, C. C. (1990). Mormyromast electroreceptor organs and their afferent fibers in mormyrid fish. III. Physiological differences between two morphological types of fibers. J Neurophysiol. **63**, 319-332.

Bell, C. C. and Grant, K. (1989). Corollary discharge inhibition and preservation of temporal information in a sensory nucleus of mormyrid electric fish. J Neurosci. **9**, 1029-1044.

Bell, C. C. and Szabo, T. (1986). Electroreception in mormyrid fish: Central anatomy. In Electroreception, eds. T. H. Bullock and W. Heiligenberg, pp. 375-421. New York: John Wiley & Sons.

Bennett, M. V. L. (1965). Electroreceptors in mormyrids. Cold Spring Harb Symp Quant Biol. **30**, 245-262.

Bennett, M. V. L. (1971). Electroreception. In Fish Physiology, vol. 5 eds. W. S. Hoar and D. J. Randall, pp. 493-568. New York and London: Academic Press.

Brand, A., Urban, R., and Grothe, B. (2000). Duration tuning in the mouse auditory midbrain. J Neurophysiol. **84**, 1790-1799.

Carlson, B. A. (2002). Electric signaling behavior and the mechanisms of electric organ discharge production in mormyrid fish. J Physiol Paris **96**, 405-419.

Carlson, B. A. (2006). A neuroethology of electrocommunication: senders, receivers, and everything in between. In Communication in Fishes, vol. 2 eds. F. Ladich S. P. Collin P. Moller and B. G. Kapoor, pp. 805-848. Enfield, NH: Science Publishers.

Carlson, B. A. (2009). Temporal-pattern recognition by single neurons in a sensory pathway devoted to social communication behavior. J Neurosci. **29**, 9417-9428.

Carlson, B. A., Hasan, S. M., Hollmann, M., Miller, D. B., Harmon, L. J. and Arnegard, M. E. (2011). Brain evolution triggers increased diversification of electric fishes. Science **332**, 583-586.

Carlson, B. A. and Hopkins, C. D. (2004). Stereotyped temporal patterns in electrical communication. Animal Behaviour **68**, 867-878.

Carlson, B. A., Hopkins, C. D. and Thomas, P. (2000). Androgen correlates of socially induced changes in the electric organ discharge waveform of a mormyrid fish. Horm Behav. **38**, 177-186.

Carlson, B. A. and Kawasaki, M. (2006). Ambiguous encoding of stimuli by primary sensory afferents causes a lack of independence in the perception of multiple stimulus attributes. J Neurosci. **26**, 9173-9183.

Carlson, B. A. and Kawasaki, M. (2007). Behavioral responses to jamming and 'phantom' jamming stimuli in the weakly electric fish *Eigenmannia*. J Comp Physiol A Neuroethol Sens Neural Behav Physiol.**193**, 927-941.

Carr, C. E. and Friedman, M. A. (1999). Evolution of time coding systems. Neural Comput. **11**, 1-20.

Chelaru, M. I. and Dragoi, V. (2008). Efficient coding in heterogeneous neuronal populations. Proc Natl Acad Sci USA **105**, 16344-16349.

Clark, B.D., Goldberg, E.M., and Rudy, B. (2009). Electrogenic tuning of the axon initial segment. Neuroscientist. **15**, 651-668.

Covey, E. and Casseday, J.H. (1999). Timing in the auditory system of the bat. Annu Rev Physiol. **61**, 457-476.

Derbin, C. and Szabo, T. (1968). Ultrastructure of an electroreceptor (Knollenorgan) in the morymrid fish Gnathonemus petersii. I. J Ultrastruct Res **22**, 469-484.

Edwards, C. J., Leary, C. J. and Rose, G. J. (2007). Counting on inhibition and rate-dependent excitation in the auditory system. J Neurosci. **27**, 13384-13392.

Edwards, C. J., Leary, C. J. and Rose, G. J. (2008). Mechanisms of long-interval selectivity in midbrain auditory neurons: Roles of excitation, inhibition, and plasticity. J Neurophysiol. **100**, 3407-3416.

Feulner, P. G., Plath, M., Engelmann, J., Kirschbaum, F. and Tiedemann, R. (2009). Electrifying love: Electric fish use species-specific discharge for mate recognition. Biol Lett. **5**, 225-228.

Fischer, B.J., Steinberg, L.J., Fontaine, B., Brette, R., and Peña, J.L. (2011). Effect of instantaneous frequency glides on interaural time difference processing by auditory coincidence detectors. PNAS **108**, 18138-18143.

Fortune, E. S., Rose, G. J. and Kawasaki, M. (2006). Encoding and processing biologically relevant temporal information in electrosensory systems. J Comp Physiol A Neuroethol Sens Neural Behav Physiol. **192**, 625-635.

Friedman, M. A. and Hopkins, C. D. (1996). Tracking individual mormyrid electric fish in the field using electric organ discharge waveforms. Animal Behaviour **51**, 391-407.

Friedman, M. A. and Hopkins, C. D. (1998). Neural substrates for species recognition in the time-coding electrosensory pathway of mormyrid electric fish. J Neurosci. **18**, 1171-1185.

Gabbiani, F. and Koch, C. (1998). Principles of spike train analysis. In Methods in Neuronal Modeling: From Ions to Networks eds. C. Koch and I. Segev, pp. 313-360. Cambridge, MA: MIT Press.

George, A. A., Lyons-Warren, A. M., Ma, X. and Carlson, B. A. (2011). A diversity of synaptic filters are created by temporal summation of excitation and inhibition. *J* Neurosci. **31**, 14721-14734.

Graff, C. and Kramer, B. (1992). Trained weakly-electric fishes, *Pollimyrus isidori* and *Gnathonemus petersii* (Mormyridae, Teleostei) discriminate between waveforms of electric pulse discharges. Ethology **90**, 279-292.

Harder, W. (1968a). Die beziehungen zwischen elektrorezeptoren, elektrischem organ, seitenlinienorganen und nervensystem bei den Mormyridae (Teleostei, pisces). Zeitschrift für vergleichende Physiologie **59**, 272-318.

Harder, W. (1968b). Zum aufbau der epidermalen sinnesorgane der Mormyridae (Mormyriformes, Teleostei). Zeitschrift für Zellforschung **89**, 212-224.

Hopkins, C. D. (1976). Stimulus filtering and electroreception: Tuberous electroreceptors in three species of Gymnotoid fish. J Comp Physiol A Neuroethol Sens Neural Behav Physiol. **111**, 171-207.

Hopkins, C. D. (1981). On the diversity of electric signals in a community of mormyrid electric fish in West Africa. Amer. Zool. **21**, 211-222.

Hopkins, C. D. and Bass, A. H. (1981). Temporal coding of species recognition signals in an electric fish. Science **212**, 85-87.

Köppl, C. (2009). Evolution of sound localisation in land vertebrates. Curr. Biol. **19**, R635-R639.

Lawhern, V., Nikonov, A.A., Wu, W., and Contreras, R.J. (2011). Spike rate and spike timing contributions to coding taste quality information in rat periphery. Front. Integr. Neurosci. **5**, 1-14.

Lissmann, H.W. and Mullinger, A.M. (1968). Organization of ampullary electric receptors in Gymnotidae (Pisces). Proc R Soc Lond B Biol Sci. **169**, 345-378.

Livingstone, M. and Hubel, D**.** (1988). Segregation of form, color, movement, and depth: anatomy, physiology, and perception. Science **240**, 740-749.

Machnik, P. and Kramer, B**.** (2008). Female choice by electric pulse duration: attractiveness of the males' communication signal assessed by female bulldog fish, Marcusenius pongolensis (Mormyridae, Teleostei). J Exp Biol. **211**, 1969-1977.

Marsat, G. and Maler, L. (2010). Neural heterogeneity and efficient population codes for communication signals. J Neurophysiol. **104**, 2543-2555.

Moller, P. and Bauer, R. (1973). 'Communication' in weakly electric fish, *Gnathonemus Petersii* (Mormyridae) II. Interaction of electric organ discharge activities of two fish. Anim. Behav. **21,** 501-512.

Moller, P., Serrier, J., and Bowling, D. (1989). Electric organ discharge displays during social encounter in the weakly electric fish *Brienomyrus niger* L. (Mormyridae). Ethology. **82**, 177-191.

Mugnaini, E. and Maler, L. (1987). Cytology and immunocytochemistry of the nucleus extrolateralis anterior of the mormyrid brain: possible role of GABAergic synapses in temporal analysis. Anat Embryol (Berl). **176**, 313-36.

Neumann, E. and Nachmansohn, D. (1975). Nerve excitability--toward an integrating concept. In Biomembranes, vol. 7 eds. H. Eisenberg E. Katchalski-Katzir and L. A. Manson, pp. 99-166. New York: Plenum Press.

Nishino, E. and Ohmori, H. (2009). The modulation by intensity of the processing of interaural timing cues for localizing sounds. Mol Neurobiol **40**, 157-165.

Nishino, E., Yamada, R., Kuba, H., Hioki, H., Furuta, T., Kaneko, T., and Ohmori, H. (2008). Sound-intensity-dependent compensation for the small interaural time difference cue for sound source localization. J Neurosci. **28**, 7153-7164.

Paintner, S. and Kramer, B. (2003). Electrosensory basis for individual recognition in a weakly electric, mormyrid fish, *Pollimyrus adspersus* (Günther, 1866). Behav. Ecol. Sociobiol. **55**, 197-208.

Peña, J. L. and Konishi, M. (2000). Cellular mechanisms for resolving phase ambiguity in the owl's inferior colliculus. Proc Natl Acad Sci USA **97**, 11787-11792.

Post, N. and von der Emde, G. (1999). The "novelty response" in an electric fish: response properties and habituation. Physiol Behav. **68**, 115-128.

Ricci, A. J., Crawford, A. C. and Fettiplace, R. (2003). Tonotopic variation in the conductance of the hair cell mechanotransducer channel. Neuron **40**, 983-990.

Rose, G. J. (2004). Insights into neural mechanisms and evolution of behaviour from electric fish. Nat Rev Neurosci. **5**, 943-951.

Sawtell, N. B., Williams, A. and Bell, C. C. (2005). From sparks to spikes: information processing in the electrosensory systems of fish. Curr Opin Neurobiol. **15**, 437-443.

Sayegh, R., Aubie, B. and Faure, P.A. (2011). Duration tuning in the auditory midbrain of echolocating and non-echolocating vertebrates. J Comp Physiol A. **197**, 571-583.

Sullivan, W. E. and Konishi, M. (1984). Segregation of stimulus phase and intensity coding in the cochlear nucleus of the barn owl. J Neurosci **4**, 1787-1799.

Sullivan, J. P., Lavoué, S. and Hopkins, C. D. (2002). Discovery and phylogenetic analysis of a riverine species flock of African electric fishes (Mormyridae: Teleostei). Evolution. **56**, 597-616.

Szabo, T. (1965). Sense organs of the lateral line system in some electric fish of the Gymnotidae, Mormyridae and Gymnarchidae. J Morphol **117**, 229-249.

Szabo, T., Ravaille, M., Libouban, S. and Enger, P. S. (1983). The mormyrid rhombencephalon: I. Light and EM investigations on the structure and connections of the lateral line lobe nucleus with HRP labeling. Brain Res. **266**, 1-19.

Szamier, R.B. and Wachtel, A.W. (1970). Special cutaneous receptor organs of fish. VI. Ampullary and tuberous organs of *Hypopomus*. J Ultrastruct Res. **30,** 450-471.

Szücs, A. (1998). Applications of the spike density function in analysis of neuronal firing patterns. J Neurosci Methods **81**, 159-67.

von der Emde, G. (1999). Active electrolocation of objects in weakly electric fish. J Exp Biol. **202**, 1205-1215.

Xu-Friedman, M. A. and Hopkins, C. D. (1999). Central mechanisms of temporal analysis in the knollenorgan pathway of mormyrid electric fish. J Exp Biol. **202**, 1311-1318.

Young, E. D. (1998). Parallel processing in the nervous system: Evidence from sensory maps. Proc Natl Acad Sci USA **95**, 933-934.

Zakon, H. H. (1986). The electroreceptive periphery. In Electroreception, eds. T. H. Bullock and W. Heiligenberg, pp. 103-156. New York: John Wiley & Sons.

Zakon, H. H. (2003). Insight into the mechanisms of neuronal processing from electric fish. Curr Opin Neurobiol. **13**, 744-750.

Chapter 3

Retrograde fluorescent labeling allows for targeted extracellular single-unit recording from identified neurons *in vivo*

A great deal of the difficulty in physiological research is due to the microscopic size of the living cell.

-E.D. Adrian, 1928

This chapter contains a previously published manuscript:

A.M. Lyons-Warren, T. Kohashi, S. Mennerick, B.A. Carlson (2013). Retrograde Fluorescent Labeling Allows for Targeted Extracellular Single-unit Recording from Identified Neurons in vivo. *J. Vis. Exp*. 26:76.

Author contributions for the above citation:

A.L-W developed the initial idea for the procedure and performed the experiments. T.K. designed the recording chamber and assisted with technical aspects. The manuscript was written by A.L-W with input from all other authors.

ABSTRACT

Retrograde transport of fluorescent dye labels a sub-population of neurons based on anatomical projection. Labeled axons can be visually targeted *in vivo*, permitting extracellular recording from identified axons. This technique facilitates recording when neurons cannot be labeled through genetic manipulation or are difficult to isolate using 'blind' *in vivo* approaches.

INTRODUCTION

The overall goal of this method is to record single-unit responses from an identified population of neurons. *In vivo* electrophysiological recordings from individual neurons are critical for understanding how neural circuits function under natural conditions. Traditionally, these recordings have been performed 'blind', meaning the identity of the recorded cell is unknown at the start of the recording. Cellular identity can be subsequently determined via intracellular[1], juxtacellular[2] or loose-patch[3] iontophoresis of dye, but these recordings cannot be pre-targeted to specific neurons in regions with functionally heterogeneous cell types. Fluorescent proteins can be expressed in a cell-type specific manner permitting visually-guided single-cell electrophysiology[4-6]. However, there are many model systems for which these genetic tools are not available. Even in genetically accessible model systems, the desired promoter may be unknown or genetically homogenous neurons may have varying projection patterns. Similarly, viral vectors have been used to label specific subgroups of projection neurons[7], but use of this method is limited by toxicity and lack of trans-synaptic specificity. Thus, additional techniques that offer specific pre-visualization to record from identified single neurons *in vivo* are needed. Pre-visualization of the target neuron is particularly useful for challenging recording conditions, for which classical single-cell recordings are often prohibitively difficult[8-11]. The novel technique described in this paper uses retrograde transport of a fluorescent dye applied using tungsten needles to rapidly and selectively label a specific subset of cells within a particular brain region based on their unique

axonal projections, thereby providing a visual cue to obtain targeted electrophysiological recordings from identified neurons in an intact circuit within a vertebrate CNS.

The most significant novel advancement of our method is the use of fluorescent labeling to target specific cell types in a non-genetically accessible model system. Weakly electric fish are an excellent model system for studying neural circuits in awake, behaving animals[12]. We utilized this technique to study sensory processing by 'small cells' in the anterior exterolateral nucleus (ELa) of weakly electric mormyrid fish. 'Small cells' are hypothesized to be time comparator neurons important for detecting submillisecond differences in the arrival times of presynaptic spikes[13]. However, anatomical features such as dense myelin, engulfing synapses, and small cell bodies have made it extremely difficult to record from these cells using traditional methods[11, 14]. Here we demonstrate that our novel method selectively labels these cells in 28% of preparations, allowing for reliable, robust recordings and characterization of responses to electrosensory stimulation.

PROTOCOL TEXT

1) Prepare Dye-Coated Needles

1.1) Sharpen a 160 μm diameter tungsten wire electrolytically[15]. Final needle tip diameters should range from 5-50 μm. The number of needles needed depends on the size of the region being labeled. We prepared 5 needles for 4 injections into ELp.

1.2) The night before the experiment, place a drop (<0.25 μL) of 2 mM dextran-conjugated Alexa Fluor 10,000 MW dye onto the distal 100 μm of each needle.

1.3) Allow the needles to air dry at room temperature, leaving concentrated dye at the tip. Store the needles at 4°C in a dark container to protect them from light.

2) Prepare Animal for Surgery

2.1) Induce general anesthesia by placing the fish in a solution of 300 mg/l MS-222 in tank water.

2.2) Weigh the fish and measure fork length (tip of snout to fork of caudal fin) and body depth (maximal dorso-ventral distance in the transverse plane). These measurements should fall within the ranges indicated in Table 1 so that the fish fits inside a recording chamber small enough to place under a water-immersion microscope objective (Fig. 1).

2.3) Immobilize and electrically silence the fish by injecting 100μL of 3 mg/ml flaxedil into the dorsal body musculature.

2.4) Fill the recording chamber (Fig. 1A) with tank water. Place the fish ventral-side down on the platform in the center of the chamber (Fig. 1). Deliver an aerated solution of

Table 1: Optimal weight, length and body depth ranges for fish.

	Mass (g)	Fork Length (cm)	Body Depth (cm)
Mean	2.42	6.20	1.14
Standard Deviation	0.64	0.52	0.18
Range	1.2-4.0	5.5-8.4	0.9-1.6

Table 1: Optimal weight, fork length (tip of snout to fork of caudal fin) and body depth (maximal dorso-ventral distance in the transverse plane) ranges allowing fish to fit in the recording chamber illustrated in Figure 1. Fish that are too small may be less likely to survive the surgery and will have a small ELp, making dye placement challenging. Fish that are too large will have a large, over-reaching cerebellum that will reduce access to ELa and ELp and may prevent lowering of the high power, water-immersion objective close enough to focus on ELa and ELp.

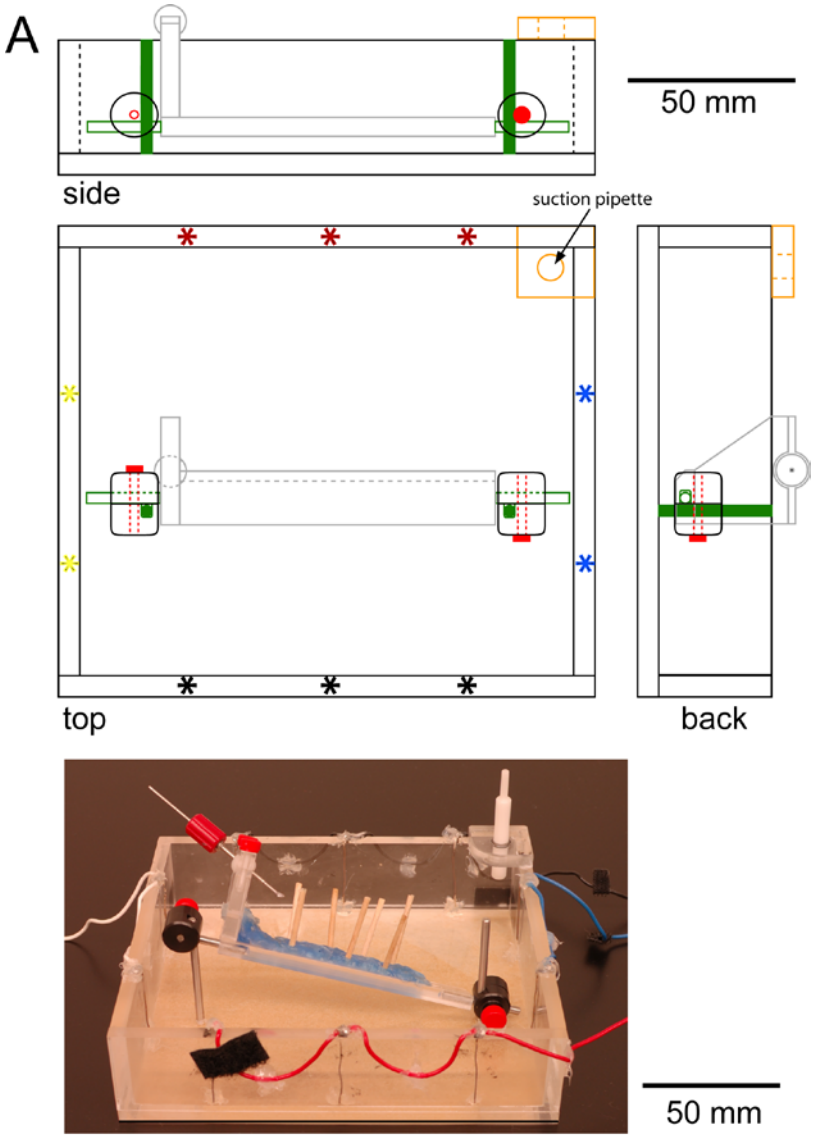
A
50 mm
side
suction pipette
top
back
50 mm
B
C
assembled
screw cap
disc 1
disc 2
screw
stainless steel head post
front
side
respiration tubing and pipette tip
50 mm

FIG 1: Specifications for a recording chamber that can fit underneath the objective of a fixed-stage epiflourescent microscope. (A) To-scale square recording chamber made from plexiglass showing top, side and back views. Paired sets of stimulating electrodes (asterisks) at the periphery allow for either transverse (red-black) or longitudinal (blue-yellow) stimulation. An additional piece of plexiglass in the corner, with a rubber-lined hole in the center (orange), holds a suction pipette that maintains a constant water level. Two vertical stainless steel posts screwed into the bottom of the chamber (solid green) connect to stainless steel posts (green outline) attached to the platform supporting the fish (light grey, detailed in C) via adjustable disc clamps. A photograph of the chamber is shown below the to-scale drawing. (B) Individual and assembled views of the circular plastic disc clamps used to secure the platform to the vertical posts. Each disc clamp has a groove (green) for a post and a center hole for the tightening screw. Disc clamps are rotated so the grooves are perpendicular to each other. Tightening the screw (red) clamps the posts in place to prevent further vertical and rotational movement of the platform. (C) Front and side to-scale views of the plexiglass platform used to hold the fish in place. The platform is coated with a layer of paraffin wax (blue) that holds wooden dowels (black bars) in place to support the fish. Tubing for respirating the fish passes through a hole in the 'headboard' of the platform and ends in a pipette tip placed in the fish's mouth. A stainless steel head post (gray bar) connects to the platform via a ball joint allowing 360 degree rotation. Stainless steel horizontal posts (green) are screwed into either end of the platform.

100 mg/l MS-222 using a pipette tip placed in the fish's mouth (1-2 ml/min). Stabilize the fish with rods fixed in wax placed on both sides of the body (Fig. 1C). Monitor the fish's health by checking for continuous blood flow in the ocular vessels and a normal body color.

2.5) Rotate the platform along its long axis and lower the back end of the platform so that one side of the dorsal surface of the fish's head is exposed above the water while the rest of the fish's body remains submerged. A small piece of Kimwipe should be placed on any non-submerged portion of the skin to prevent drying.

3) Surgery (Figure 2)

The basic surgical procedure described here is well established and reliably used for blind *in vivo* recordings in mormyrids[16]. For other applications, expose the desired regions for labeling and recording. The region containing axon terminals of the cells of interest must be reachable by a sharp needle. The region containing more proximal segments of those same axons must have sufficient space above the tissue to accommodate the working distance of the water-immersion lens (2 mm in our case).

3.1) Apply a 0.4% solution of lidocaine to the exposed surface of the head using a Q-tip.

3.2) Using a scalpel blade, cut the perimeter of a rectangular piece of skin. Remove the rectangle using a pair of forceps. The size of the rectangle will scale with fish size, but should be approximately 3mm X 5mm for a 6.2 cm fish (Fig. 2A). The lateral edge of the rectangle should align with the center of the eye, the anterior edge of the rectangle

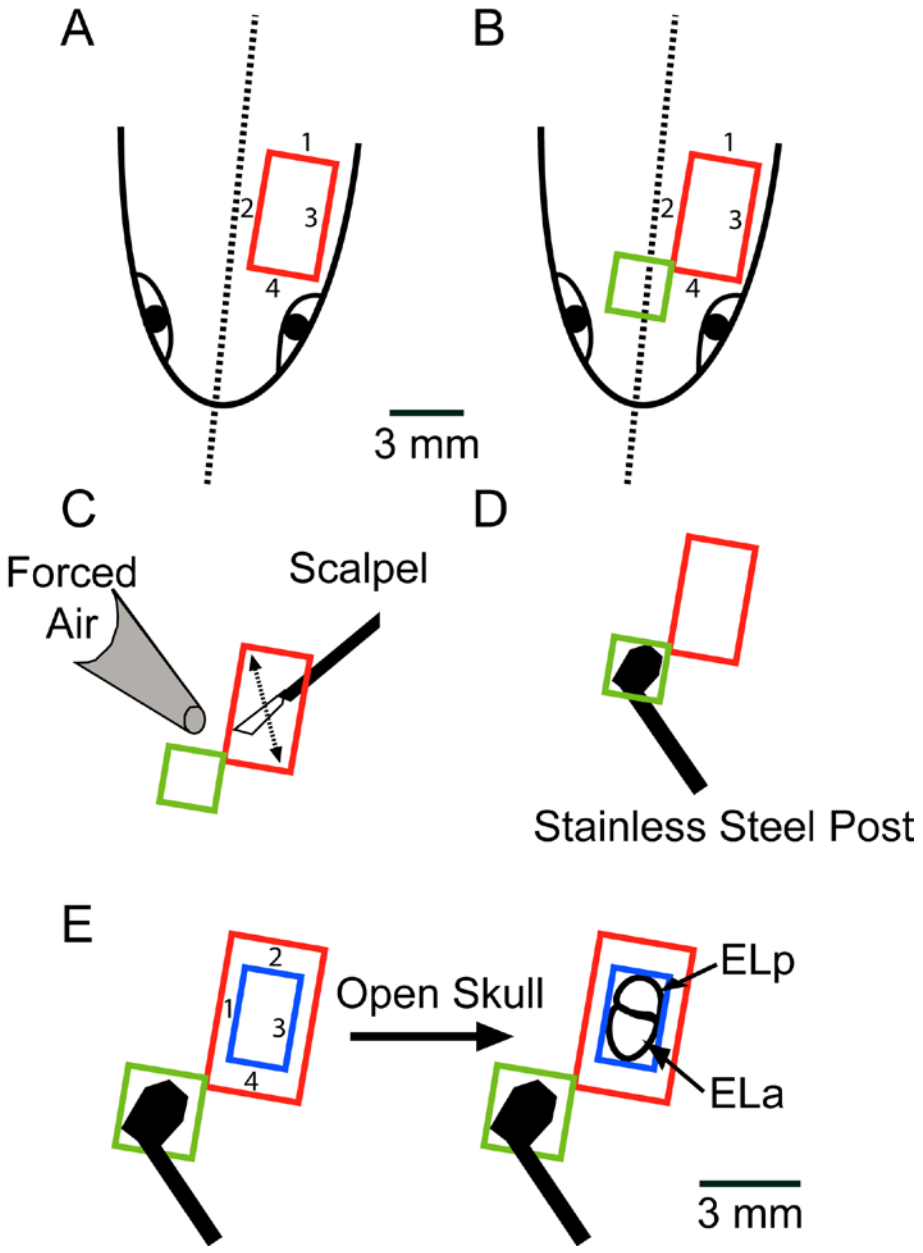

FIG 2: Schematic overview of surgery looking down at the dorsal surface of the head. (A) Make four cuts, in the order indicated, to remove a rectangular piece of skin (red). (B) Extend the opening anteromedially to remove an additional rectangular piece of skin (green). (C) Scrape off any remaining fat or ligaments by moving the scalpel blade as indicated by the arrow and dry the surface completely with Kimwipes and forced air. (D) Glue a stainless steel post to the skull using Super Glue. Scale bar in A applies to A-D. (E) Use a dental drill to make four cuts, in the order indicated, to remove a rectangular piece of bone (blue), exposing the anterior and posterior exterolateral nuclei (ELa and ELp, respectively).

should be just posterior to the eye, and the medial edge of the rectangle should be just lateral of the fish's midline.

3.3) Expand the exposed skull region anteromedially to expose an additional 2.5 mm square non-overlapping area (Fig. 2B).

3.4) Completely clear and dry the exposed surface of the skull using the scalpel blade to scrape away any excess tissue and Kimwipes and forced air to dry the surface (Fig. 2C).

3.5) Glue a metal post to the anteromedial exposed skull region using Super Glue. Wait until the glue is completely dry (Fig. 2D).

3.6) Remove a rectangle of skull, approximately 2mm X 4mm for a 6.2 cm fish. Use a dental drill with a ~0.5 mm diameter ball mill carbide tip to thin the perimeter of the rectangle. Then, using a scalpel and forceps, cut the perimeter of the rectangle and peel it away to expose the underlying brain. Additional drilling or cutting with small scissors may be necessary to fully expose EL (Fig. 2E). If muscle bleeding occurs, an electrocautery unit may be used.

3.7) Cut away both the dura mater (pigmented) and the pia mater (clear) using spring scissors or a needle and remove the cut portions with a pair of forceps. The anterior and posterior portions of EL (ELa and ELp, respectively) are now visible (Fig. 3A)

4) Retrograde Labeling of Axons of Interest

4.1) Position a manipulator with a dye-coated needle (made in Step 1) above the target region containing axons of interest, in our case ELp.

4.2) Swiftly insert the needle approximately 25 μm into the tissue. Wait 15-30 seconds,

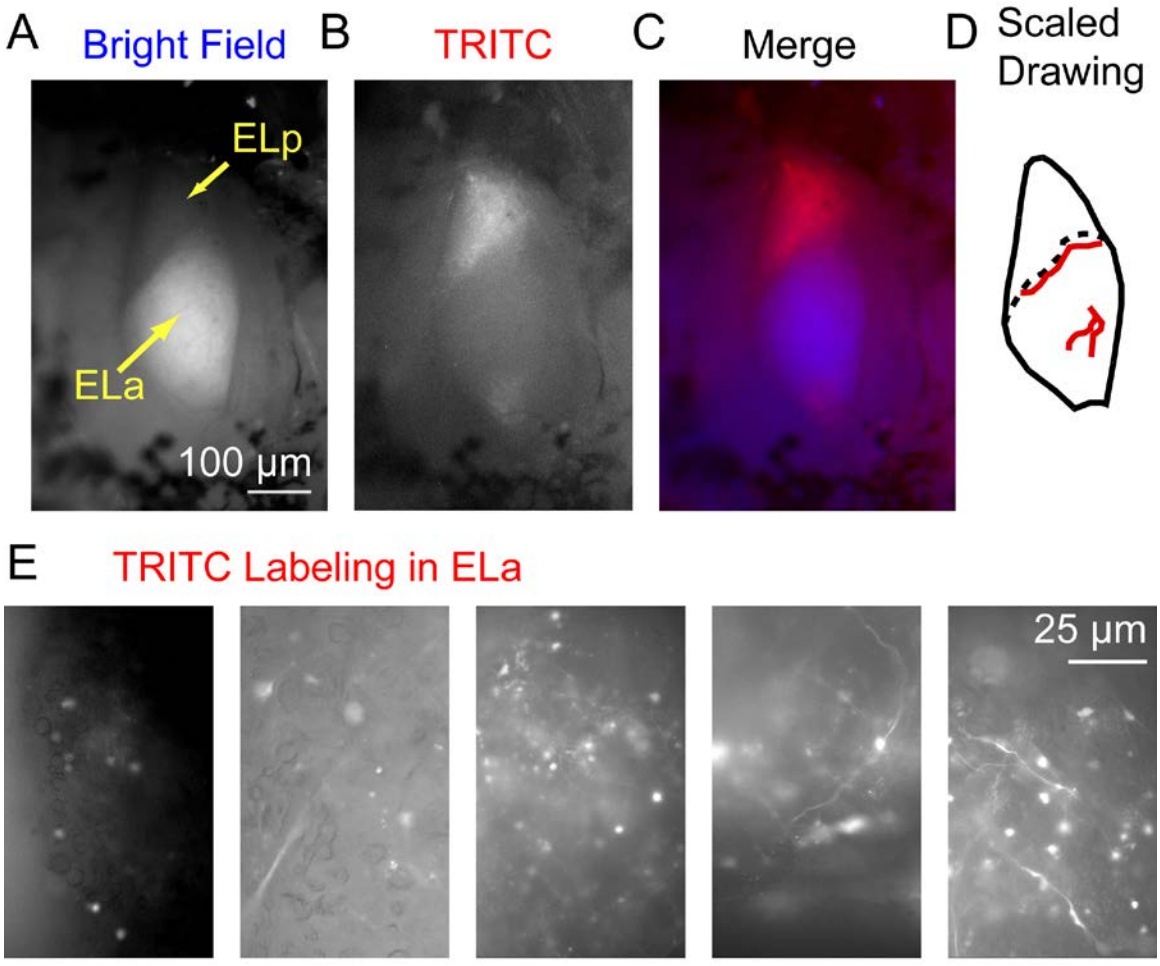

FIG 3: Fluorescent labeling in the posterior exterolateral nucleus 3 hours after injection of dextran-conjugated Alexa Fluor 568. (A) The anterior and posterior exterolateral nuclei (ELa and ELp, respectively) visualized with bright field illumination from above. Note that the extensive myelination within ELa gives it a relatively bright appearance that distinguishes it from ELp. (B) The same area visualized using epifluorescence viewed through a TRITC filter. (C) A merged image using blue for A (brightfield) and red for B (TRITC). (D) Example of a scaled drawing of ELa and ELp including major blood vessels (red lines) that can be used as landmarks to identify the exact location of labeled axons visible only under high magnification (the exact location of blood vessels varies from fish to fish). Dotted line indicates the border between ELa and ELp. (E) Sample images acquired using a TRITC filter from 5 different preparations illustrating a range of successful labeling patterns of Small cell axons and somas in ELa.

until all the dye has come off, and then retract the needle.

4.3) Repeat with additional fresh needles as needed, placing each one in a different location so that the dye is distributed throughout the target region. We used 3-5 needles per preparation.

4.4) Rinse excess dye from the cavity with Hickman's ringer solution.

4.5) Wait at least 2 hours for dye uptake and transport.

5) Visualization of Axons of Interest

5.1) Place the recording chamber, along with the fish, underneath the objective of an upright, fixed-stage epifluorescent microscope. As the body of the fish occludes light penetration, both white and fluorescent light sources must come from above. Careful placement of a fiber optic light source above the skull cavity allows satisfactory brightfield images. For epifluorescence viewing, fluorescence filter specifications should match the absorption/emission spectrum of the dye.

5.2) Switch respiration to fresh tank water and maintain the same flow rate. Place a ground wire in the exposed brain cavity and connect to the ground of the recording headstage (see 6.3).

5.3) Place a pair of recording electrodes next to the base of the tail and connect to a differential amplifier and recording device (e.g. audio monitor, oscilloscope, or computer) to monitor the electric organ discharge command (EODC). After the fish recovers from anesthesia, the EODC can be used as an indicator of the fish's condition.

5.4) Prepare a scaled sketch of the brain region viewed at low magnification. Include major blood vessels as landmarks (may vary from fish to fish) to identify the exact location of labeled axons visible only under high magnification (Fig. 3D).

5.5) Confirm dye placement. First view entire tissue with brightfield illumination for orientation (Fig. 3A). Then view with fluorescent illumination (Fig. 3B). ELp will have diffuse labeling (Fig. 3B,C). Minimize fluorescence excitation to limit the photodynamic and phototoxic effects of the dye.

5.6) Use the vessels as landmarks to locate ELa under high magnification. Illuminate with fluorescent light while searching for a labeled axon near the surface. (Fig. 4).

6) Record Extracellular Activity

6.1) Pull suction recording electrodes using 1 mm OD, 0.58 mm ID borosilicate capillary glass with filament. Ideal tip size will depend on the diameter of the target axons, which in our case is 0.1-0.2 μm[17]. For our application, electrode tip diameters were 1.5 ± 0.4 μm (range: 1.0-2.4 μm) with a 5 mm long, narrow shank in order to approach labeled axons without moving the surrounding densely packed tissue.

6.2) Fill electrodes with filtered Hickman's ringer solution. Final tip resistance is 45.2 ± 38.0 MΩ (range: 16 to 155 MΩ).

6.3) Place the electrode in an electrode holder with a pressure port and connect it to an amplifier headstage mounted on a manipulator. Run a pressure line from the pressure port to a T-junction ending in a manometer and a syringe for monitoring and controlling pressure, respectively.

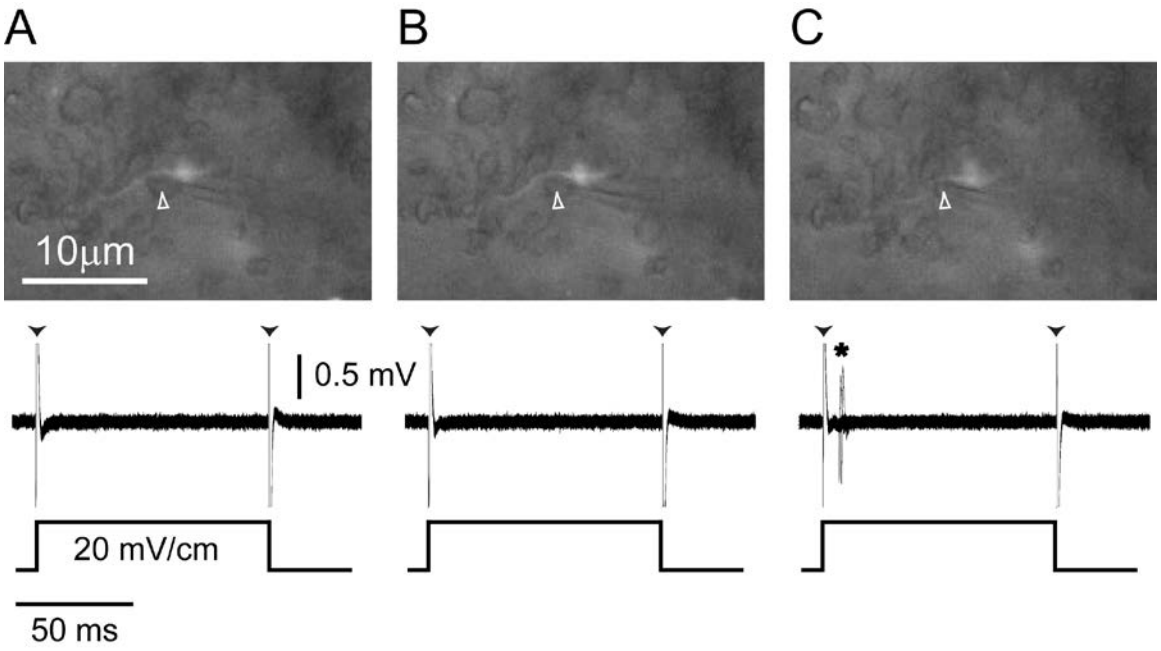

FIG 4: Single-unit extracellular recording from a labeled axon. (A) Recording electrode (arrow head) under positive pressure placed adjacent to a labeled small cell axon in ELa (top) records only edge artifact (arrow heads) in response to a 100 ms 20 mV/cm monophasic, contralateral-positive, transverse square pulse (bottom). (B) Releasing outward pressure from the electrode (arrow head) causes the axon to move slightly towards the electrode (top) but there are still no responses to the stimulus (bottom). (C) Slight negative pressure pulls the axon into the electrode (top, arrow head) and action potentials in response to stimulus onset are now visible (bottom, asterisk). Bottom portions of all three panels are overlaid responses to 20 repetitions of the stimulus.

6.4) Connect the headstage to an amplifier and an analog-to-digital acquisition device.

6.5) With 30 mbar outward pressure in the electrode line, place an electrode next to a labeled axon. A low-light level camera interfaced with imaging software is used to visualize pipette placement. Start near the tissue surface and advance the electrode towards the axon. As you approach the axon, the outward pressure should cause a slight, but noticeable movement of the axon.

6.6) While the electrode is next to the axon, (Fig. 4A, top) record the potential at the electrode while presenting test stimuli (in our case, we used 100 ms monophasic positive and negative transverse pulses at an intensity of 20 mV/cm; Fig. 1A). Action potentials should not be observed, although an electrical artifact confirms proper recording/stimulation (Fig. 4A, bottom).

6.7) Release the outward pressure in the electrode and repeat stimulation/recording. Action potentials should still not be observed (Fig. 4B).

6.8) Apply slight (125 ± 25 mbar) suction to the electrode and repeat stimulation /recording. Action potentials should now be observed in response to stimulation (Fig. 4C). Spontaneous activity may also occur. If action potentials are not observed, release the suction, clear the electrode with slight pressure, move the electrode slightly, and attempt suction again. Once action potentials are visible, close the pressure line.

6.9) Stimulate and record as desired.

7) Termination and Disposal

7.1) Once all desired recordings are complete, switch to respiration with 100 mg/l MS-222 until the EODC has stopped. No EODC should be detected for at least 10 minutes.

7.2) Dispose of the fish according to institutional guidelines and approved animal care protocols.

RESULTS

For our particular application, we are interested in studying stimulus coding by central sensory neurons. Successful recordings from labeled axons allow analysis of single-unit responses to sensory stimulation[18]. Figure 5A shows representative action potentials evoked by transverse electrosensory stimulation using bipolar electrodes located on the insides of the left and right walls of the recording chamber. Spike times can be presented as a spike raster plot (Fig. 5B). A 25 ms pre-stimulus recording window shows the low level of spontaneous activity. This particular ELa small cell is long-pass tuned to stimulus duration at a stimulus intensity of 6 mV/cm, increasing the number of spikes per repetition as stimulus duration increases (Fig. 5C). The mean first spike latency is 4.28 ± 0.16 ms, consistent with the expected latency for small cells in ELa[11].

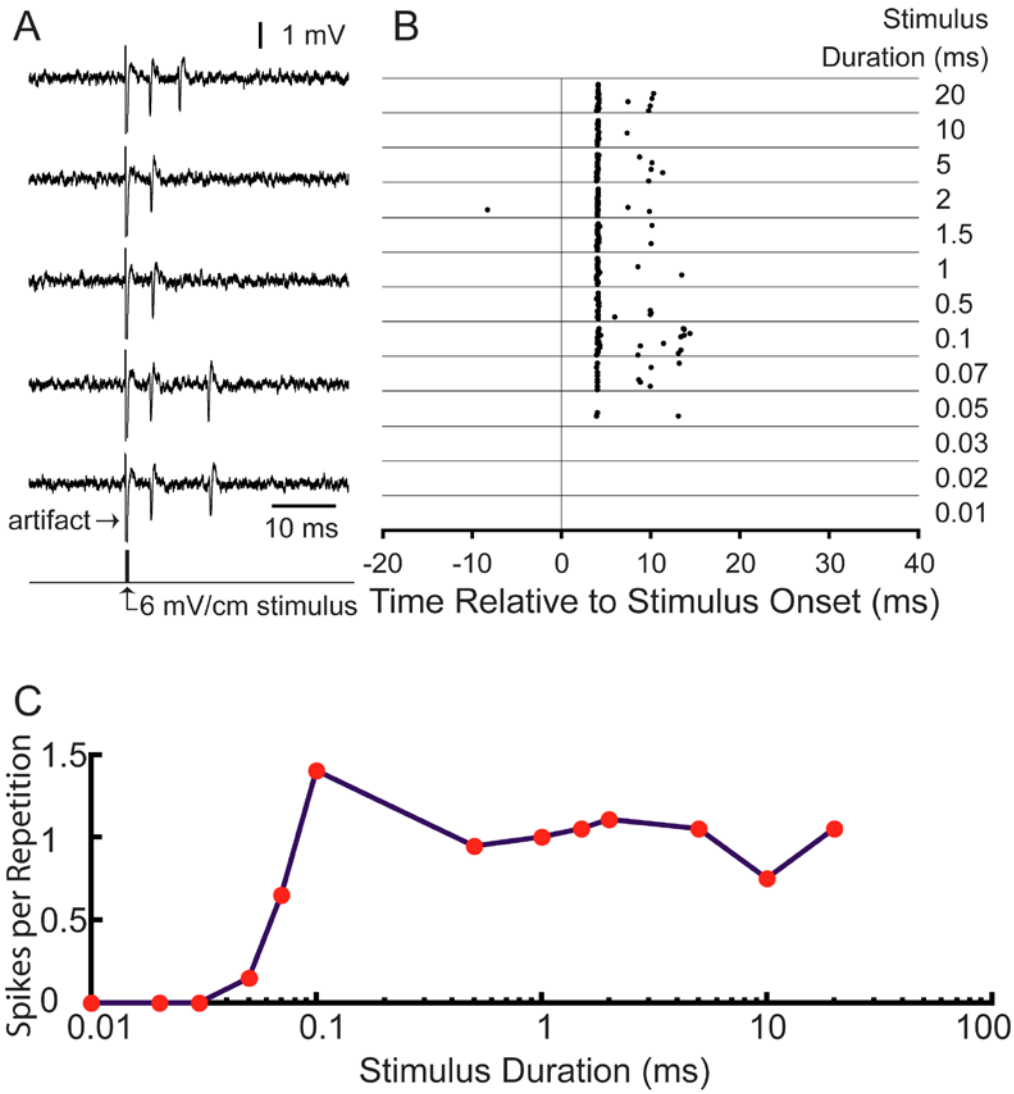

FIG 5: Representative results using this technique. (A) 5 sample traces showing action potentials evoked by a 0.1 ms 6 mV/cm monophasic, contralateral-positive, transverse square pulse stimulus. (B) Raster plot showing spike times during 20 repetitions of a 75 ms recording window for the same unit stimulated at time 0 with 6 mV/cm stimuli at the range of durations listed on the right. (C) Duration tuning curve quantifying the responses displayed in the raster as spikes per stimulus repetition.

DISCUSSION

Once mastered, this technique will allow one to target identified neurons, including individual axons, for *in vivo* recordings in many model systems. In addition, this technique allows one to reliably record spike output from neurons with unique anatomical characteristics that make traditional *in vivo* recording methods challenging. We have utilized this technique to record from ELa small cells in mormyrid weakly electric fish. Previous attempts to study the tuning properties of small cells were unsuccessful due to challenging recording conditions[11, 14]. Similar anatomical features create barriers to obtaining single-unit recordings from many different vertebrate auditory and electrosensory neurons[8-10]. To overcome these challenges in our system, we took advantage of the fact that small cells are the only cells in ELa that project to ELp. Thus, retrograde transport of dye placed in ELp limits labeling in ELa to small cell somas and axons. Fluorescent labeling of the axons allowed precise electrode placement next to labeled axons, making single-unit recordings from identified cells possible despite inaccessible somas. We attempted somatic recordings, but were unsuccessful, probably due to the surrounding engulfing synapses[11,17]. However, somatic labeling was clearly visible suggesting that this technique could be used to target somatic recordings in other cell types and other circuits. Fluorescent labeling of neurons through retrograde transport *in vivo* has been used for guiding targeted recordings *in vitro*[19-21]. A similar technique was used for targeted *in vivo* recordings from motor neurons in zebrafish spinal cord[22]. Our work represents a novel expansion of this approach, in which both labeling and recording are done *in vivo* within the brain. Our method demonstrates that *in vivo*

labeling of CNS areas with a retrograde tracer can be expanded to the study of other intact circuits with similarly selective projection neurons. For example, in mammalian auditory processing, the inferior colliculus (IC) serves as an important relay center for inputs from multiple rhombencephalic structures[23]. Dye injection into the IC would selectively label the projection cells from each of these nuclei. The superior colliculus (SC) serves a similar function for vision[24]. Spinal cord preparations are particularly well suited for this technique, as the spinal cord is easily accessed, dye injection can occur far from the recording site, and it can be combined with intracellular recording and filling of select neurons to acquire more detailed anatomical information[25]. Finally, tract-tracing is a well established technique used throughout the central nervous system to map complex circuitry[26]. Our method can be utilized to add functional information to these studies as has been done with calcium-sensitive indicators in cat visual cortex[27].

The surgery, which is well established, reliable, and regularly used for blind *in vivo* recordings[16], must be completed with minimal bleeding and no damage to the surface of the brain to allow the animal and the tissue to survive. With practice, the surgery and dye application can be completed in 30-45 minutes. We successfully labeled small cell axons in 67% of the preparations. Most preparations have only 1 or 2 visible labeled axons, but some have as many as 8. Of the 119 labeled units attempted, we obtained single-unit recordings from 26 units distributed over 12 preparations (Table 2). Thus, data were collected from 41% of preparations with labeled axons for an overall success rate of 28%.

The critical aspect of dye application is labeling depth. Shallow insertion of the

Table 2: Success rates for each dye injection method.

Application Site	Dye Type	Fish attempted	Label in ELa	Label in ELp	Units attempted	Recordings
ELa	Alexa Fluor injection	32	26 (81.2%)	19 (59.4%)	50	4 (8.0%)
	Alexa Fluor soaked filter paper	1	0	0	0	0
	Di-I in DMSO	8	6 (75.0%)	0	0	0
	Di-O crystals	5	3 (60.0%)	2 (40.0%)	9	0
ELp	Solid Alexa Fluor crystals	2	0	2 (100%)	0	0
	Alexa Fluor coated tungsten wires	43	29 (67.4%)	41 (95.3%)	119	26 (21.8%)

Table 2: Success rates for each dye injection method. Methods are divided based on injection site and dye type. For each method, the total number of fish attempted and the percentage of these experiments that resulted in successful labeling in ELa and ELp is shown. Note that the targeted recording area is the opposite of the application site (highlighted boxes). For the injection site, dye uptake was considered successful with labeling of both somas and axons. In contrast, at the recording site, only preparations with labeled axons were counted as successful labeling experiments. The total number of attempted units and the percentage of these units that resulted in successful recordings are also shown.

tungsten wire will result in the dye being washed away. However, if the penetration is too deep, labeled axons will not be visible for targeting. Further, some mechanical damage to the cell must occur for the dye to be adequately taken up[25, 28]. However, too much damage will kill the cells. We attempted labeling with other dyes and other methods (Table 2), including anterograde labeling through dye injection into ELa paired with recording from labeled axons in ELp (Table 3). We hypothesize that anterograde labeling was not successful because labeling was limited to cells with somatic damage, making them unresponsive. Additionally, pre-synaptic terminals may have been disturbed. By contrast, retrograde labeling minimizes both of these concerns. The amount and location of dye application can be modified according to the particular circuit being studied. Maximal labeling occurs with the greatest dye concentration, which we achieved using coated tungsten wires. However, for labeling axons with deep projections, dye may come off a tungsten needle as it is advanced. In these cases, pressure injection would be more appropriate. Dye uptake and transport are rapid, with labeled axons in our preparation being visible as early as 2 hours post-injection and additional labeled axons appearing as late as 6 hours post-injection. Thus, labeling and recording can be accomplished in a single day, eliminating technical difficulties associated with survival surgery. Timing will vary for each application depending on the distance required for dye transport.

Another critical aspect is electrode placement. It is important to enter the tissue close to the site of the labeled axon to prevent clogging of the tip. For dense tissue such as in ELa, a long, thin shank on the recording electrode minimizes excess movement of

Table 3: Quantities of dye applied for each of the three mechanisms used to inject Alexa Fluor into ELa

	# of injection sites	Average volume per injection (µL)	Range of volumes per injection (µL)	Average total injection volume (µL)	Range of total injection volumes (µL)
Microinjector with Hamilton	3 or 4	0.144	0.091 - 0.91	0.516	0.378 - 0.669
Nanoinjector with glass pipette	2 - 4	0.069 (fixed)	Fixed volume injected 1-6 times	0.621	0.414 - 0.966
Microinjector with glass pipette	2 - 6	0.093	0.058 - 0.202	0.360	0.252 - 0.540

Table 3: Quantities of dye applied for each of the three mechanisms used to inject Alexa Fluor into ELa (first method from table 2). Dye injection into ELa was performed with both a nanoinjector and a microinjector using either a 33 gauge Hamilton syringe needle or a pulled glass capillary pipette. We varied the number of injection sites, the volume per injection and the total volume of dye injection.

surrounding tissue. If a successful recording is not achieved on the first attempt, repeat with fresh electrodes until a recording is obtained or the tissue is disrupted to the point at which the axon is no longer visible. However, it is also important to quickly place the electrode next to the axon to minimize the amount of fluorescent exposure, which can cause phototoxicity, bleaching and may affect physiological properties of the cell[29-31]

Once a segment of axon is successfully suctioned into the recording electrode, recordings can be obtained for several hours. If units are consistently lost in less than 1 hour, consider making smaller electrode tips to prevent the axon from slipping out. On the other hand, too small of a tip may result in clogging, low signal-to-noise, or damage to the axon. A steady decrease in spike amplitude and the 'return' of a unit with additional suction is an indication that the tip is too large. Too much suction may cause irreparable damage to the axon. One solution is to allow a small leak in the air line so the pressure slowly returns to zero. Rapidly equalizing the pressure will result in a transient relative-outward 'push' which may expel the axon.

Although this technique represents a major advantage for obtaining targeted recordings from identified projection neurons, it will not be useful for distinguishing local interneurons, as dye would be taken up by all cell types at the injection site. Theoretically, the use of multiple fluorophores with separate injection sites may allow this method to be expanded. For example, comparison of single- versus double-labeling could be used to distinguish interneurons from projection neurons following dual injections at two points in the circuit[32]. Similarly, retrograde tracers can be combined with other advanced imaging techniques, such as two-photon imaging, as was done

recently in zebra finch High Vocal center (HVc)[32]. Also, recording regions are limited to those near the surface when using epifluorescence microscopes, as we were only able to resolve 1 μm structures within the first 30 μm of tissue. However, this depth could be extended through the use of other microscopy techniques, such as two-photon microscopy[33] or objective-coupled planar illumination microscopy[34]. Overall, this technique represents an important advancement in the study of neural circuits *in vivo* because it can be used to record from single neurons in many different circuits in a variety of model systems – including those that are relatively inaccessible.

ACKNOWLEDGMENTS

Funding provided by the National Science Foundation (IOS-1050701 to B.A.C.), the National Institutes of Health (NS54174 to S.M. and F30DC0111907 to A.M.L-W.), the Uehara Memorial Foundation and the Japan Society for the Promotion of Science (G2205 to T.K.). We thank Julian Meeks for his support and guidance on the topic of extracellular axonal recordings. We thank Carl Hopkins for providing a prototype recording chamber.

REFERENCES

1. Meeks, J.P., Jiang, X. & Mennerick, S. Action potential fidelity during normal and epileptiform activity in paired soma-axon recordings from rat hippocampus. J Physiol **566**, 425-441 (2005).
2. Pinault, D. A novel single-cell staining procedure performed *in vivo* under electrophysiological control: morpho-functional features of juxtacellularly labeled thalamic cells and other central neurons with biocytin or Neurobiotin. J Neurosci Methods **65**, 113-136 (1996).
3. Joshi, S. & Hawken, M.J. Loose-patch-juxtacellular recording *in vivo*--a method for functional characterization and labeling of neurons in macaque V1. J Neurosci Methods **156**, 37-49 (2006).
4. Margrie, T.W. *et al.* Targeted whole-cell recordings in the mammalian brain *in vivo*. Neuron **39**, 911-918 (2003).
5. Lima, S.Q., Hromádka, T., Znamenskiy, P. & Zador, A.M. PINP: A new method of tagging neuronal populations for identification during *in vivo* electrophysiological recording. PLoS One **4**, e6099 (2009).
6. Foust, A., Popovic, M., Zecevic, D. & McCormick, D.A. Action potentials initiate in the axon initial segment and propagate through axon collaterals reliably in cerebellar Purkinje neurons. J Neurosci **30**, 6891-6902 (2010).
7. Norgren, R.B. Jr. & Lehman, M.N. Herpes simplex virus as a transneuronal tracer. Neurosci Biobehav Rev **22**, 695-708 (1998).
8. Joris, P.X. A dogged pursuit of coincidence. J Neurophysiol **96**, 969-972 (2006).

9. Heiligenberg, W. & Rose, G. Phase and amplitude computations in the midbrain of an electric fish: Intracellular studies of neurons participating in the jamming avoidance response of Eigenmannia. J Neurosci **5**, 515-531 (1985).

10. Morales, E. *et al.* Releasing the peri-neuronal net to patch-clamp neurons in adult CNS. Pflügers Archiv European J Physiol **448**, 248-258 (2004).

11. Friedman, M.A. & Hopkins, C.D. Neural substrates for species recognition in the time-coding electrosensory pathway of mormyrid electric fish. J Neurosci **18**, 1171-1185 (1998).

12. Hitschfeld, É.M., Stamper, S.A., Vonderschen, K., Fortune, E.S. & Chacron, M.J. Effects of restraint and immobilization on electrosensory behaviors of weakly electric fish. ILAR J **50**, 361-372 (2009).

13. Xu-Friedman, M.A. & Hopkins, C.D. Central mechanisms of temporal analysis in the knollenorgan pathway of mormyrid electric fish. J Exp Biol **202**, 1311-1318 (1999).

14. Amagai, S., Friedman, M.A. & Hopkins, C.D. Time coding in the midbrain of mormyrid electric fish. I. Physiology and anatomy of cells in the nucleus exterolateralis pars anterior. J Comp Physiol A: Neuroethol Sens Neural Behav Physiol **182**, 115-130 (1998).

15. Brady, J. A simple technique for making very fine, durable dissecting needles by sharpening tungsten wire electrolytically. Bull World Health Organ **32**, 143-144 (1965).

16. Carlson, B.A. Temporal-pattern recognition by single neurons in a sensory pathway devoted to social communication behavior. J Neurosci **29**, 9417-9428 (2009).

17. Mugnaini, E. & Maler, L. Cytology and immunocytochemistry of the nucleus extrolateralis anterior of the mormyrid brain: possible role of GABAergic synapses in temporal analysis. Anat Embryol (Berl*)* **176**, 313-336 (1987).

18. Lyons-Warren, A.M., Kohashi, T., Mennerick, S., & Carlson, B.A. Detection of submillisecond spike timing differences based on delay-line anticoincidence detection. J. Neurophysiol **110**, 2295-2311 (2013).

19. Colin, W., Donoff, R.B. & Foote, W.E. Fluorescent latex microspheres as a retrograde tracer in the peripheral nervous system. Brain Res **486**, 334-339 (1989).

20. Katz, L.C., Burkhalter, A. & Dreyer, W.J. Fluorescent latex microspheres as a retrograde neuronal marker for *in vivo* and *in vitro* studies of visual cortex. Nature **310**, 498-500 (1984).

21. Brown, S.P. & Hestrin, S. Intracortical circuits of pyramidal neurons reflect their long-range axonal targets. Nature **457**, 1133-1136 (2009).

22. Drapeau, P., Ali, D.W., Buss, R.R. & Saint-Amant, L. *In vivo* recording from identifiable neurons of the locomotor network in the developing zebrafish. J Neurosci Methods **88**, 1-13 (1999).

23. Pollak, G.D., Burger, R.M. & Klug, A. Dissecting the circuitry of the auditory system. Trends Neurosci **26**, 33-39 (2003).

24. Wurtz, R.H. & Albano, J.E. Visual-motor function of the primate superior colliculus. Annu Rev Neurosci **3**, 189-226 (1980).

25. O'Malley, D.M., Zhou, Q. & Gahtan, E. Probing neural circuits in the zebrafish: a suite of optical techniques. Methods **30**, 49-63 (2003).

26. Vercelli, A., Repici, M., Garbossa, D. & Grimaldi, A. Recent techniques for tracing pathways in the central nervous system of developing and adult mammals. Brain Res Bull **51**, 11-28 (2000).

27. Ohki, K., Chung, S., Ch'ng, Y.H., Kara, P. & Reid, R.C. Functional imaging with cellular resolution reveals precise micro-architecture in visual cortex. Nature **433**, 597-603 (2005).

28. Gahtan, E. & O'Malley, D.M. Rapid lesioning of large numbers of identified vertebrate neurons: applications in zebrafish. J Neurosci Methods **108**, 97-110 (2001).

29. Higure, Y., Katayama, Y., Takeuchi, K., Ohtubo, Y. & Yoshii, K. Lucifer Yellow slows voltage-gated Na^+ current inactivation in a light-dependent manner in mice. J Physiol **550**, 159-167 (2003).

30. Mennerick, S. *et al.* Diverse voltage-sensitive dyes modulate GABAA receptor function. J Neurosci **30**, 2871-2879 (2010).

31. Oxford, G.S., Pooler, J.P. & Narahashi, T. Internal and external application of photodynamic sensitizers on squid giant axons. J Membr Biol **36**, 159-173 (1977).

32. Roberts, T.F., Tschida, K.A., Klein, M.E. & Mooney, R. Rapid spine stabilization and synaptic enhancement at the onset of behavioural learning. Nature **463**, 948-952 (2010).

33. Min, W., Freudiger, C.W., Lu, S. & Xie, X.S. Coherent nonlinear optical imaging: beyond fluorescence microscopy. Annu Rev Phys Chem **62**, 507-530 (2011).

34. Holekamp, T.F., Turaga, D. & Holy, T.E. Fast three-dimensional fluorescence imaging of activity in neural populations by objective-coupled planar illumination microscopy. Neuron **57**, 661-672 (2008).

Chapter 4

Detection of submillisecond spike timing differences based on delay-line anti-coincidence detection

The question of the timing of the impulses in the different fibres of a nerve trunk has a considerably importance in the case of the sensory nerves.

-E.D. Adrian, 1928

This chapter contains a previously published manuscript:

A.M. Lyons-Warren, T. Kohashi, S. Mennerick, B.A. Carlson (2013). Detection of submillisecond spike timing differences based on delay-line anti-coincidence detection. *J. Neurophysiol*. 10: 2295-311.

Author contributions for the above citation:

A.M.L-W performed all experiments except for tract tracing and confocal imaging, which T.K. performed. B.A.C. performed modeling. A.M.L-W and B.A.C. performed data analysis. All authors contributed to conceptualization and discussion of the experiments and analyses. The manuscript was written by A.M.L-W and B.A.C. with input from S.M. and T.K.

ABSTRACT

Detection of submillisecond interaural timing differences is the basis for sound localization in reptiles, birds and mammals. Although comparative studies reveal that different neural circuits underlie this ability, they also highlight common solutions to an inherent challenge: processing information on timescales shorter than an action potential. Discrimination of small timing differences is also important for species recognition during communication amongst mormyrid electric fishes. These fishes generate a species-specific electric organ discharge (EOD) that is encoded into submillisecond-to-millisecond timing differences between receptors. Small, adendritic neurons (Small Cells) in the midbrain are thought to analyze EOD waveform by comparing these differences in spike timing, but direct recordings from Small Cells have been technically challenging. Here we use a fluorescent labeling technique to obtain visually guided extracellular recordings from individual Small Cell axons. We demonstrate that Small Cells receive 1-2 excitatory inputs from one or more receptive fields with latencies that vary by over 10 ms. This wide range of excitatory latencies is likely due to axonal delay lines, as suggested by a previous anatomical study. We also show that inhibition of Small Cells from a calyx synapse shapes stimulus responses in two ways: through tonic inhibition that reduces spontaneous activity, and through precisely timed, stimulus-driven, feed-forward inhibition. Our results reveal a novel delay-line anti-coincidence detection mechanism for processing submillisecond timing differences, in which excitatory delay lines and precisely timed inhibition convert a temporal code into a population code.

INTRODUCTION

Temporal coding, in which information is encoded into the precise timing of action potentials, is common in sensory systems (VanRullen et al. 2005). In some cases, behavioral sensitivity can reach the submillisecond or even submicrosecond range, several orders of magnitude shorter than a typical action potential (Kawasaki 1997; Moiseff and Konishi 1981; Simmons 1979). Understanding this hyperacute temporal sensitivity provides insight into general properties of temporal processing and the diverse neural mechanisms that can support it (Carr and Friedman 1999).

The best studied examples of submillisecond temporal discrimination involve detection of interaural timing differences (ITDs) for sound localization (Ashida and Carr 2011; Köppl 2009; Schnupp and Carr 2009). In birds and reptiles, ITDs are analyzed through delay-line coincidence detection of binaural excitatory inputs (Carr and Konishi 1990; Carr et al. 2009; Funabiki et al. 2011). In mammals, ITD detection also relies on coincidence detection of binaural excitatory inputs, but the mechanistic basis for ITD tuning remains controversial and cannot be explained by axonal delay lines (Brand et al. 2002; Grothe et al. 2010; McAlpine and Grothe 2003; Roberts et al. 2013; van der Heijden et al. 2013). In both systems, inhibition appears to play important but different roles in shaping binaural processing (Grothe 2003; Roberts et al. 2013; Yamada et al. 2013). One general theme that emerges is that submillisecond temporal processing is implemented using similar neural substrates that are combined in unique ways by different circuits (Carr and Friedman 1999; Carr and Soares 2002; Carr et al. 2001; Kawasaki 2009).

Mormyrid fishes communicate using a species-specific electric organ discharge (EOD) consisting of 1-5 distinct phases and a total duration ranging from ~0.1-20 ms (Carlson et al. 2011; Hopkins 1981). Sharp temporal features of the EOD waveform, particularly the relative timing of phase onsets and offsets, are used for species recognition and mate choice (Arnegard et al. 2006; Feulner et al. 2009; Hopkins and Bass 1981). For example, in the Ivindo River of Gabon there are at least 21 mormyrid species/morphs living in sympatry, each having a distinctive EOD (Arnegard et al. 2010; Carlson et al. 2011; Hopkins 1981). Thus, detecting subtle timing differences among EOD waveforms is an essential computation that fish must perform in their natural environment.

EODs are encoded by peripheral electroreceptors distributed throughout the surface of the skin called knollenorgans (KOs), which respond with a single, fixed latency spike to the onset of inward currents (Bennett 1965; Harder 1968). Variation in the location and orientation of KOs with respect to external electric fields results in different receptors receiving local EOD stimuli with different polarities and intensities (Hopkins 1986; Hopkins and Bass 1981). As a result, different KOs respond to distinct edges of an EOD waveform, thereby encoding EODs into spike timing differences among the population of receptors (Baker et al. 2013).

These timing differences are thought to be analyzed by Small Cells in the midbrain anterior exterolateral nucleus (ELa) (Fig. 1*A*) (Baker et al. 2013; Xu-Friedman and Hopkins 1999). Small Cells receive excitatory inputs from ascending axons and GABAergic input from local interneurons called Large Cells via a calyx synapse

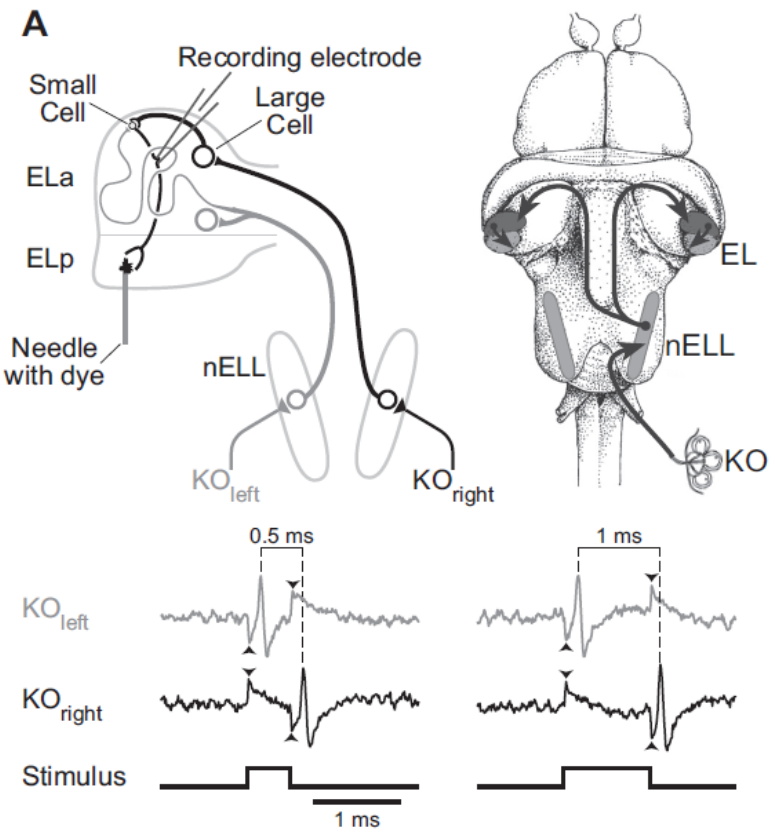

FIG 1: Retrograde labeling allows for visually guided extracellular recordings from Small Cell axons. (A) Schematic representation of the knollenorgan (KO) electrosensory pathway. KOs generate short-latency spikes in response to inward current caused by changes in voltage across the skin surface. In response to an electrical stimulus, KOs on opposite sides of the body experience opposite stimulus polarities. Thus, when recording from a single KO, the responses to normal and reversed polarity stimuli reveal how KOs on opposite sides of the body would respond to a single stimulus (Hopkins and Bass 1981; Lyons-Warren et al. 2012). Here, we show the spiking responses of a single KO, recorded extracellularly, to normal (simulating KO_{left}) and reversed (simulating KO_{right}) polarity square pulses of two different durations (0.5 ms; left, 1 ms; right). The stimuli are shown in the bottom trace, and stimulus artifact can be seen at stimulus onset and offset (black arrowheads). The difference in spike timing between KO_{left} and KO_{right} codes for pulse duration. These spike timing differences are relayed with high temporal fidelity from the hindbrain nucleus of the electrosensory lateral line lobe (nELL) to the midbrain exterolateral nucleus (EL). EL has two components, anterior (ELa) and posterior (ELp). nELL axons synapse onto large GABAergic interneurons (Large Cells) soon after entering ELa, and then travel for up to 7 additional mm, synapsing on dozens of Small Cells throughout ELa. Small Cells also receive GABAergic input from Large Cell calyx synapses. Small Cell axons provide the only projection from ELa to ELp. Thus, dye placed in ELp (gray needle) selectively labels Small Cells through retrograde transport.

(Friedman and Hopkins 1998; George et al. 2011; Mugnaini and Maler 1987). Incoming axons synapse on Large Cells immediately after entering ELa and then continue on a convoluted path for up to 7 mm, synapsing on dozens of Small Cells along the way (Friedman and Hopkins 1998). The variable length of the axons projecting to Small Cells are suggestive of delay-lines that establish variation in the relative timing of excitatory and inhibitory input (Xu-Friedman and Hopkins 1999). This observation led to a delay-line anti-coincidence detection model, in which the processing of submillisecond spike timing differences results from a combination of precisely timed inhibition and delayed excitation arising from different receptive fields (Friedman and Hopkins 1998). Unfortunately, it is difficult to record from Small Cells due to their distinctive anatomical features, so we do not know how they actually perform temporal comparisons. Therefore, we developed a fluorescence-based method to directly target Small Cell axons for extracellular recording (Lyons-Warren et al. 2013). To determine how Small Cells code for peripheral timing differences, we recorded responses to spatially uniform, square pulse electric stimuli that allowed us to precisely manipulate the relative timing of KO responses on opposite sides of the body (Fig. 1*A*). Our data provide empirical evidence in support of a novel delay-line anti-coincidence detection mechanism for processing submillisecond timing differences.

MATERIALS AND METHODS

Animals. We used developmentally mature individuals of both sexes of the weakly electric mormyrid fish *Brienomyrus brachyistius*. Fish were purchased from commercial distributors and housed in community aquariums at a temperature of 26-28 ºC and conductivity of 200-400 μS/cm, with a 12:12 hour light:dark cycle. Fish were fed live black worms four times per week. Prior to all procedures, fish were anesthetized in 300 mg/l tricaine methanesulfonate (MS-222) and then paralyzed with either 20-100 μl of 0.3 mg/ml gallamine triethiodide (for KO recordings) or with 100 μL of 3 mg/ml gallamine triethiodide (for evoked potential and Small Cell recordings). They were then placed on a platform, supported with vertical rods, and respirated by a tube placed in the mouth that fed aerated water across the gills. For evoked potential and Small Cell recordings, we respirated fish under general anesthesia (100 mg/l MS-222) throughout surgery and we applied lidocaine as a local anesthetic before performing a craniotomy. Fish were brought out of general anesthesia before all recordings. To monitor fish health during experiments, we recorded the descending EOD command from the spinal cord using a pair of electrodes placed next to the caudal peduncle (Carlson 2003). Fish used for KO recordings were returned to their home tank after recovering from the paralytic. Fish used for Small Cell and evoked potential recordings were placed back under general anesthesia after all recordings were completed before being euthanized. All procedures were in accordance with guidelines established by the National Institutes of Health (NIH) and were approved by the Animal Care and Use Committee at Washington University in St. Louis.

KO Recordings. We obtained non-invasive, *in vivo* extracellular recordings from KOs as previously described (Arnegard et al. 2006; Bennett 1965; Hopkins and Bass 1981; Lyons-Warren et al. 2012). We used 3 fish ranging in size from 11.2 to 13.0 cm standard length. We used relatively large fish for these recordings because larger fish have more KOs and can be more reliably dosed with gallamine triethiodide to allow for a full recovery after the experiment. Previous studies did not find any differences in KO physiology with respect to fish size. Electrodes were forged from 1.0 mm OD, 0.5 mm ID borosilicate glass by heating the distal end and bending the last 1 cm to a 10 degree angle. The electrode was then filled with tank water, connected to the headstage of a DC amplifier (A-M Systems model 1600), and placed just above an individual KO. Monophasic square pulse stimuli were generated using isolated square pulse generators (A-M Systems model 2100), attenuated (Hewlett Packard 350D), and then delivered as a constant-current stimulus directly through the recording electrode, using bridge balance to minimize artifact. Thus, KO stimuli consisted of localized current pulses injected directly into the receptor organ and referenced to ground. Stimulus intensities varied from 0.5-5.7 nA. For isointensity tuning curves, stimuli were monophasic positive square pulses ranging in duration from 0.01 to 100 ms. For paired pulse experiments, the stimulus was a 50 ms monophasic positive square pulse followed by a 0.3 ms monophasic positive square pulse with delays of 0.1 to 10 ms between the end of the first pulse and the start of the second pulse. In both experiments, each stimulus was presented for 10, 20 or 30 repetitions. KO electrical activity was amplified 10x and digitized at

195.3 kHz (Tucker-Davis Model RP2.1). Responses were saved using custom software (Matlab).

Small Cell Recordings. We obtained extracellular single unit recordings from 76 retrogradely labeled Small Cell axons in 37 fish as described in detail in a companion methods paper (Lyons-Warren et al. 2013). Individuals ranged from 5.5-8.6 cm in standard length. We were limited to using fish ≤8.6 cm in standard length because the compound microscope objective constrained the size of the recording chamber (Lyons-Warren et al. 2013). Sharpened tungsten wires coated in 2 mM dextran-conjugated Alexa Fluor 10,000 MW dye were inserted 1-4 times approximately 25 μm deep into the posterior exterolateral nucleus (ELp) for dye placement. Small Cells are the only neurons in ELa that project to ELp, so this provided a means of selectively labeling these neurons within ELa (Fig. 1*A*). Recording electrodes were made from 1 mm OD, 0.58 mm ID borosilicate glass pulled to a 1.0-2.4 μm tip, and they were then filled with filtered Hickman's Ringer and connected to a headstage (Axon instruments CV-7B). After 2-6 hours for dye uptake and retrograde transport, an electrode under positive pressure was placed next to a labeled axon in ELa visualized using an upright, fixed-stage epifluorescent microscope. Suction was then used to bring the axon into the recording electrode. We attempted to obtain intracellular whole-cell recordings from labeled Small Cell somas, but we were unable to obtain a membrane seal. We also attempted intracellular whole-cell recordings from Small Cells *in vitro* using both slice (George et al. 2011) and whole-brain (Ma et al. 2013) preparations. However, even when visualizing Small Cells at high magnification *in vitro*, it was difficult to obtain a membrane seal, and

on rare instances when a seal was achieved the resulting intracellular recordings were of low quality (low, unstable resting potential and no ability to drive spiking). Finally, we attempted sharp intracellular recordings from Small Cells *in vitro*, but these also resulted in low quality recordings and an inability to drive spiking with current injection. These difficulties most likely relate to the extensive myelination within ELa, the small size of the cells (diameter = 5-7 μm), and synaptic terminals from other cells covering most of the soma (Friedman and Hopkins 1998; Mugnaini and Maler 1987). Thus, we are currently limited to using extracellular recordings from Small Cells in this study.

Monophasic square pulse stimuli were generated using isolated square pulse generators (A-M Systems model 2100), attenuated (Hewlett Packard 350D), and then delivered as global electrosensory stimuli to the tank in one of two orientations, transverse or longitudinal (Lyons-Warren et al. 2013). Transverse stimuli were delivered between 3 vertically oriented silver wires located on the left wall of the chamber and 3 vertically oriented silver wires located on the right wall of the chamber, resulting in a uniform electric field vector between the left and right sides of the fish. Longitudinal stimuli were delivered between 2 vertically oriented silver wires located on the front wall of the chamber and 2 vertically oriented silver wires located on the back wall of the chamber, resulting in a uniform electric field vector between the head and tail of the fish. After getting a unit, we used both monophasic positive and negative 100 ms square pulses to determine which stimulus orientation (transverse vs. longitudinal), polarity (normal vs. reversed), and intensities elicited a response. We then used the preferred stimulus orientation to assess duration tuning to both stimulus polarities, and when

possible, to multiple stimulus intensities. If a unit responded to both stimulus orientations, then duration tuning was assessed for both orientations whenever possible. Stimulus intensities were calibrated in units of mV/cm at the fish's position, but with the fish absent.

The duration tuning of a unit was determined by presenting monophasic positive and negative stimuli ranging in duration from 1 μs to 20 ms. The specific durations presented were chosen to best capture the tuning of each particular unit. Each stimulus was presented as either 1 set of 20 or 4 sets of 5 repetitions each. An inhibitory corollary discharge in the hindbrain timed to the fish's own EOD prevents the knollenorgan pathway from responding to stimuli arriving 2-4 ms after the fish's own EOD (Bell and Grant 1989). Therefore, a sweep was discarded if a spinal EOD command occurred during 5 ms windows preceding both stimulus edges.

Responses were obtained using a Multiclamp 700B amplifier (Molecular Devices). Recorded signals were low-pass filtered using a 10 kHz 8-pole Bessel filter, digitized at 166-200 kHz using a Digidata 1322A 16-bit A/D converter, and acquired in pCLAMP software (Molecular Devices). Pipette capacitance compensation was automatically adjusted using Multiclamp 700B commander software. Either a threshold or a template search function was used to identify the timing of each spike in each sweep using Clampex software (Molecular Devices). In some recordings, there appeared to be two separate units, likely due to an unlabeled axon in close proximity to the target axon. For these recordings, we used principal components analysis to confirm that multiple units were present and to separate waveforms so that the units could be analyzed separately.

We used 12 waveform parameters that resulted in clearly separated units: peak amplitude, time to peak, rise time, rise slope, decay time, decay slope, half-width, area, anti-peak amplitude, time to anti-peak, time to rise to half-amplitude, and time to decay from half-amplitude. We used data from all recorded units in subsequent analyses.

To test for inhibition of Small Cells we used two different techniques. First, we used a complex stimulus protocol consisting of a 50 ms monophasic square stimulus (long pulse) at a polarity that elicited a response to the leading edge followed by a shorter pulse of the same polarity. The duration of the short pulse was the minimum duration that reliably elicited a response when presented alone, which ranged from 0.1-0.5 ms depending on the unit. The short pulse was presented at delays ranging from 0.1-25 ms after the end of the long pulse. As a control, we presented a 100 ms pulse with a second long pulse timed so the 'excitatory' edges occurred at the same intervals as in the paired pulse experiment, but without an 'inhibitory' edge between them. Second, we applied SR-95531 (gabazine), a competitive inhibitor of $GABA_A$ receptors (Lindquist et al. 2005). Inhibitory synapses are located on the Small Cell soma, which is not necessarily proximal to our recording site (Mugnaini and Maler 1987). Therefore, we used bolus application of 5-50 μl of a 1-10 mM solution in Hickman's Ringer (Bremner et al. 2006). The cavity surrounding ELa holds 100-500 μl of Ringer, so we estimate the final concentration of gabazine to be between 100 and 600 μM, which is above saturating levels (Lindquist et al. 2005). In a separate experiment using evoked potential recordings (see below) we demonstrated that the effects of gabazine application on Small Cell activity are due to local actions within ELa, not effects on upstream GABAergic synapses.

Spike Response Analysis. To analyze Small Cell spike times, we generated peri-stimulus time histograms using a bin size of 1 ms, and then divided by the number of stimulus repetitions. The average bin height during the pre-stimulus baseline period plus three standard deviations was set as a criterion response level. This criterion was then subtracted from the entire histogram, and all bins with a value greater than zero were considered part of the response. First-spike latency (FSL) was calculated as the median latency from stimulus edge to first spike across repetitions. We also calculated time-locked response latency (TLL). The window for determining TLL was defined as the tallest bin in the peri-stimulus time histogram plus an additional 0.5 ms on either side of this bin. We then calculated the median and standard deviation of all spike times falling within this window. We used the median rather than the mean to eliminate the effect of outliers in skewing the FSL and TLL. For most units, the mean and median of FSL and TLL were in close agreement. However, some units were more variable in their responses, resulting in large outliers that skewed the mean away from the center of the distribution.

When 100 ms stimuli were tested at multiple intensities, we used the highest intensity tested for analyzing response timing to ensure uniformity. Recordings from KO receptors reveal that response probability and temporal precision increase with stimulus intensity (Lyons-Warren et al. 2012). Response magnitude was determined as the area of all bins post stimulus presentation greater than the baseline criterion, in units of spikes/stimulus. Duration tuning curves were generated by plotting response magnitude as a function of stimulus duration and smoothed using a Savitzky-Golay filter in Matlab with a polynomial order of 1 and a frame size of 3. Tuning categorization was based on

which parts of the smoothed curve were greater than 50% of the maximal response. Paired pulse experiments for both Small Cells and KOs were analyzed using peri-stimulus time histograms. We quantified responses to the two pulses as the height of the tallest bin following each stimulus edge, and then determined the ratio of the response to the second pulse relative to the first pulse.

Statistical Analysis. All statistical analyses were performed using Statistica 6.1 (StatSoft, Inc.). Because Small Cell duration tuning could change with both stimulus intensity and polarity, we treated each tuning curve as an independent sample in statistical analyses of duration tuning. Due to small sample sizes in some cases and deviations from normality in others, we used nonparametric tests for all statistical comparisons between groups. For pair-wise comparisons between independent groups, we used the Mann-Whitney U Test. For pair-wise comparisons of repeated measurements, we used the Wilcoxon Matched Pairs Test. For comparing multiple, independent groups, we used the Kruskal-Wallis one-way ANOVA. We used linear regression to test for correlations between variables. All tests were two-tailed with $\alpha = 0.05$. We did not perform multiple comparisons on any data set.

Evoked Field Potential Recordings. Evoked potentials were recorded from the ELa as described previously (Carlson 2009; Lyons-Warren et al. 2012). We recorded from one fish having a standard length of 12.0 cm. We chose a relatively large fish for this because we have found that evoked potential amplitudes in ELa generally scale with fish size. We delivered transverse, 0.5 ms monophasic square pulses at an intensity of 20 mV/cm using 3 vertically oriented silver wires located on the left and right sides of the

chamber as described for Small Cell recordings. 10 repetitions of the stimulus were delivered at a range of latencies after the fish's EOD command. After obtaining baseline responses, we added 15 μL of 5 mM gabazine in Hickman's Ringer to the brain cavity surrounding ELa/ELp. The same stimuli were presented immediately after application and then repeatedly until 5 hours after application.

Modeling. To determine how differences in the latency of excitation relative to inhibition could impact Small Cell responses to variation in peripheral spike timing differences, we generated leaky integrator neurons (Dayan and Abbott 2001) as

$$C_m \frac{dVm}{dt} = I_E(t) + I_I(t) - \frac{V_m}{R_m}$$

where V_m is the membrane potential, C_m is the membrane capacitance (10 μF), R_m is the membrane resistance (200 MΩ), and I_E(t) and I_I(t) represent excitatory and inhibitory synaptic currents. Based on the anatomy of the circuit (Friedman and Hopkins 1998; Mugnaini and Maler 1987) and our recordings of Small Cell responses to square-pulse stimulation, we modelled two conditions: excitatory input in response to one stimulus edge with inhibitory input to the other edge; and separate excitatory inputs in response to both stimulus edges with inhibitory input to a single edge. We varied the latency of excitatory inputs from 0 to 10 ms, and we kept the inhibitory latency constant at 0 ms. This models excitatory latencies that vary from 0 to 10 ms relative to inhibitory latencies, which matches observed anatomical variation in axonal path lengths to Small Cells (Friedman and Hopkins 1998) and our observed spike latencies. We modelled all synaptic conductances as alpha functions (Dayan and Abbott 2001) using the equation

$$g_s(t) = \frac{g_{\max} t}{\tau_s} e^{(1-t/\tau_s)}$$

where g_s is the synaptic conductance, g_{max} is the maximum conductance, and τ_s is the time constant of the conductance. We set τ_E to 0.5 ms and τ_I to 1 ms, and g_{maxE} to 1 nS and g_{maxI} to 10 nS. These values were chosen so as to reflect inhibition that is slow and strong relative to excitation. Varying these parameters affected the specific quantitative output of the model, but did not affect the patterns of duration tuning observed when varying excitatory synaptic latency.

To incorporate the effects of long-pass peripheral filtering by knollenorgan electroreceptors on responses to variation in pulse duration (Lyons-Warren et al. 2012), we scaled synaptic conductances using a sigmoidal function

$$s(d) = \frac{1}{1 + e^{-40(d-0.1)}}$$

where d is stimulus duration and $s(d)$ is a scaling factor that varies from 0 to 1. The other parameters were set so as to replicate the general peripheral filtering observed among knollenorgans (Lyons-Warren et al. 2012).

The excitatory and inhibitory synaptic currents were determined from their respective conductances and driving forces as

$$I_s(t) = g_s(V_m - V_r)$$

where V_r is the reversal potential, which was set at +60 mV depolarized relative to rest for excitatory currents and -20 mV hyperpolarized relative to rest for inhibitory currents. We presented square-pulse stimuli of both polarities ranging in duration from 0.01 to 10 ms. We measured the maximum depolarization of each model neuron as a function of

duration and then characterized duration tuning by normalizing the responses of each model neuron to the maximum response. We also characterized the duration tuning of each neuron after removing the inhibitory input to simulate the effects of blocking inhibition on duration tuning.

Stereology counts. We used Stereo Investigator by MBF Bioscience to perform stereology counts of nELL and Small Cell somas from three fish ranging in size from 8.9 to 10.2 cm in standard length (Gundersen et al. 1988). We used 50 μm serial transverse sections from paraformaldehyde-fixed brain tissue stained with cresyl violet. We used every section that included nELL or ELa for generating counts, which ranged from a total of 19-21 sections with nELL and 12-15 sections with ELa. In each section, the region of interest was outlined. Counting grids and frames were selected based on the density and regularity of cells in the region of interest, using a counting grid of 125 μm x 125 μm for nELL and 150 μm x 150 μm for ELa. The optical fractionator selected a random box in each grid space at the specified counting frame of 100 μm x 100 μm for nELL and 50 μm x 50 μm for ELa. A counter was used to mark the cells of interest. The total number of counters was extrapolated based on the area of the tissue to determine the total number of cells. We repeated this procedure for the left and right nELL and ELa of each fish to estimate the total number of nELL and ELa somas. Gunderson's coefficient of error (m=1) was ≤0.05 for all counts (Gundersen et al. 1988). To estimate the number of nELL projections to Small Cells, we multiplied estimates of total nELL soma numbers in each fish by 1.1 to account for the ~10% of nELL neurons that project bilaterally to ELa (Friedman and Hopkins 1998), and then we multiplied this by 54.5, the median number

of Small Cells that individual nELL axons project to (Friedman and Hopkins 1998). We choose the median rather than the mean because only 4 nELL axons were systematically analyzed in this previous study (these 4 axons projected to 33, 44, 65 and 72 Small Cells). For each fish, we then determined the ratio of estimated nELL terminals to Small Cell somas.

Axonal labeling. After general anesthesia, two fish (one with a standard length of 6.4 cm and a second of 13.3 cm) were transcardially perfused with ice-cold Hickman's Ringer followed by 4% paraformaldehyde. The brains were post fixed for 24 hours at 4°C, and then removed from the skull. Dye was placed in the left and right nELL by inserting sharpened tungsten wires coated in DiI or DiO paste throughout the anterior-posterior extent of nELL. The brains were then embedded in a gelatin block and stored in 4% paraformaldehyde at 37-42ºC for 14-16 weeks to allow for dye transport. We cut 50 μm horizontal sections on a vibratome, washed them in 0.1 M phosphate buffer, and then stained cell nuclei using Hoechst 34580 (2 μg/ml, 5 min incubation at room temperature). Slices were wet mounted in 0.1 M phosphate buffer and cover slipped for imaging on a confocal microscope.

RESULTS

Targeted recordings from Small Cells

We obtained extracellular recordings from Small Cells using a retrograde labeling technique that allowed us to target individual axons (Fig. 1*A*, *B*) (Lyons-Warren et al. 2013). To determine whether excitatory inputs arose from ipsilateral or contralateral receptive fields and characterize their latency, we recorded responses of 70 units to 100 ms square-pulse stimuli presented in a transverse orientation. Although this duration is outside the behaviorally relevant range of EOD durations, it allowed us to distinguish responses to different stimulus edges. 30 units (42.9%) responded to contralateral-positive (down) edges, 17 (24.3%) responded to ipsilateral-positive (up) edges, and 23 (32.8%) responded to both edges. These numbers roughly agree with anatomical evidence showing twice as many axons from the contralateral vs. ipsilateral hindbrain (Szabo et al. 1983).

First spike latency (FSL), the median time from stimulus edge to the first spike, ranged from 2.2 to 39.8 ms (Fig. 1*C*). Time locked latency (TLL), the median time from stimulus edge to spikes that were time-locked to that edge, ranged from 2.2 to 13.4 ms (Fig. 1*C*). Some units did not respond with a time-locked spike on every stimulus repetition, skewing the FSL to an unreasonably high value due to spontaneous spiking (the reason for calculating TLL). Both distributions exceed the reported FSL values of 2.5-3 ms for incoming axons and Large Cells, the only other neurons in ELa (Amagai et al. 1998), further demonstrating that our recordings were from Small Cells. Based on an estimated conduction speed of 0.5 m/s for axons <1 μm in diameter (Waxman and

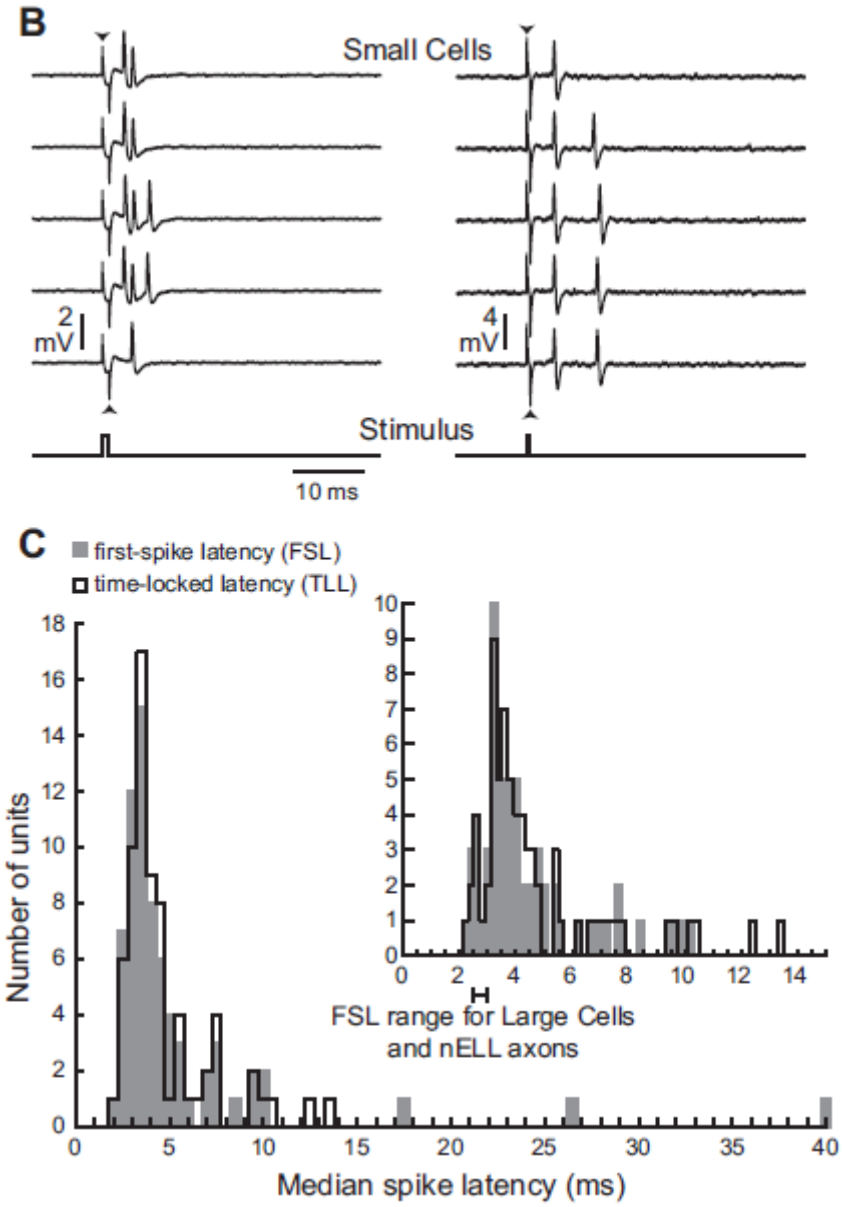

FIG 1: Retrograde labeling allows for visually guided extracellular recordings from Small Cell axons. (B) Extracellular recordings from two different Small Cell axons, one showing responses to a 1 ms, 18.4 mV/cm stimulus (left) and a second showing responses to a 0.5 ms, 10 mV/cm stimulus (right). The stimuli are shown in the bottom trace, and stimulus artifact can be seen at stimulus onset and offset (black arrowheads). (C) Histogram of median first-spike latencies (FSL, gray) and time-locked latencies (TLL, black) from the stimulus edge (bin size = 0.5 ms). Inset shows the same result at a finer resolution (bin size = 0.2 ms) for the subset of latencies ranging from 1-15 ms. Large Cells and nELL axons have a FSL range of 2.5-3 ms (Amagai et al. 1998).

Bennett 1972) and axon lengths up to 7 mm (Friedman and Hopkins 1998), we calculated a 14 ms maximum latency difference for excitatory inputs to Small Cells, close to the observed range of TLL values (11.2 ms). In small diameter axons, increased axonal length results in increased temporal jitter (Wang et al. 2008). Therefore, if differences in TLL are due to variation in the lengths of nELL axons, units with higher TLL should have increased jitter. Indeed, median TLL was positively correlated with TLL standard deviation for all units that responded with at least 1 spike/stimulus (linear regression: n=68, r^2=0.34, P<0.00001).

Small Cells are diverse in their responses to peripheral spike timing differences

We used monophasic square pulses of different durations to measure Small Cell responses to variation in peripheral spike timing differences. Although square pulses do not capture the complexity of natural EOD waveforms, they can be used to precisely manipulate the relative timing of KO receptor spikes on opposite sides of the body (Fig. 1*A*). Further, square pulses that elicit the same KO spike timing differences as a natural conspecific EOD elicit similar behavioral responses (Hopkins and Bass 1981).

We presented square pulses of both positive and negative polarity ranging in duration from 1 μs to 90 ms at 1 (n=40), 2 (n=16) or ≥3 (n=11) intensities. We illustrate the resulting duration tuning curves using two plots, one on the left representing negative polarity square pulses and one on the right representing positive polarity square pulses (Fig. 2). The x-axis of the negative polarity plot on the left is reversed (duration increases to the left). Presented in this way, the two x-axes can be viewed as a single axis that

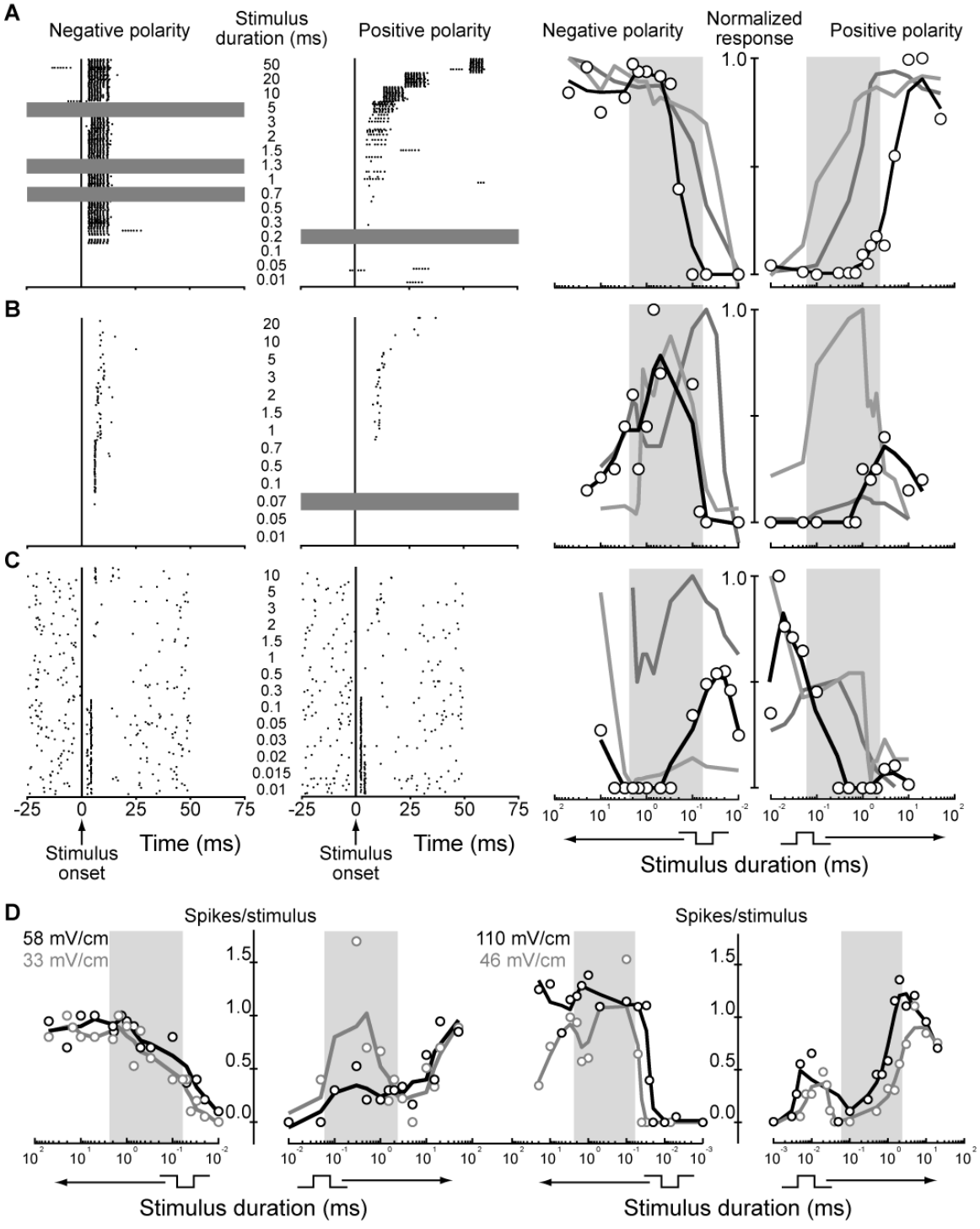
A
Negative polarity
Stimulus duration (ms)
Positive polarity
Negative polarity
Normalized response
Positive polarity
50
20
10
5
3
2
1.5
1.3
1
0.7
0.5
0.3
0.2
0.1
0.05
0.01
1.0
B
20
10
5
3
2
1.5
1
0.7
0.5
0.1
0.07
0.05
0.01
C
10
5
3
2
1.5
1
0.5
0.3
0.1
0.05
0.03
0.02
0.015
0.01
-25
0
25
50
75
Stimulus onset
Time (ms)
Stimulus duration (ms)
D
Spikes/stimulus
58 mV/cm
33 mV/cm
110 mV/cm
46 mV/cm
1.5
1.0
0.5
0.0

FIG 2: Small Cells are diverse in their tuning to peripheral spike timing differences. Raster plots (left) and smoothed tuning curves (right) from representative long-pass Small Cells (*A*) that responded preferentially to longer square-pulse durations, band-pass Small Cells (*B*) that responded preferentially to intermediate durations, and band-stop Small Cells (*C*) that responded preferentially to long and short durations. Rasters show spike times in response to 20 sweeps of each stimulus for both monophasic negative (left portion of raster) and positive (right portion of raster) stimuli (gray horizontal shading indicates durations not tested). Time is relative to stimulus onset. Responses were quantified as the mean number of spikes above baseline per stimulus repetition. The resulting data points (open circles in right panels) were then scaled to the maximum value within the unit and smoothed (black lines in right panels). In each case, smoothed tuning curves from two additional units of the same tuning type (light and dark gray) are also shown. The duration tuning curves are plotted on two axes, one on the left for negative polarity and one on the right for positive polarity, with the x-axis of the negative polarity plot reversed (stimulus duration increases to the left). Together, the two plots can be viewed as sharing a single x-axis that represents the relative timing of upward and downward stimulus edges. Gray background shading on tuning curves indicates the behaviorally relevant range of durations (Lyons-Warren et al. 2012). *D*: Tuning curves (not normalized) of example units that changed tuning with changes in intensity (left) and polarity (both).

represents the relative timing of upward and downward stimulus edges. 46 units had consistent duration tuning to all polarities and intensities tested that elicited a response: 35 (76%) were long-pass tuned (Fig. 2*A*), 6 (13%) were band-pass tuned, (Fig. 2*B*), and 5 (11%) were band-stop tuned (Fig. 2*C*). 20/62 units tested at both polarities (32%) had different duration tuning to positive and negative polarity stimuli (e.g. Fig. 2*D*); long-pass paired with non-long-pass was the most common (*n*=18). Of 27 units tested at multiple intensities, 16 (59%) changed their tuning with changes in intensity (e.g. Fig. 2*D*).

For most units, responses varied widely over the behaviorally relevant range of durations (Fig. 2), defined as the duration of the shortest EOD phase (60 μs) to the longest total EOD duration (2.37 ms) among conspecific EODs (Carlson et al. 2000). This represents the total possible range of KO receptor spike timing differences in response to conspecific EODs (Lyons-Warren et al. 2012). To determine how much Small Cell responses varied across this behaviorally relevant range, we calculated the difference between the minimum and maximum responses within this range for all tuning curves (*n*=220). On average, responses varied within the behaviorally relevant range by 1.17 ± 0.08 spikes/stimulus (range = 0-6.94 spikes/stimulus).

Primary electroreceptors (KOs) are long-pass tuned at threshold intensities (Lyons-Warren et al. 2012). We confirmed that KOs are also long-pass tuned at higher intensities (not shown). Thus, Small Cell duration tuning is more diverse than receptor duration tuning. Further, Small Cells are the first place in the circuit where inputs from

widely separated receptive fields converge. We therefore hypothesized that Small Cell duration tuning results from integrating multiple synaptic inputs.

Small Cell responses to complex stimuli suggest precisely timed inhibition

We hypothesized that Small Cells receive precisely timed inhibition from Large Cells based on several lines of evidence: Large Cell axons give rise to large, calyceal synapses onto Small Cell somas (Friedman and Hopkins 1998; Mugnaini and Maler 1987); Large Cells are GABAergic (George et al. 2011; Mugnaini and Maler 1987); and Large Cells respond to stimulus edges with a single, short-latency, time-locked spike (Amagai et al. 1998; Friedman and Hopkins 1998). We used a complex stimulus protocol to test for inhibition in response to the stimulus edge that did not elicit spiking. We presented a 50 ms stimulus that elicited an excitatory response to the leading edge, followed by a shorter pulse at a range of delays following the trailing edge (Fig. 3*A*, *top*). A response was consistently seen following the first edge of the long pulse. However, a response to the leading edge of the second pulse only occurred for sufficiently long delays. We determined the minimum delay where the magnitude of the response to the second pulse was >50 % of the response to the first pulse, which varied from 0.1 to 25 ms (Fig. 3*B, asterisks*). As a control, we presented a 100 ms pulse with a second overlapping pulse such that the 'excitatory' edges were presented at the same intervals as in the paired pulse experiment, but without an 'inhibitory' edge between them (Fig. 3*A*, *bottom*). In this case, the response to the second pulse was >50% of the response to the first pulse at all "delays" tested (Fig. 3*B*).

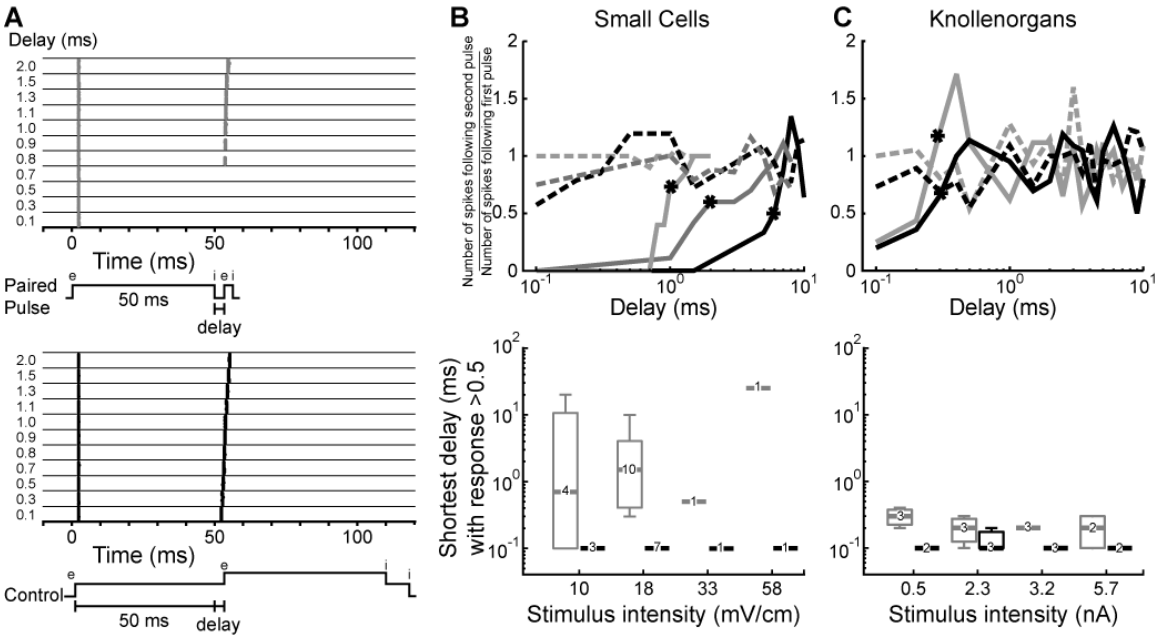

FIG 3: Paired pulse stimuli suggest functional inhibition of Small Cells elicited by the non-responsive stimulus edge. *A*: Representative rasters of the spiking responses of an individual Small Cell to electrosensory stimulation in paired pulse (*top*) and control (*bottom*) experiments. Time locked spikes occur following presumed excitatory edges (labeled 'e'). The test pulse was presented at varying delays following the presumed inhibitory edge (labeled 'i'). *B*: Responses to the paired pulse (solid) and control (dashed) experiments from three representative units showed a failure to respond to the test pulse at varying delays. Asterisks indicate shortest delays with a response >50%. Box plots showing medians, quartiles, and ranges of shortest delays with a response >50% for all units tested in response to paired pulse (gray) and control (black) across 4 different intensities are shown below (numbers refer to sample size for each condition). *C*: Responses to the paired pulse (solid) and control (dashed) experiments from two representative knollenorgans along with a box plot summary from all recorded knollenorgans below.

We performed the same experiment on KOs. KO responses to the second pulse were also blocked at short delays, but these delays were much shorter than those of Small Cells (Fig. 3*C*). Therefore, the blocking of Small Cell responses cannot be explained by peripheral effects, supporting the hypothesis that Small Cells receive inhibitory input in response to one edge of a stimulus that is strong enough to block responses to excitatory inputs. It is not clear why different Small Cells had 'inhibitory' windows of different durations, but this could reflect differences in excitatory latency, differences in the time course of IPSPs, and/or differences in intrinsic physiology. The relatively short delays over which KO responses were reduced were likely due to the direct integration of depolarizing and hyperpolarizing currents by KOs. KOs act as AC filters that respond to changes in current intensity (Bennett 1965). Thus, the trailing edge of a depolarizing current pulse results in a transient hyperpolarization and decrease in excitability, which would reduce responses to a depolarizing current pulse delivered after a short delay.

GABAergic inhibition reduces spontaneous activity and blocks responses to excitatory input

To directly test whether Small Cells receive functional GABAergic inhibition from Large Cells, we bath applied SR-95531 (gabazine), a competitive antagonist of $GABA_A$ receptors, to the cavity surrounding ELa (Fig. 4*A*). We tested 7 units with vehicle: 6 of these had no spontaneous activity before vehicle application, whereas one had relatively high spontaneous activity (Fig. 4*B*). After applying vehicle, the 6 units without spontaneous activity remained silent (Fig. 4*B*), and there was no significant

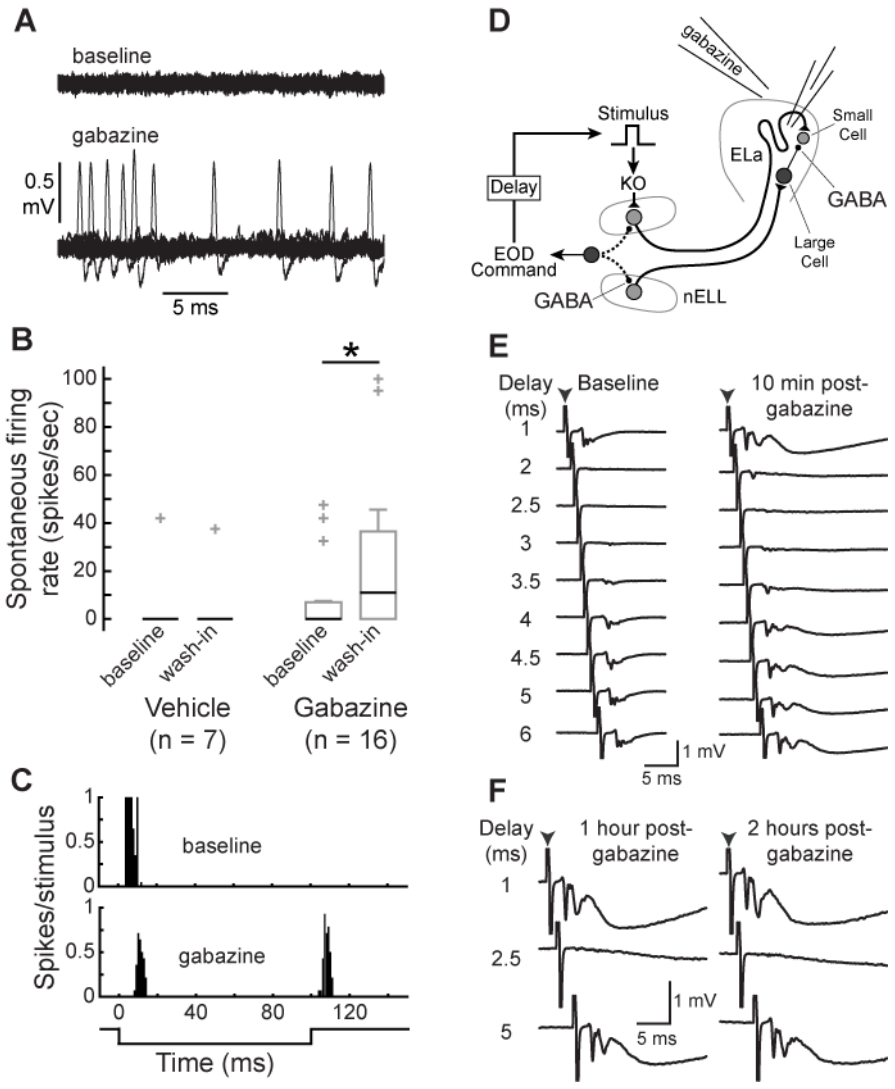

FIG 4: Gabazine affects Small Cell activity due to local actions in ELa. A: Example of increased spontaneous firing rate of a Small Cell after gabazine application. Twenty repetitions of a 25 ms recording of spontaneous activity are superimposed, revealing an average spontaneous firing rate of 0 spikes/second under baseline conditions (top) and 20 spikes/second after gabazine application (bottom). B: Box plots showing spontaneous firing rates of Small Cells (median is in black; quartiles, non-outlier range, and outlier data points are in grey) before and after application of gabazine or vehicle revealed a significant increase following gabazine application (Wilcoxon matched pairs test: n=16, z=2.4, P<0.05), but not vehicle application (Wilcoxon matched pairs test: n=7, z=0, P=1). C: Representative peri-stimulus histogram of spike times in response to a 100 ms stimulus before (top) and after (bottom) gabazine application from a single unit shows a response to one edge under baseline conditions, but a response to both edges in the absence of inhibition. D: Schematic representation of the knollenorgan pathway leading

up to Small Cells, illustrating the locations of GABAergic synapses and an experiment to test whether gabazine application to ELa affects GABAergic transmission in the hindbrain. The electromotor command that initiates EOD production also triggers inhibitory GABAergic input to the hindbrain nELL through a corollary discharge pathway (dotted lines). This command-triggered inhibition blocks sensory responses in nELL for a brief window of time after each EOD. To assess functional inhibition in nELL, we delivered a sensory stimulus at different delays after the EOD command while recording evoked field potentials in ELa before and after delivering gabazine to the cavity surrounding ELa. E: Evoked potentials recorded in ELa in response to a stimulus (0.5 ms, 20 mV/cm, arrowhead indicates stimulus artifact) are blocked at delays of 2 to 4 ms both before (left) and 10 minutes after (right) gabazine application, indicating that gabazine is not reaching the hindbrain GABA receptors. F: Responses are still blocked at delays of 2 to 4 ms after 1 (left), 2 (right), and 5 (not shown) hours following gabazine application.

change in spontaneous activity (Wilcoxon matched pairs test: n=7, z=0, P=1). We tested 16 units with gabazine: 11 of these had no spontaneous activity before gabazine application, but only 5 of them remained silent after gabazine application (Fig. 4*B*). Thus, gabazine caused a significant increase in the spontaneous activity of Small Cells (Wilcoxon matched pairs test: n=16, z=2.4, P<0.05), suggesting they are tonically inhibited at rest. In addition, of three units that responded to only one edge of the 100 ms stimulus prior to gabazine application, two responded to both edges after gabazine application (e.g. Fig. 4*C*). This suggests the existence of an excitatory input in response to one of the edges that was previously masked by inhibition.

Changes in Small Cell activity following application of gabazine could be due to effects on GABAergic synapses onto Small Cells or GABAergic synapses in the hindbrain nucleus of the electrosensory lateral line lobe (nELL) (Figs. 1*A*, 4*D*). In nELL, GABAergic inhibition triggered by the electromotor command blocks responses to the fish's own EOD (Bell and Grant 1989). Although the fish were paralyzed during our experiments and therefore could not emit EODs, we could record the spinal motor neuron activity representing a fictive EOD (Carlson 2003). To determine whether gabazine application affected GABAergic synapses in nELL, we recorded evoked potentials in ELa in response to a stimulus pulse presented at a range of delays after the fictive EOD (Fig. 4*D*). Under baseline conditions, the evoked potential was blocked when the stimulus was presented 2-4 ms after the fictive EOD (Fig. 4*E*), due to the command-triggered GABAergic inhibition in nELL. Following application of gabazine, this evoked potential became larger and longer lasting, but it was still blocked at delays of 2-4 ms

following the fictive EOD (Fig. 4*E*), even several hours after gabazine application (Fig. 4*F*). Therefore, the effects of gabazine application on Small Cell activity were limited to local actions within ELa. Large Cells are the only GABAergic neurons in ELa, and their projections are limited to within ELa (Friedman and Hopkins 1998; George et al. 2011; Mugnaini and Maler 1987). Thus, we conclude that the effects of gabazine application on Small Cell activity are due to blocking inhibition at the Large Cell to Small Cell synapse.

Some Small Cells receive multiple excitatory inputs

Both mammalian and avian sound localization depends critically on binaural excitatory inputs converging onto time comparator neurons (Ashida and Carr 2011; Köppl 2009; Schnupp and Carr 2009). We found that 23 out of 70 units (32.8%) exhibited a spiking response to both edges of 100 ms stimuli, suggesting that some Small Cells likewise receive convergent excitatory inputs originating from the left and right sides of nELL (e.g. Fig. 5*A*). In some cases, application of gabazine unmasked responses to both stimulus edges (e.g. Fig. 4*C*). If responses to both edges are driven by excitatory inputs from different axons, each with its own delay, then we would expect no correlation in response latency (TLL) to each edge, which was indeed the case (Fig. 5*B*; linear regression: n=23, r^2=0.02, P>0.4).

To determine whether ELa anatomy would allow for multiple excitatory inputs to individual Small Cells, we used stereology (Gundersen et al. 1988) to estimate the total numbers of nELL neurons and Small Cells. Combined with data showing that ~10% of nELL axons project bilaterally to ELa and that each axon terminates on ~54.5 Small

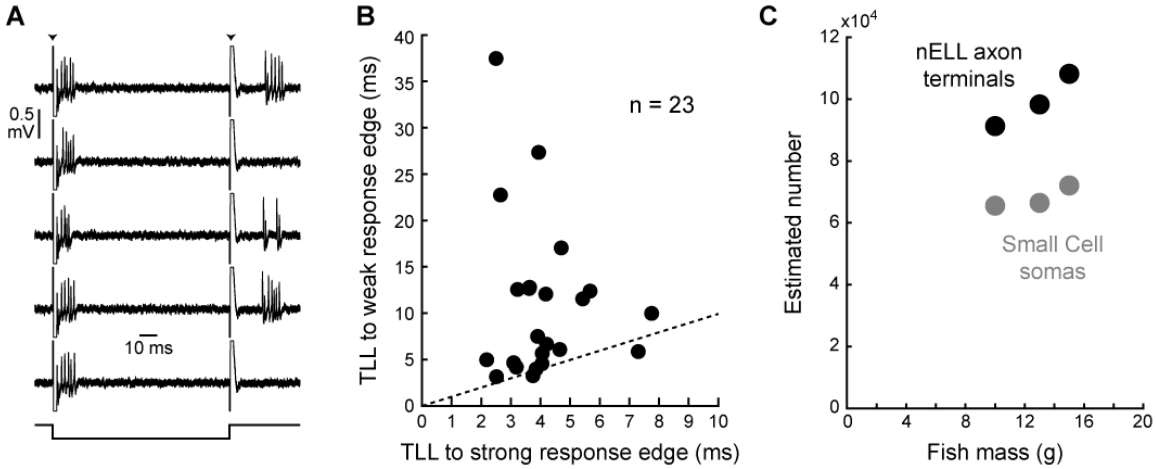

FIG 5: Some Small Cells receive multiple excitatory inputs from different receptive fields. A: An example of a unit that responded to both positive-going and negative-going stimulus edges, with different latencies and response strengths. The stimulus (100 ms, 32.6 mV/cm) is shown in the bottom trace, and stimulus artifact can be seen at stimulus onset and offset (black arrowheads). B: TLL in response to the edge eliciting a higher magnitude response (strong) was not correlated with TLL to the other edge (weak) (linear regression: n=23, r2=0.02, P>0.4). Dotted line is 1:1. C: Estimated numbers of Small Cells and nELL axon terminals onto Small Cells from three fish. The numbers of Small Cells and nELL somas from both sides of the brain were estimated using stereology, and the numbers of axon terminals per nELL soma were estimated using published data on nELL axonal projection patterns (Friedman and Hopkins 1998), as described in the Materials and Methods.

Cells (Friedman and Hopkins 1998), the estimated ratio of nELL terminals to Small Cell somas ranged from 1.4 to 1.5 (Fig. 5*C*), suggesting that individual Small Cells receive 1-2 excitatory inputs each.

To further test whether Small Cells receive multiple excitatory inputs from different receptive fields, we stained the left and right nELLs with different lipophilic dyes. This resulted in densely labeled fiber tracts projecting into ELa and allowed us to distinguish contralateral from ipsilateral axons (Fig. 5*D*, *E*). Small Cells are adendritic, and all synaptic inputs to them are therefore on the soma (Friedman and Hopkins 1998; Mugnaini and Maler 1987). Because of their small size, the nuclei of Small Cells are located within <2 μm of the cell membrane (Mugnaini and Maler 1987). Thus, we used a nuclear stain to identify Small Cells scattered throughout ELa, and identified putative synaptic inputs as closely apposed nuclear and punctate axonal stain (Fig. 5*D*, *E*). Electron microscopic studies have demonstrated that about 80% of putative synapses identified on the basis of axonal puncta located close to the cell membrane are functional synapses (Feldmeyer et al. 2006; Feldmeyer et al. 2002; Lübke et al. 1996; Markram et al. 1997; Mishchenko et al. 2010; Wang et al. 2002). Using this criterion, we found several labeled Small Cells that appeared to receive synaptic inputs from both sides of nELL (Fig. 5*D*, *E*), providing an additional piece of evidence for the convergence of bilateral excitatory inputs onto Small Cells.

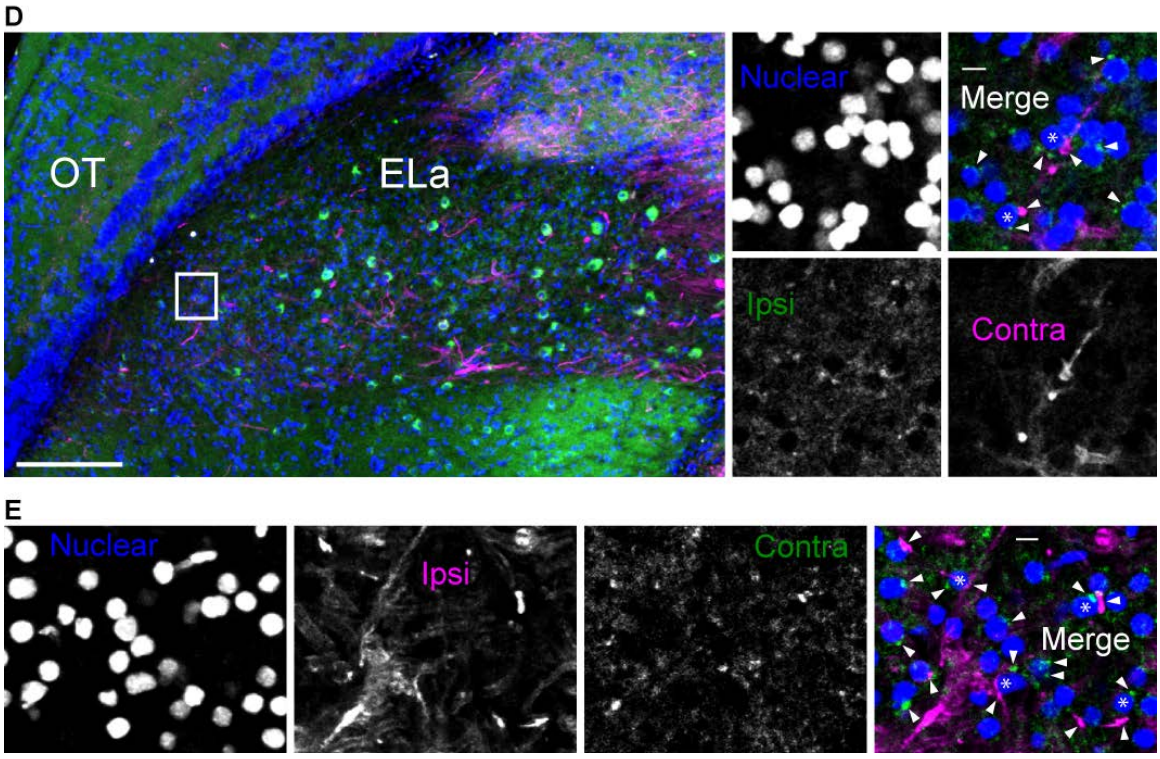

FIG 5: Some Small Cells receive multiple excitatory inputs from different receptive fields. D: Ipsilateral nELL axons labeled with DiO (green) and contralateral nELL axons labeled with DiI (magenta) colocalized adjacent to individual Small Cell somas (blue) in the left ELa. The large image to the left shows ELa based on a maximum intensity projection from six 2.53-µm slices (Scale bar = 100 µm). The adjacent optic tectum (OT) also had labeled axons, likely due to labeling of hindbrain regions other than nELL during dye injection. The smaller images to the right show an expanded view of the enclosed box, illustrating colocalization of ipsilateral and contralateral nELL terminals next to Small Cell nuclei, based on a maximum intensity projection from two 1.14-µm slices (Scale bar = 5 µm). Arrowheads indicate putative synaptic boutons, asterisks indicate Small Cell nuclei where putative ipsilateral and contralateral boutons colocalized. E: Labeled axons and Small Cell nuclei from the right ELa of the same brain, based on a maximum intensity projection from four 1.14-µm slices (Scale bar = 5 µm).

Variation among Small Cells can be explained by differences in excitatory latency

Unlike the long, winding projections from nELL axons to Small Cells, the inputs from nELL axons to Large Cells and from Large Cells to Small Cells are both direct (Friedman and Hopkins 1998). This suggests that inhibitory latencies are relatively uniform among Small Cells and that variation in duration tuning is determined primarily by differences in excitatory latency. Axonal delay lines to Small Cells (Friedman and Hopkins 1998) and our observed spike latencies (Fig. 1*C*) suggest that excitatory latencies can vary from about 0 to 10 ms relative to Large Cell latencies. Finally, some Small Cells appear to receive separate excitatory inputs in response to the two stimulus edges (Fig. 5). To determine whether these features of synaptic input to Small Cells could explain the observed diversity of duration tuning, we modeled Small Cells as leaky integrator neurons receiving excitatory and inhibitory synaptic inputs with different relative latencies (Fig. 6). Each model neuron received excitatory input in response to one stimulus edge, and either inhibitory input or both excitatory and inhibitory input in response to the other stimulus edge. We varied the excitatory latencies from 0 to 10 ms relative to the inhibitory latency (set at 0 ms), and we scaled the inhibitory conductances to be larger and longer lasting than the excitatory conductances (see Materials and Methods for details). Finally, we incorporated a long-pass filter of duration that scaled the synaptic conductances to simulate the observed peripheral filtering imposed by KO electroreceptors (Lyons-Warren et al. 2012).

The resulting model neurons had the same types of duration tuning observed among actual Small Cells, including long-pass, band-pass, and band-stop. None of the

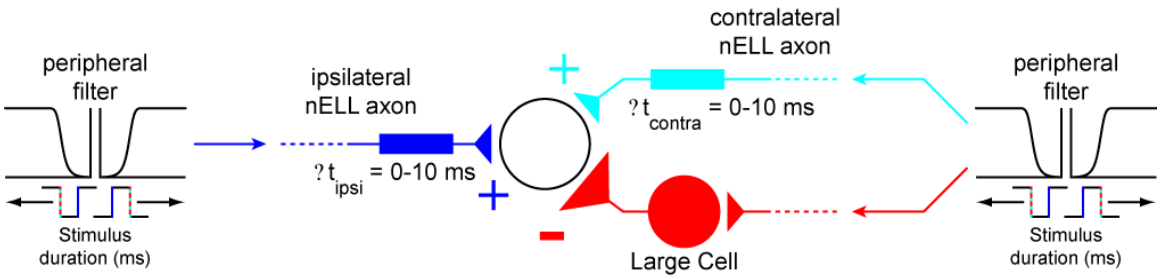

FIG 6: Schematic illustrating the modeling of synaptic integration by Small Cells. Each cell was modeled as a leaky integrator neuron that received excitation in response to the rising stimulus edge (ipsilateral), and either inhibition only or inhibition plus excitation in response to the falling stimulus edge (contralateral). Inhibitory latencies were set at 0 ms, and excitatory latencies (Δt_{ipsi} and Δt_{contra}) were varied from 0 to 10 ms. Synaptic conductances were simulated as alpha-functions (see Materials and Methods for details). These conductances were passed through a sigmoidal filter that modeled the effects of peripheral long-pass filtering by knollenorgans, thereby reducing synaptic input strength at short durations.

model cells responded to short durations because of the long-pass peripheral filter. Variation in responses to longer durations among model neurons was caused by differences in excitatory latency, which determined which stimulus durations resulted in overlapping excitation and inhibition, and in the case of model neurons with two excitatory inputs, overlapping excitatory inputs in response to the two edges. To illustrate, we show simulation traces for three different stimuli along with duration tuning curves under three different scenarios (Fig. 7*A*): ipsilateral excitation (7 ms latency) with contralateral inhibition (0 ms latency) but no contralateral excitation (*left*); ipsilateral excitation (7 ms latency) with contralateral inhibition (0 ms latency) and contralateral excitation (0 ms latency) (*middle*); and ipsilateral excitation (7 ms latency) with contralateral inhibition (0 ms latency) and contralateral excitation (5 ms latency) (*right*). The arrowheads above the duration tuning curves correspond to the example traces shown above.

Figure 7*B* shows heat maps that illustrate how duration tuning changes with variation in ipsilateral excitatory latency for model neurons under three different scenarios: ipsilateral excitation with contralateral inhibition (0 ms latency) but no contralateral excitation (*left*); ipsilateral excitation with contralateral inhibition (0 ms latency) and contralateral excitation (0 ms latency) (*middle*); and ipsilateral excitation with contralateral inhibition (0 ms latency) and contralateral excitation (5 ms latency) (*right*). In each heat map, the x-axis shows stimulus duration, the y-axis shows ipsilateral excitatory latency, and the color indicates normalized synaptic response. The asterisks to the right of each heat map correspond to the ipsilateral excitatory latencies of the example

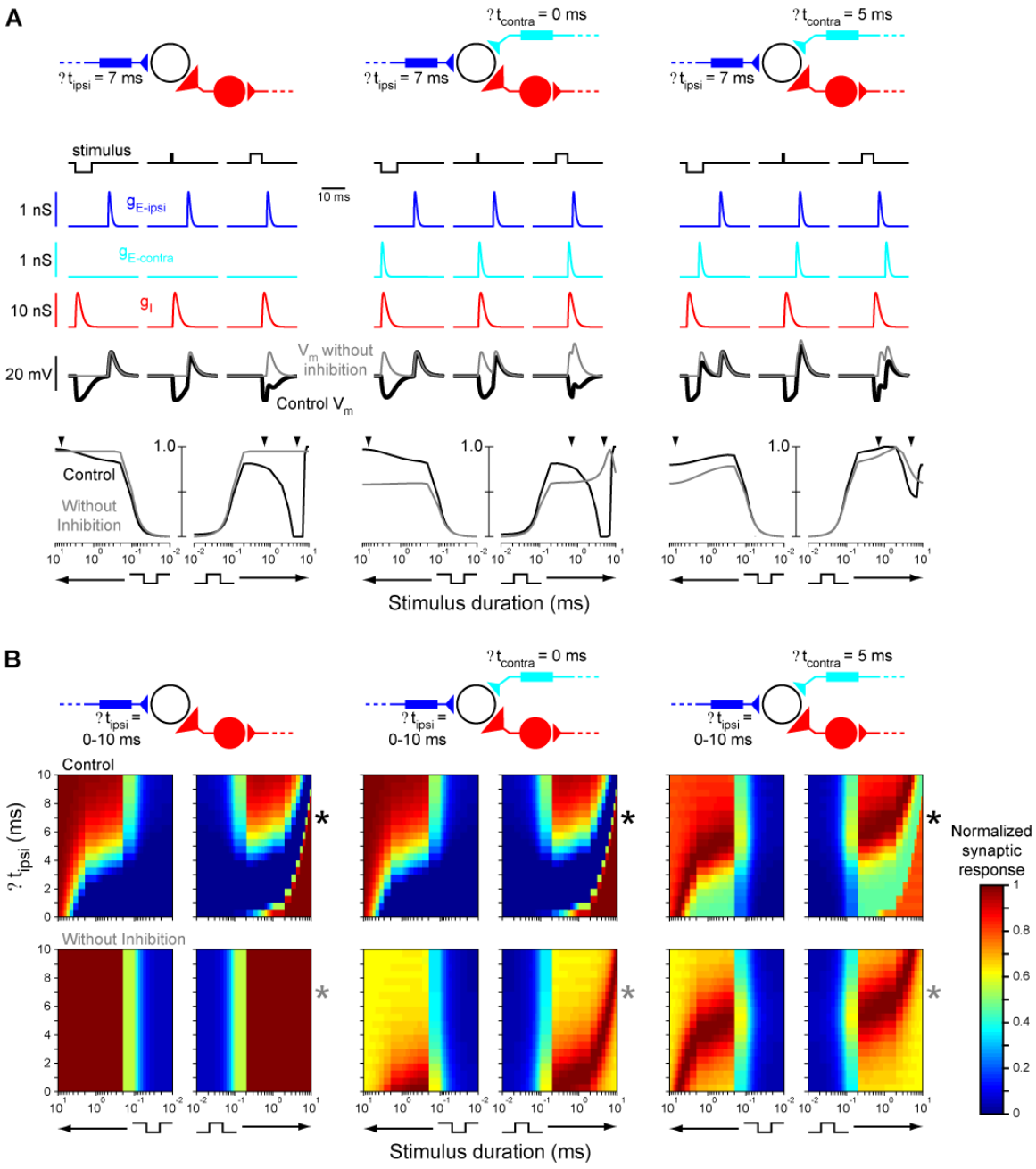

FIG 7: Model neurons that integrate inhibition in response to one stimulus edge and variably delayed excitation in response to one or both stimulus edges recreate the diversity in duration tuning observed among Small Cells.

(A) Example simulation traces and duration tuning curves from three model neurons, each having ipsilateral excitation with Δt_{ipsi} = 7 ms and contralateral inhibition with 0 ms latency. The model neuron in the left panel does not receive contralateral excitatory input. The other two model neurons receive contralateral excitation with Δt_{contra} set at 0 ms (middle panel) or 5 ms (right panel). For all three model neurons, synaptic conductances (gE-ipsi in blue, gE-contra in cyan, gI in red) and membrane potential (control Vm in black, Vm without inhibition in grey) are shown in response to a 7 ms reversed polarity stimulus (left), 0.7 ms normal polarity stimulus (middle), and 5 ms normal polarity stimulus (right). Changes in stimulus duration alter the relative timing of different synaptic inputs, and the stimulus durations at which these inputs overlap are determined by their relative latencies. The duration tuning curves show the normalized response of each model neuron for both stimulus polarities for durations ranging from 0.01 to 10 ms under control conditions (black) and after removing the inhibitory input (gray). Arrowheads indicate the durations corresponding to the sample traces shown above. (B) Duration tuning changes with variation in excitatory latency. The left panel shows the tuning of model neurons that receive ipsilateral excitation and contralateral inhibition only, with Δt_{ipsi} varying from 0 to 10 ms. The other two panels show the tuning of model neurons that also receive contralateral excitation with Δt_{contra} set at 0 ms (middle panel) or 5 ms (right panel). In the heat maps, the x-axis represents stimulus duration (right plot = normal polarity, left plot = reversed polarity) and the y-axis represents Δt_{ipsi}. Thus, each row represents the duration tuning of a single model neuron with a given Δt_{ipsi}, with responses normalized to its maximum response and colored as indicated in the scale to the right. The lower plots illustrate duration tuning of the same model neurons after removing the inhibitory synaptic input. The asterisks indicate the Δt_{ipsi} (7 ms) that corresponds to the example traces and tuning curves shown in (A).

model neurons shown in Figure 7*A*.

Long-pass tuning was always observed at relatively short excitatory latencies, whereas band-pass and band-stop tuning were only observed at longer excitatory latencies (Fig. 7*B*). When there is a relatively short excitatory latency, contralateral inhibition will block excitation at short stimulus durations (Fig. 8*A, top*). With longer excitatory latencies, however, inhibition and excitation can interact at longer durations, thereby establishing more complex patterns of tuning (Fig. 8*A, bottom*). To see whether this prediction held for recordings from actual Small Cells, we analyzed the relationship between TLL and duration tuning. Extracellular recording does not allow for a direct determination of synaptic latency, but TLL can serve as a proxy for excitatory latency. When considering the units that only responded to one stimulus edge, the TLL of long-pass tuning curves (n=68) was significantly shorter than the TLL of band-pass (n=11) and band-stop (n=17) tuning curves (Kruskal-Wallis ANOVA: $H_{2,96}$=14.6, P<0.001), as predicted by our model (Fig. 8*B*).

For long-pass tuning curves with relatively short excitatory latencies, our model also predicted differences in tuning curve shape depending on whether excitation was to the leading or trailing edge (Fig. 7*B*, compare opposite polarity stimuli). When excitation is to the trailing edge of the stimulus, a longer stimulus duration is required to elicit a response compared to when excitation is to the leading edge of the stimulus. The reason for this is that when excitation leads inhibition, the stimulus only needs to be long enough for the excitation to arrive before the onset of inhibition (Fig. 8*C, top*). When excitation trails inhibition, however, the stimulus needs to be long enough for the excitation to

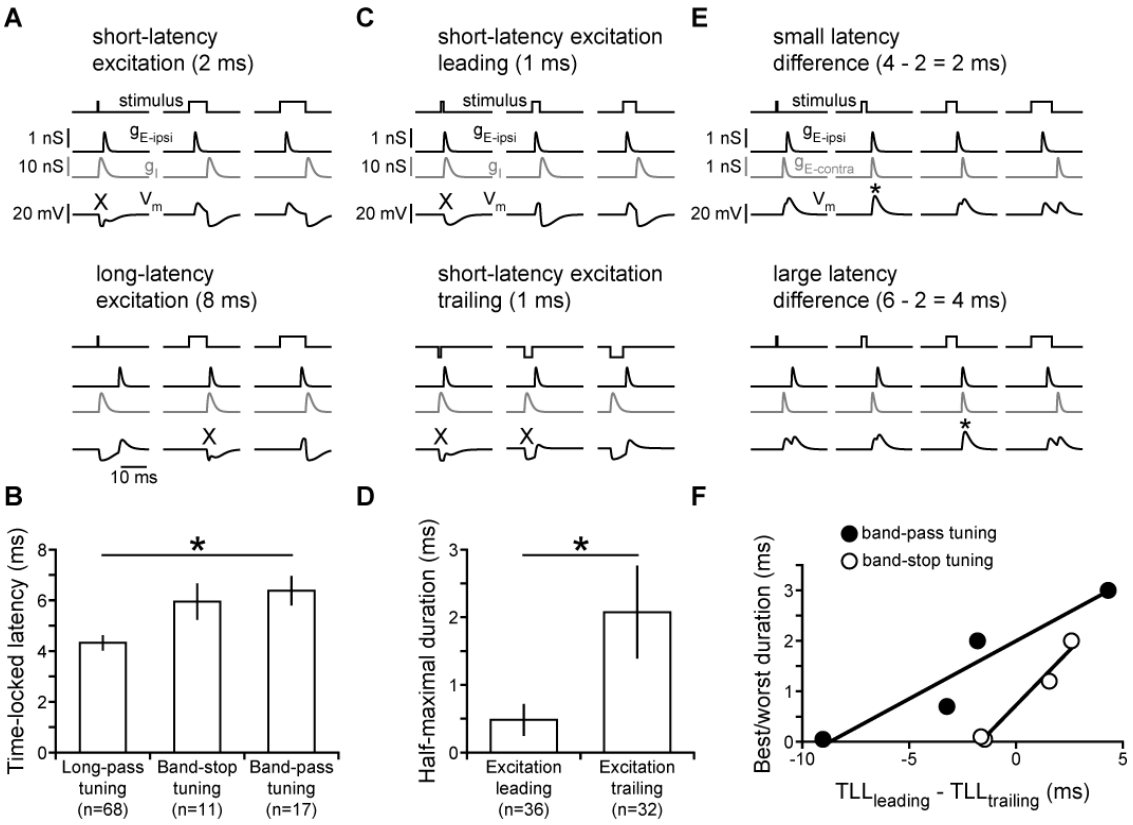

FIG 8: Responses to peripheral spike timing differences are determined by the relative latency of excitation and inhibition. (*A*) Model simulations illustrating how short-latency excitation combined with contralateral inhibition gives rise to long-pass tuning (*top*), whereas long-latency excitation combined with contralateral inhibition gives rise to band-stop tuning (*bottom*) (*B*) As predicted by the model, long-pass tuning curves of actual recorded units had significantly shorter TLL than band-stop or band-pass tuning curves (Kruskal-Wallis ANOVA: $H_{2,96}$=14.6, P<0.001). (*C*) Model simulations illustrating how reversing the sequence of excitation and inhibition by changing stimulus polarity results in responses to shorter durations when excitation is leading (*top*) compared to when excitation is trailing (*bottom*). For A and C, 'X' shows stimuli for which excitation is blocked by inhibition, resulting in responses <50% of maximum. (*D*) As predicted by the model, long-pass tuning curves of actual recorded units had a significantly shorter minimum duration for eliciting a half-maximal response when excitation was to the trailing, rather than leading, edge of the stimulus (Mann-Whitney U test: z=3.5, P<0.001). (*E*) Model simulations illustrating how variation in the relative latencies of two excitatory inputs leads to different durations at which these two inputs are coincident, resulting in the strongest response (asterisks). (*F*) As predicted by the model for units that responded to both edges, the difference between the TLL of each excitatory edge was significantly correlated with the best duration of band-pass tuning curves (linear regression: r^2=0.90, P<0.05) and worst duration of band-stop tuning curves (linear regression: r^2=0.97, P<0.05).

arrive after the inhibitory synaptic potential has ended (Fig. 8*C, bottom*). To test this hypothesis in our recordings from actual Small Cells, we compared the minimum duration where responses reached >50% of the maximal response for stimulus polarities in which excitation was to the leading or trailing edge. As predicted by our model, the half-maximal duration of excitation-leading long-pass tuning curves (n=36) was significantly shorter than the half-maximal duration of excitation-trailing long-pass tuning curves (n=32) (Fig. 8*D*; Mann-Whitney U test: z=3.5, P<0.001).

In our model neurons, interactions between separate excitatory inputs to the two stimulus edges also contributed to complex patterns of duration tuning such as band-pass and band-stop tuning (Fig. 7). This is because excitation will be maximal for stimulus durations that cause these two excitatory inputs to arrive simultaneously (Fig. 8*E*). Therefore, in our recordings from actual band-pass and band-stop Small Cells that responded to both edges, we compared the difference in TLL to the two edges with their 'best' and 'worst' stimulus durations, respectively (Fig. 8*F*). Despite the small number of units that met these criteria (n=4 each), there was a significant correlation between difference in TLL and best duration of band-pass units (linear regression: r^2=0.90, P<0.05), as well as worst duration of band-stop units (linear regression: r^2=0.97, P<0.05). Thus, several predictions of our computational model are supported by correlations between TLL and duration tuning among Small Cells, supporting the hypothesis that variation in excitatory latency contributes to the wide diversity of Small Cell tuning that we observed. It is important to note, however, that Small Cells may also differ in other respects, including passive and active membrane properties as well as the strengths and

time courses of excitatory and inhibitory synaptic currents. In the absence of intracellular recordings, it is not yet possible to evaluate the potential contribution of these factors to variation in Small Cell tuning.

Stimulus-driven feed-forward inhibition shapes Small Cell responses to peripheral spike timing differences

To directly test the role of GABAergic inhibition from Large Cells in establishing Small Cell duration tuning, we quantified tuning before and after gabazine application. Due to space constraints, susceptibility of recordings to mechanical disturbance during drug delivery, and normal difficulties with maintaining stable long-term recordings, it was difficult to hold a unit long enough to get complete tuning curves after drug application. Nevertheless, we were able to collect a total of 32 tuning curves from 5 units after gabazine application. The multiple tuning curves from each unit included tuning curves to both stimulus polarities, as well as to different stimulus intensities, but not repetitions of the same polarity and intensity.

Our modeling results predict that different patterns of duration tuning result from inhibition blocking excitation at different stimulus durations, due to variation in excitatory latency. For long-pass neurons with relatively short excitatory latencies, our model predicts that inhibition blocks excitation only at short durations, thereby increasing the minimum duration for eliciting a response (Figs. 7*B*, 8*A*). Thus, after removing inhibition from long-pass model neurons, there was a decrease in the minimum duration for eliciting a response (Fig. 7*B*). In recordings from actual long-pass units, blocking

inhibition by applying gabazine had a similar effect, leading to increased responses to short stimulus durations (Fig. 9*A*). Among all long-pass tuning curves tested, gabazine application resulted in a significant decrease in the minimum stimulus duration that elicited a response greater than 50% of the maximum response (Fig. 9*A*; Wilcoxon matched pairs test: n=16, z=2.9, P<0.01). This supports our model prediction that inhibition contributes to long-pass tuning by blocking responses to short duration stimuli.

For band-pass and band-stop neurons with relatively long excitatory latencies, our model predicts that inhibition blocks excitation at longer durations (Figs. 7*B*, 8*A*). Overall, this results in weak responses to the shortest durations due to the peripheral filter, increasing responses as duration increases, and then decreasing responses due to inhibition as duration increases further (Fig. 7*B*). Thus, after removing inhibition from band-pass and band-stop model neurons, the secondary decrease in response at relatively long durations disappeared (Fig. 7*B*). In recordings from actual band-pass and band-stop units, blocking inhibition by applying gabazine had a similar effect, resulting in an increased response at longer durations that had previously elicited weak responses. For example, the neuron shown in Fig. 9*B* was band-stop tuned to both polarities, but became long-pass tuned after gabazine application because the decrease in response to longer duration stimuli no longer occurred. For all band-pass and band-stop tuning curves tested, we identified the minimum duration at which further increases in duration resulted in responses that dropped below 50% of the maximum response. We then determined the total range of durations above this value that elicited a response less than 50% of the maximum response, and compared this to the total range of durations below this criterion

after gabazine application. Among all band-pass and band-stop tuning curves tested, gabazine application resulted in a significant decrease in the range of durations that elicited a response less than 50% of the maximum response (Fig. 9*B*; Wilcoxon matched pairs test: n=13, z=2.4, P<0.05). This supports our model prediction that inhibition contributes to band-pass and band-stop tuning by blocking responses to stimuli over a particular range of durations.

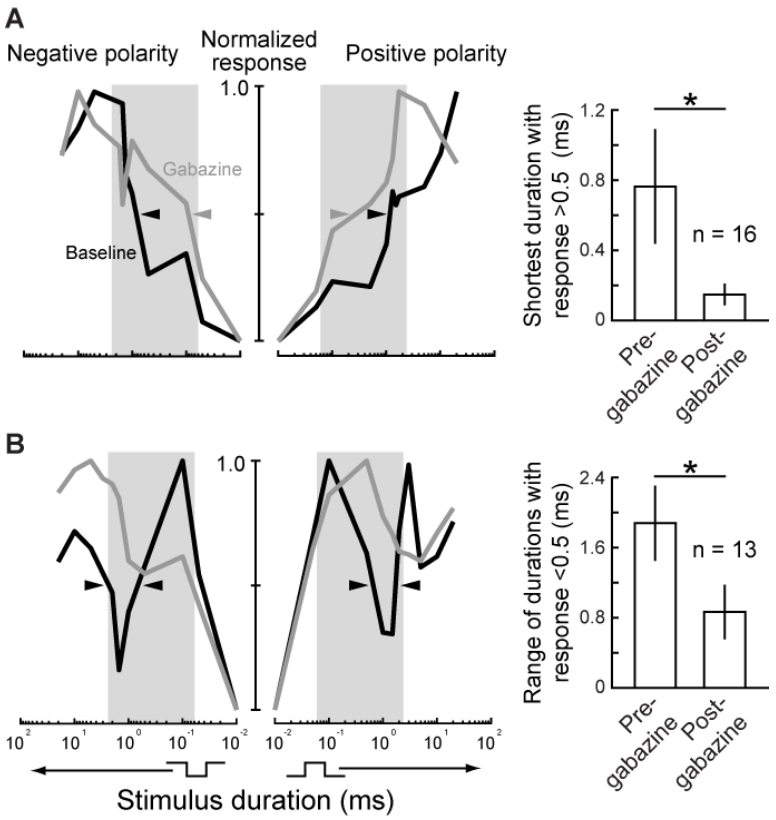

FIG 9: Blocking inhibition in ELa affects Small Cell responses to peripheral spike timing differences. (A) Smoothed, normalized tuning curves from a representative long-pass Small Cell before and after gabazine application, presented as in Fig. 2. This cell had long-pass tuning to both stimulus polarities before and after gabazine application. However, the minimum duration eliciting a response >0.5 decreased after gabazine application for both polarities (arrowheads), suggesting that inhibition was affecting excitatory input to the Small Cell at short durations. The bar graph to the right shows the minimum duration eliciting a response >0.5 (mean ± sem) for all 16 tuning curves that were long-pass before gabazine application. After gabazine application, there was a significant decrease in the minimum duration eliciting a response >0.5 (Wilcoxon matched pairs test: n=16, z=2.9, P<0.01). (B) Smoothed, normalized tuning curves from a representative band-stop Small Cell before and after gabazine application. This cell had band-stop tuning to both stimulus polarities, but the tuning to both polarities changed to long-pass after gabazine application. The band-stop portion of the tuning curves that was <0.5 of the maximum response before gabazine (arrowheads) was no longer present after gabazine application, suggesting that inhibition was responsible for the decreased response at these durations. The bar graph to the right shows the range of durations eliciting a response <0.5 (mean ± sem) for all 13 tuning curves that were either band-pass or band-stop before gabazine application. After gabazine application, there was a significant decrease in the range of durations eliciting a response <0.5 (Wilcoxon matched pairs test: n=13, z=2.4, P<0.05).

DISCUSSION

Small Cells are diverse in their responses to variation in peripheral spike timing differences and are the first location where inputs from widely separated receptive fields converge. Our results suggest several factors that determine the responses of individual cells: variation in excitatory latency, likely due to axonal delay lines (Friedman and Hopkins 1998); feed-forward inhibition, likely mediated by Large Cell calyces (Friedman and Hopkins 1998; George et al. 2011; Mugnaini and Maler 1987); multiple excitatory inputs from different receptive fields for some cells; and variation in the relative timing of excitation and inhibition owing to latency differences and the relative timing of stimulus edges.

Variation in excitatory latency determines which peripheral timing differences the cell will respond to. Excitation will be greatest when two excitatory inputs arrive in synchrony, but the strong inhibition from the calyx synapse will effectively silence any excitation. Combined with the peripheral long-pass filter (Lyons-Warren et al. 2012), this mechanism can establish different temporal filters of spike timing differences. Specific predictions of this model regarding the relationship between excitatory latency and duration tuning, and the effects of blocking inhibition on duration tuning, were supported by our extracellular data. Our model can also explain changes in tuning with changes in stimulus intensity. As intensity increases, additional receptive fields will be activated, leading to the recruitment of additional inputs.

Mechanisms for detecting submillisecond timing differences have been well studied in auditory pathways that use interaural timing differences (ITDs) to locate

azimuthal sound sources (Ashida and Carr 2011; Köppl 2009; Schnupp and Carr 2009). There is strong evidence in birds and reptiles for the canonical Jeffress model (1948), in which a counter-current organization of ipsilateral and contralateral projections to the nucleus laminaris (NL) converts a temporal code into a place code through delay-line coincidence detection (Carr and Konishi 1990; Carr et al. 2009; Funabiki et al. 2011). By contrast, binaural projections to the mammalian medial superior olive (MSO) do not appear to include delay lines (McAlpine and Grothe 2003; Smith et al. 1993). Instead, binaural excitation and inhibition convert a temporal code into a rate code, in which azimuthal sound location is represented by the relative firing rates of neurons in the left and right MSO (Brand et al. 2002; Grothe et al. 2010; van der Heijden et al. 2013). Our data suggests a novel mechanism for processing spike timing differences that combines features of both sound localization pathways, including axonal delay lines and precisely timed feed-forward inhibition. Integration of precisely timed excitation and inhibition is also thought to establish sound duration tuning in the midbrains of mammals and amphibians (Aubie et al. 2009; Leary et al. 2008; Sayegh et al. 2011).

Our results provide empirical support for the delay-line anti-coincidence detection model of Friedman & Hopkins (Friedman and Hopkins 1998). However, our findings also add to this model by revealing multiple excitatory inputs to some cells, an important role for tonic inhibition, and greater diversity of Small Cell response patterns than first predicted. In its original formulation, the model predicted that all Small Cells would be long-pass tuned to square-pulse duration, with variation in excitatory latency determining the minimum cut-off duration that Small Cells would respond to (Xu-Friedman and

Hopkins 1999). However, Small Cell duration tuning was more diverse than this for three reasons. First, the periphery imposes a long-pass filter before stimulus information reaches Small Cells (Lyons-Warren et al. 2012). Second, relatively long excitatory latencies result in coincident excitation and inhibition at durations that are longer than the cut-off of this peripheral filter. Third, multiple excitatory inputs from different receptive fields result in coincident excitation at certain durations.

Thus, while the original model proposed a population code in which the number of responsive Small Cells codes for square-pulse duration (Xu-Friedman and Hopkins 1999), our results suggest a distributed population code in which the identity of responsive cells codes for duration. Individual Small Cells respond equally well to a wide range of stimulus durations, polarities, and intensities, such that they cannot individually code for specific stimuli. However, the tuning of each cell is unique, meaning that different stimuli will elicit responses from distinct populations of Small Cells.

Monophasic square pulses provide a convenient stimulus for precisely manipulating the timing of receptor responses to study the decoding of peripheral timing differences. However, natural EOD waveforms are more complex than square pulses, typically consisting of multiple phases of different durations (Carlson et al. 2011; Hopkins 1981). Variation in the polarity and intensity of an EOD stimulus across the body surface results in a mosaic of peripheral timing differences as opposed to the simple "start-stop" responses to uniform square-pulse stimuli that we elicited (Baker et al. 2013). Thus, in a natural context, the particular timing difference that an individual Small Cell will experience depends on the receptive fields of its synaptic inputs and on the polarity

and intensity of the EOD at those locations. Relative movements of the signaling and receiving fish will further complicate the matter, causing this mosaic of timing differences to shift. Nevertheless, just as changes in square-pulse duration alter the relative timing of peripheral inputs to Small Cells, so too will changes in EOD waveform and sender position alter the relative timing of these inputs. Thus, our findings suggest that both EOD waveform and sender position are represented as a distributed population code among Small Cells. This contrasts with the mammalian MSO, which converts a temporal code into a rate code, and the avian NL, which converts a temporal code into a place code.

Although the source of much speculation, it remains unclear why different circuits have evolved different mechanisms and recoding strategies for processing submillisecond timing differences (Köppl 2009; Schnupp and Carr 2009). Why would mormyrids utilize yet another strategy? We recently found that at near threshold stimulus intensities, when the temporal code for EOD waveform breaks down, variation in KO tuning establishes a peripheral population code for stimulus duration (Lyons-Warren et al. 2012). Thus, there are two peripheral codes operating at different intensities, a population code at low intensities and a temporal code at high intensities. It may be that the temporal code is converted into a population code so that two different peripheral codes come to be represented as a single, unified population code centrally. A similar argument has been proposed to explain different strategies for ITD processing. Mammals use both ITDs and interaural level differences (ILDs) for azimuthal sound localization (Macpherson and Middlebrooks 2002). Since sound intensity is represented using a rate code, the MSO

may convert ITDs from a temporal code to a rate code so that both features are in the same "currency" (Schnupp and Carr 2009). Birds, however, use ILDs for elevational sound localization; because ITDs and ILDs represent different information, it may not be necessary to convert them into a common coding scheme.

Another reason that mormyrids may convert a temporal code into a population code is that this circuit must deal with the coding of both spatial and identity information into complex patterns of timing differences among many receptors. By contrast, the mammalian MSO and avian/reptilian NL only need to perform a binaural timing comparison for the sole purpose of azimuthal sound localization. Population codes are able to more efficiently and more accurately represent a large number of stimuli than codes based on individual neurons (Averbeck et al. 2006), and they may be well suited to representing the high dimensionality and variability of electric signals that ELa must deal with.

Multipolar neurons in ELp integrate the outputs of many Small Cells along their extensive dendritic arbors (Xu-Friedman and Hopkins 1999). This high degree of convergence makes ELp neurons ideally suited to detecting coherent spiking among distinct subpopulations of Small Cells, and this likely represents the first step in decoding Small Cell population activity (Amagai 1998). Further, sensory stimulation will result in coherent synaptic input to ELp from many Small Cells, but spontaneous inputs will be uncorrelated. Thus, even though spontaneous activity among Small Cells was generally quite low, this convergence should help prevent the propagation of spontaneous activity

and ensure reliable sensory coding. Indeed, ELp neurons have low levels of spontaneous synaptic activity and no spontaneous spiking *in vivo* (Amagai 1998; Carlson 2009).

To our knowledge, this study is the first to document functional roles for an inhibitory calyx. We propose that just as the excitatory calyx of Held functions to increase the reliability of synaptic transmission (Borst and van Hoeve 2012), the calyx structure of the Large Cell-to-Small Cell synapse is particularly effective at blocking excitation. It is somewhat puzzling that some Small Cells receive excitation in response to a stimulus edge that is normally blocked by inhibition in response to that same edge. It may be that coincident excitatory inputs in response to two edges can overcome this inhibition, similar to the anteroventral cochlear nucleus in mice (Chanda and Xu-Friedman 2010). In mammalian MSO neurons, it was recently shown that inhibition increases the linearity and temporal precision of binaural coincidence detection (Roberts et al. 2013). Inhibition in response to the same stimulus edge as excitation could also shorten the window for excitatory integration (Pouille and Scanziani 2001). Conversely, delayed excitation in response to the same stimulus edge as inhibition could effectively shorten the inhibitory window. Finally, even though excitation and inhibition were often elicited by a single stimulus edge in our preparation, these inputs may have arisen through adjacent, but separate receptive fields. Slight changes in stimulus orientation during natural social interactions could differentially activate these receptive fields, which would be reflected in the resulting Small Cell output.

We also found evidence suggesting tonic inhibition of Small Cells. This could arise through tonic activation of $GABA_A$ receptors by ambient GABA at the Large Cell

terminal, spontaneous miniature IPSPs, spontaneous spiking of Large Cells, or a separate source of GABAergic inhibition. We consider the latter two possibilities highly unlikely. Intracellular recordings from nELL axons and Large Cells reveal little, if any, spontaneous firing (Amagai et al. 1998; Friedman and Hopkins 1998). In addition, the cytology and anatomy of ELa has been well described, and there is no evidence for any neurons other than Small Cells, Large Cells, and nELL axons (Friedman and Hopkins 1998; George et al. 2011; Mugnaini and Maler 1987). Tonic excitation and inhibition due to low ambient levels of neurotransmitter have been well described (Cavelier et al. 2005; Semyanov et al. 2004). The extensive synaptic cleft formed by the calyx may limit the diffusion and clearance of GABA, resulting in high ambient levels that remain long after presynaptic spiking. Although the exact mechanism remains unknown, it is clear that tonic inhibition of Small Cells reduces spontaneous firing, which increases the fidelity of stimulus coding by limiting spiking to stimulus-driven events, similar to the effect of tonic inhibition on mechanosensory coding by cerebellar granule cells (Duguid et al. 2012). Further, a tonic inhibitory conductance would decrease the membrane time constant, thereby decreasing temporal integration windows and increasing the precision of coincidence (or anti-coincidence) detection (Cavelier et al. 2005; Häusser and Clark 1997).

ACKNOWLEDGEMENTS

This research was supported by grants from the National Science Foundation (IOS-1050701 to B.A.C.), the National Institutes of Health (NS54174 to S.M., F30DC0111907 to A.M.L-W. and NIH Neuroscience Blueprint Center Core Grant P30-NS057105 to Washington University) and the Uehara Memorial Foundation and the Japan Society for the Promotion of Science (G2205 to T.K.). We thank Joseph Bernardi for assistance with KO recordings.

REFERENCES

Amagai S. (1998). Time coding in the midbrain of mormyrid electric fish. II. Stimulus selectivity in the nucleus exterolateralis pars posterior. J Comp Physiol A. **182**, 131-143.

Amagai, S., Friedman, M.A., and Hopkins, C.D. (1998). Time coding in the midbrain of mormyrid electric fish. I. Physiology and anatomy of cells in the nucleus exterolateralis pars anterior. J Comp Physiol A Neuroethol Sens Neural Behav Physiol. **182**, 115-130.

Arnegard, M.E., Jackson, B.S., and Hopkins, C.D. (2006). Time-domain signal divergence and discrimination without receptor modification in sympatric morphs of electric fishes. J Exp Biol. **209**, 2182-2198.

Arnegard ME, McIntyre PB, Harmon LJ, Zelditch ML, Crampton WGR, Davis JK, Sullivan JP, Lavoué S, and Hopkins CD. (2010). Sexual signal evolution outpaces ecological divergence during electric fish species radiation. Am Nat **176**, 335-356.

Ashida, G., and Carr, C.E. (2011). Sound localization: Jeffress and beyond. Curr Opin Neurobiol. **21**, 745-751.

Aubie, B., Becker, S., and Faure, P.A. (2009). Computational models of millisecond level duration tuning in neural circuits. J Neurosci. **29**, 9255-9270.

Averbeck BB, Latham PE, and Pouget A. (2006). Neural correlations, population coding and computation. Nat Rev Neurosci **7**, 358-366.

Baker C, Kohashi T, Lyons-Warren A, Ma X, and Carlson B. (2013). Multiplexed temporal coding of electric communication signals in mormyrid fishes. J Exp Biol **216**, 2365-2379.

Bell, C.C., and Grant, K. (1989). Corollary discharge inhibition and preservation of temporal information in a sensory nucleus of mormyrid electric fish. J Neurosci. **9**, 1029-1044.

Bennett MVL. (1965). Electroreceptors in mormyrids. Cold Spring Harbor Symp Quant Biol **30**, 245-262.

Borst JGG, and van Hoeve JS. (2012). The calyx of Held synapse: From model synapse to auditory relay. Annu Rev Physiol **74**, 199-224.

Brand, A., Behrend, O., Marquardt, T., McAlpine, D., and Grothe, B. (2002). Precise inhibition is essential for microsecond interaural time difference coding. Nature **417**, 543-547.

Bremner, L., Fitzgerald, M., and Baccei, M. (2006). Functional GABAA-receptor–mediated inhibition in the neonatal dorsal horn. J Neurophysiol. **95**, 3893-3897.

Carlson, B.A. (2003). Single-unit activity patterns in nuclei that control the electromotor command nucleus during spontaneous electric signal production in the mormyrid *Brienomyrus brachyistius*. J Neurosci. **23**, 10128-10136.

Carlson, B.A. (2009). Temporal-pattern recognition by single neurons in a sensory pathway devoted to social communication behavior. J Neurosci. **29**, 9417-9428.

Carlson BA, Hasan SM, Hollmann M, Miller DB, Harmon LJ, and Arnegard ME. (2011). Brain evolution triggers increased diversification of electric fishes. Science **332**, 583-586.

Carlson BA, Hopkins CD, and Thomas P. (2000). Androgen correlates of socially induced changes in the electric organ discharge waveform of a mormyrid fish. Horm Behav **38**, 177-186.

Carr, C., and Friedman, M. (1999). Evolution of time coding systems. Neural Comput. **11**, 1-20.

Carr, C.E., and Konishi, M. (1990). A circuit for detection of interaural time differences in the brain stem of the barn owl. J Neurosci. **10**, 3227-3246.

Carr CE, and Soares D. (2002). Evolutionary convergence and shared computational principles in the auditory system. Brain Behav Evol **59**, 294-311.

Carr CE, Soares D, Parameshwaran S, and Perney T. (2001). Evolution and development of time coding systems. Curr Opin Neurobiol **11**, 727-733.

Carr, C.E., Soares, D., Smolders, J., and Simon, J.Z. (2009). Detection of interaural time differences in the alligator. J Neurosci. **29**, 7978-7990.

Cavelier P, Hamann M, Rossi D, Mobbs P, and Atwell D. (2005). Tonic excitation and inhibition of neurons: ambient transmitter sources and computational consequences. Prog Biophys Mol Bio **87**, 3-16.

Chanda, S., and Xu-Friedman, M.A. (2010). Neuromodulation by GABA converts a relay into a coincidence detector. J Neurophysiol. **104**, 2063-2074.

Dayan P, and Abbott L. Theoretical Neuroscience: Computational and Mathematical Modeling of Neural Systems. Cambridge, MA: The MIT Press, 2001.

Duguid I, Branco T, London M, Chadderton P, and Häusser M. (2012). Tonic inhibition enhances fidelity of sensory information transmission in the cerebellar cortex. J Neurosci **32**, 11132-11143.

Feldmeyer D, Lübke J, and Sakmann B. (2006). Efficacy and connectivity of intracolumnar pairs of layer 2/3 pyramidal cells in the barrel cortex of juvenile rats. J Physiol **575**, 583-602.

Feldmeyer D, Lübke J, Silver RA, and Sakmann B. (2002). Synaptic connections between layer 4 spiny neurone- layer 2/3 pyramidal cell pairs in juvenile rat barrel cortex: physiology and anatomy of interlaminar signalling within a cortical column. J Physiol **538**, 803-822.

Feulner, P.G.D., Plath, M., Engelmann, J., Kirschbaum, F., and Tiedemann, R. (2009). Electrifying love: electric fish use species-specific discharge for mate recognition. Biol Lett. **5**, 225-228.

Friedman, M.A., and Hopkins, C.D. (1998). Neural substrates for species recognition in the time-coding electrosensory pathway of mormyrid electric fish. J Neurosci. **18**, 1171-1185.

Funabiki K, Ashida G, and Konishi M. (2011). Computation of interaural time difference in the owl's coincidence detector neurons. J Neurosci **31**, 15245-15256.

George, A.A., Lyons-Warren, A.M., Ma, X., and Carlson, B.A. (2011). A diversity of synaptic filters are created by temporal summation of excitation and inhibition. J Neurosci. **31**, 14721-14734.

Grothe, B. (2003). New roles for synaptic inhibition in sound localization. Nat Rev Neurosci. **4**, 540-550.

Grothe, B., Pecka, M., and McAlpine, D. (2010). Mechanisms of sound localization in mammals. Physiol Rev. **90**, 983-1012.

Gundersen, H.J.G., Bagger, P., Bendtsen, T.F., Evans, S.M., Korbo, L., Marcussen, N., MØller, A., Nielsen, K., Nyengaard, J.R., Pakkenberg, B., *et al.* (1988). The new stereological tools: Disector, fractionator, nucleator and point sampled intercepts and their use in pathological research and diagnosis. APMIS **96**, 857-881.

Harder W. (1968). Die beziehungen zwischen elektrorezeptoren, elektrischem organ, seitenlinienorganen und nervensystem bei den Mormyridae (Teleostei, Pisces). Z Vergl Physiol **59**, 272-318.

Häusser M, and Clark BA. (1997). Tonic synaptic inhibition modulates neuronal output pattern and spatiotemporal synaptic integration. Neuron **19**, 665-678.

Hopkins, C.D. (1981). On the diversity of electrical signals in a community of mormyrid electric fish in West Africa. Amer. Zool. **21**, 211-222.

Hopkins, C.D. (1986). Temporal structure of non-propagated electric communication signals. Brain Behav Evol **28**, 43-59.

Hopkins, C.D., and Bass, A.H. (1981). Temporal coding of species recognition signals in an electric fish. Science **212**, 85-87.

Jeffress, L.A. (1948). A place theory of sound localization. J Comp Physiol Psychol. **41**, 35-39.

Kawasaki M.(2009). Evolution of time-coding systems in weakly electric fishes. Zool Sci **26**, 587-599.

Kawasaki M. (1997). Sensory hyperacuity in the jamming avoidance response of weakly electric fish. Curr Opin Neurobiol **7**, 473-479.

Köppl, C. (2009). Evolution of sound localisation in land vertebrates. Current Biology **19**, R635-R639.

Leary, C.J., Edwards, C.J., and Rose, G.J. (2008). Midbrain auditory neurons integrate excitation and inhibition to generate duration selectivity: An in vivo whole-cell patch study in anurans. J Neurosci. **28**, 5481-5493.

Lindquist, C.E.L., Laver, D.R., and Birnir, B. (2005). The mechanism of SR95531 inhibition at GABAA receptors examined in human α1β1 and α1β1γ2S receptors. J Neurochem. **94**, 491-501.

Lübke J, Markram H, Frotscher M, and Sakmann B. (1996). Frequency and dendritic distribution of autapses established by layer 5 pyramidal neurons in the developing rat neocortex: comparison with synaptic innervation of adjacent neurons of the same class. J Neurosci **16**, 3209–3218.

Lyons-Warren, A.M., Hollmann, M., and Carlson, B.A. (2012). Sensory receptor diversity establishes a peripheral population code for stimulus duration at low intensities. J Exp Biol. **215**, 2586-2600.

Lyons-Warren, A.M., Kohashi, T., Mennerick, S., and Carlson, B.A. (2013). Retrograde fluorescent labeling allows for targeted extracellular single-unit recording from identified neurons in vivo. J. Vis. Exp. **76,** e3921.

Ma X, Kohashi T, and Carlson BA. (2013). Extensive excitatory network interactions shape temporal processing of communication signals in a model sensory system. J Neurophysiol **110**, 456-469.

Macpherson EA, and Middlebrooks J. (2002). Listener weighting of cues for lateral angle: the duplex theory of sound localization revisited. J Acoust Soc Am **111,** 2219-2236.

Markram H, Lübke J, Frotscher M, Roth A, and Sakmann B. (1997). Physiology and anatomy of synaptic connections between thick tufted pyramidal neurones in the developing rat neocortex. J Physiol **500**, 409-440.

McAlpine, D., and Grothe, B. (2003). Sound localization and delay lines - do mammals fit the model? Trends Neurosci. **26**, 347-350.

Mishchenko Y, Hu T, Spacek J, Mendenhall J, Harris KM, and Chklovskii DB. (2010). Ultrastructural analysis of hippocampal neuropil from the connectomics perspectiv. Neuron **67**, 1009-1020.

Moiseff A, and Konishi M. (1981). Neuronal and behavioral sensitivity to binaural time differences in the owl. J Neurosci **1**, 40-48.

Mugnaini, E., and Maler, L. (1987). Cytology and immunocytochemistry of the nucleus extrolateralis anterior of the mormyrid brain: possible role of GABAergic synapses in temporal analysis. Anat Embryol (Berl). **176**, 313-336.

Pouille, F., and Scanziani, M. (2001). Enforcement of Temporal Fidelity in Pyramidal Cells by Somatic Feed-Forward Inhibition. Science **293**, 1159-1163.

Roberts MT, Seeman SC, and Golding NL. (2013). A mechanistic understanding of the role of feedforward inhibition in the mammalian sound localization circuitry. Neuron **78**, 923-935.

Sayegh, R., Aubie, B., and Faure, P. (2011). Duration tuning in the auditory midbrain of echolocating and non-echolocating vertebrates. J Comp Physiol A Neuroethol Sens Neural Behav Physiol. **197**, 571-583.

Schnupp JWH, and Carr CE. (2009). On hearing with more than one ear: lessons from evolution. Nat Neurosci **12**, 692-697.

Semyanov A, Walker MC, Kullman DM, and Silver RA. (2004). Tonically active GABAA receptors: modulating gain and maintaining the tone. Trends Neurosci **27**, 262-269.

Simmons J. (1979). Perception of echo phase information in bat sonar. Science **204**, 1336-1338.

Smith, P., Joris, P., and Yin, T. (1993). Projections of physiologically characterized spherical bushy cell axons from the cochlear nucleus of the cat: evidence for delay lines to the medial superior olive. J Comp Neurol. **331**, 245-260.

Szabo, T., Ravaille, M., Libouban, S., and Enger, P.S. (1983). The mormyrid rhombencephalon: I. Light and EM investigations on the structure and connections of the lateral line lobe nucleus with HRP labelling. Brain Res. **266**, 1-19.

van der Heijden M, Lorteije JAM, Plauska A, Roberts MT, Golding NL, and Borst JGG. (2013). Directional hearing by linear summation of binaural inputs at the medial superior olive. Neuron **78**, 936-948.

VanRullen, R., Guyonneau, R., and Thorpe, S.J. (2005). Spike times make sense. Trends Neurosci. **28**, 1-4.

Wang, S.S.H., Shultz, J.R., Burish, M.J., Harrison, K.H., Hof, P.R., Towns, L.C., Wagers, M.W., and Wyatt, K.D. (2008). Functional trade-offs in white matter axonal scaling. J Neurosci. **28**, 4047-4056.

Wang Y, Gupta A, Toledo-Rodriguez M, Wu CZ, and Markram H. (2002). Anatomical, physiological, molecular and circuit properties of nest basket cells in the developing somatosensory cortex. Cerebral Cortex **12**, 395-410.

Waxman, S., and Bennett, M. (1972). Relative conduction velocities of small myelinated and non-myelinated fibres in the central nervous system. Nat New Biol. **238**, 217-219.

Xu-Friedman, M.A., and Hopkins, C.D. (1999). Central mechanisms of temporal analysis in the knollenorgan pathway of mormyrid electric fish. J Exp Biol **202**, 1311-1318.

Yamada R, Okuda H, Kuba H, Nishino E, Ishii TM, and Ohmori H. (2013). The cooperation of sustained and phasic inhibitions increases the contrast of ITD-tuning in low-frequency neurons of the chick nucleus laminaris. J Neurosci **33**, 3927-3938.

Chapter 5

Conclusions and future directions

It does not bridge the gap between stimulus and sensation, but at least it shows that the gap is a little narrower than it was before.

-E.D. Adrian, 1928

SUMMARY AND SIGNIFICANCE

Nervous systems encode information using both the rate and timing of action potentials (Ainsworth et al., 2012; Ferster and Spruston, 1995). While rate codes can achieve submillisecond resolution (Montemurro et al., 2007), temporal codes are more suited to encoding timing information on this rapid timescale (Panzeri et al., 2010). Temporal codes are used to process sensory information on a submillisecond time scale in vision (Gollisch and Meister, 2008; Victor, 2000), audition (Grothe and Klump, 2000; Sayegh et al., 2011), and smell (Bathellier et al., 2008). Given the variety of proposed mechanisms for encoding submillisecond timing information, it is critical to compare approaches used by different species in order to appropriately extrapolate common principles (Carlson, 2012).

Electrosensory processing in mormyrid weakly electric fish is an ideal model system for this task because these fish are time coding experts, able to discriminate 2 μsec timing differences using a dedicated, easily accessible neural circuit (Carr, 1993; Paintner and Kramer, 2003; Zakon, 2003). Importantly, this circuit contains anatomical features that have been shown in other time coding systems including delay-lines and coincidence detectors. These similarities allow for direct cross-mechanism comparisons. We began our investigation of electrosensory processing by looking at peripheral receptors called knollenorgans which respond to positive changes in electrical charge (Hopkins and Bass, 1981). Because knollenorgans only respond to positive changes, different receptors will respond to the start or end of an electrical signal depending on their relative body location. This creates a start-stop temporal code for stimulus duration.

However, at lower stimulus intensities, knollenorgans exhibit decreased temporal precision, or jitter (Lyons-Warren et al., 2012). Time locked responses used to detect interaural time differences in cats are similarly intensity dependent (Michelet et al., 2012). We showed that knollenorgans are tuned to both duration and frequency with variation in tuning between receptors. Tuning variation results in a unique combination of knollenorgan responses for each stimulus duration, suggesting a population code for stimulus duration. This population code is important because it provides an additional source of information about stimulus duration not influenced by jitter.

Interestingly, a subgroup of mormyrid fish termed Clade A have a broad distribution of KOs across the entire body, the number of which increases nonlinearly with increasing body size (Carlson et al., 2011; Harder, 1968). Each of these KO has 1-10 sensory cells, all innervated by the same primary afferent (Harder, 1968). Primary afferents project to nELL where they make 1- 4 club endings onto each nELL cell soma they contact, further increasing temporal fidelity. Similarly, each nELL cell will receive inputs from 1- 4 KOs. Notably, each KO projects to 3-11 nELL cells (Bell and Grant, 1989). Simultaneous convergence and divergence increases heterogeneity across a population of neurons, in this case the nELL cells. Increasing variation in a population of cells increases the efficiency of a population code (Marsat and Maler, 2010).

Due to the complex nature of sensory integration, all information is inevitably converted to a population code (Ainsworth et al., 2012). For example, rats use first spike latency following whisker movement to encode stimulus location, which is converted to a population code in barrel cortex (Petersen et al., 2001). Similarly, in electrosensory

processing, both the temporal code and the population code originating in the periphery will ultimately merge into a single midbrain population code (Lyons-Warren et al., 2012).

Our experiments revealed a population code for stimulus duration created by diversity in peripheral filters operating in parallel with a start-stop temporal code. Notably, peripheral filtering also impacts temporal coding. Signals arrive in the midbrain already long-pass tuned, contributing to diversity of time comparator neuron responses. Peripheral filters similarly impact the input to a temporal code in the detection of interaural time differences for which monaural inputs must be spectrotemporally matched to maximally excite the coincidence detector (Fischer et al., 2011).

Next we addressed central mechanisms of temporal coding. There are three cellular elements in the anterior portion of the exterolateral nucles (ELa): Large Cells, Small Cells and hindbrain axons from the nucleus of the electrosensory lateral line (nELL). Large Cells and nELL axons exhibit time locked, long-pass tuned responses to a single stimulus edge (Amagai et al., 1998). Friedman and Hopkins demonstrated anatomical evidence for delay-lines by filling individual nELL axons with biocytin (Friedman and Hopkins, 1998). Large Cells make GABAergic calyceal synapses onto Small Cells (Friedman and Hopkins, 1998; George et al., 2011; Mugnaini and Maler, 1987). Based on these findings, Friedman and Hopkins proposed a delay-line anti-coincidence detection mechanism which predicts that all Small Cells will be long-pass tuned to stimulus duration (Xu-Friedman and Hopkins, 1999). To directly test their model, we recorded from Small Cells.

Cells with small somas are difficult to record from (Rose and Fortune, 1996). Small Cells in ELa are particularly challenging to record from because their somas are engulfed by calyceal synapses from Large Cells (Friedman and Hopkins, 1998; Mugnaini and Maler, 1987). Further, ELa contains large amounts of myelin which clogs the sharp electrodes required for intracellular recordings. Even if an electrode can remain unclogged, in my experience, trying to record from Small Cells is like trying to stab a small balloon. For all of these reasons, no one has been able to record from Small Cells despite considerable effort (Amagai et al., 1998; Friedman and Hopkins, 1998). Still, recording from Small Cells is the most direct way to measure how submillisecond spike timing differences are processed in this circuit. Therefore, we designed a novel method to record from Small Cell axons. We applied fluorescent dye to a nucleus adjacent to ELa, the posterior portion of the exterolateral nucleus (ELp). The dye labeled all elements in ELp including Small Cell axons. Small Cell axons retrogradely transported dye to ELa (Lyons-Warren et al., in press). Small Cell axons are the only element to go from ELp to ELa, and therefore all labeling in ELa is specific to Small Cells. Visualizing these labeled axons allowed us to target them with extracellular recording electrodes. Recording from axons rather than somas avoided the challenges associated with calyceal synapses. Further, the larger extracellular electrode was less likely to clog. This method will be generally useful for recording from other small or inaccessible cells in other systems.

Using retrograde labeling to visualize Small Cell axons, we characterized the response properties of 76 Small Cells. Contrary to the predictions of the Friedman-

Hopkins model, we showed that some Small Cells are band-pass or band-stop tuned to stimulus duration. Across the population of Small Cells there was variation in tuning between units, and within units between polarity and intensity. We investigated the source of this variation by analyzing both the inhibitory and excitatory inputs to Small Cells. We showed evidence of blanking inhibition following the non-responsive edge of a 50 ms square pulse. We also showed that removing inhibition changed tuning properties in 5 Small Cells. Unexpectedly, tuning did not reflect peripheral filtering after removal of inhibition, leading us to hypothesize multiple excitatory inputs. Indeed, we observed 23 Small Cells that responded to both edges of a stimulus under control conditions, suggesting multiple excitatory inputs. We also observed 2 units that exhibited a response to a previously non-responsive edge after pharmacological blockade of inhibition. Based on our experiments, we propose a new model for submillisecond spike time detection using a combination of blanking inhibition corresponding to one edge of a stimulus and variably delayed excitation corresponding to one or both edges of a stimulus.

The model for discriminating submillisecond differences in stimulus duration proposed in this thesis parallels the existing models for encoding submillisecond stimulus duration in previously described systems. Specifically, many models for detecting stimulus duration utilize a "start-stop" temporal code in which time comparator neurons receive inputs corresponding to the beginning and end of the stimulus (Aubie et al., 2009). Pulse duration tuning in bat inferior colliculus is GABA dependent (Jen and Feng, 1999) and duration tuning in frogs involves integration of excitatory and inhibitory inputs (Leary et al., 2008). The critical distinction between these models and the model for

electrosensory duration tuning proposed here is the specific way inhibition contributes to creating duration tuned responses. Importantly, the existence of duration tuned neurons has been shown in mice although there is no clear mechanism for how these neurons arise (Brand et al., 2000). Therefore it is important to consider a mechanism similar to electrosensory duration tuning when analyzing duration tuned neurons in other systems.

Mechanisms of duration tuning have not been studied in other species of weakly electric fish. However, wave type weakly electric fish can detect phase timing differences as small as 400 nsec and are therefore similarly useful for studying submillisecond spike time detection (Carr et al., 1986a). Specifically, mechanisms of phase detection in the weakly electric fish *Eigenmannia* share several interesting parallels with mormyrid electrosensory processing. Stimulus phase is encoded by peripheral receptors and then processed by time comparators in the midbrain that receive delayed inputs, similar to coincidence detectors in sound localization. Notably, delay-lines in *Eigenmannia* are generated through widely branching dendrites, rather than axons (Carr et al., 1986b).

Finally, one of the best studied mechanisms for detecting submillisecond spike time differences is the comparison of interaural time differences to determine where a sound is coming from (Ashida and Carr, 2011; Grothe et al., 2010). Interestingly, multiple mechanisms for sound localization have been shown to include a role for inhibition (Batra et al., 1997; Brand et al., 2002; Burger et al., 2011). Inhibition can create a more specific response by blocking coincidence detection under select conditions such as occurs with side suppression (Mori, 1997). This mechanism is most similar to the

blanking inhibition proposed in this thesis. Alternatively, inhibition can preferentially block a sub-set of excitatory inputs based on the timing of each signal to convert a temporal code into a rate code as occurs in the medial superior olive in mammals (Grothe et al., 2010). Similarly, we observe that the order of excitation and inhibition - determined by stimulus polarity - is essential for Small Cell tuning. Finally, inhibition can prevents neurons from responding to single inputs and thus convert them into coincidence detectors as in the anteroventral cochlear nucleus in mice (Chanda and Xu-Friedman, 2010). Similarly, $GABA_B$ receptors in gerbil medial superior olive modulate both excitatory and inhibitory currents to sharpen ITD selectivity (Fischl et al., 2012).

One of the novel findings of this work is the first functional description of an inhibitory calyceal synapse. Excitatory calyces have been extensively studied in the anteroventral cochlear nucleus, the lateral geniculate nucleus, and the cerebellum (Borst, 2010). This raises the question, do inhibitory calyxes not exist in other systems or have they just not been discovered? The novelty of the calyx structure and its presence in pathways utilizing temporal coding suggests a very specific purpose requiring such unique morphology. Therefore, it will be useful to actively look for inhibitory calyceal synapses in circuits that could benefit from precise and reliable inhibition.

FUTURE DIRECTIONS

My results suggest a novel mechanism for submillisecond spike time detection using precisely timed delayed excitation and precisely timed inhibition. I demonstrated functional inhibition using two methods, complex stimuli and pharmacological

application of an inhibitory blocker. However, application of both drug and vehicle was technically challenging. Therefore, it will be important to expand pharmacological studies using new drug application techniques such as iontophoresis. Ideally, extensive trials will be done with each application method to identify an accurate success rate for each method. The best method can then be used to test gabazine on a larger sample size as well as testing other inhibitory blockers such as strychnine hydrochloride which blocks glycine receptors. These experiments will reveal what percentage of Small Cells derive their tuning from inhibition.

In a departure from the previously proposed model by Friedman and Hopkins, my results suggest multiple excitatory inputs from different receptive fields to some Small Cells. I support this conclusion with multiple lines of evidence including tuned responses in the absence of inhibition and histological approximations of the ratio of Small Cell somas to nELL axonal projections. However, there are two direct tests of the multiple excitatory input hypotheses that should be completed. First, serial reconstruction of electron micrographs of ELa can be used to quantify the number of excitatory and inhibitory synapses onto each Small Cell. While this will not distinguish the source of these synapses, spatially distinct excitatory boutons would suggest multiple excitatory inputs. Although technically challenging, electron microscopy combined with bilateral labeling of nELL axons in different colors would allow direct quantification of how many Small Cells receive excitatory inputs from the left, right or both sides of the hindbrain. Second, recording from Small Cells while stimulating local receptive fields can be used to quantify how many distinct receptive fields elicit an excitatory or inhibitory response.

Finally, I investigated the mechanisms of tuning at Small Cells, but I did not look at how tuned Small Cells contribute to later processing. As Small Cells project in a topographical manner from ELa to ELp (Friedman and Hopkins, 1998) it may be interesting to correlate Small Cell recording location along the medial-lateral axis with tuning properties of ELp neurons.

CONCLUSIONS

Processing information on a submillisecond timescale represents an especially interesting computational challenge because such short intervals are below the resolution of a single action potential. In this thesis I have provided evidence for a novel mechanism for detecting submillisecond spike time differences in electrosensory processing. I have demonstrated an important role for peripheral filtering in sensory processing that impacts how sensory signals are coded. Peripheral filters should be considered both as tuning mechanisms in their own right, and as contributors to central processing. Further, I have designed and utilized a novel method for recording from small time comparator neurons in *vivo*. Hopefully this method will facilitate progress in understanding time comparator neurons in other systems. Finally, I have proposed a novel mechanism for detecting submillisecond spike time differences in mormyrid weakly electric fish. This work may be useful for understanding related areas including submillisecond duration tuning in other systems and identifying a common role of inhibition in processing interaural time differences for sound localization.

REFERENCES

Ainsworth, M., Lee, S., Cunningham, M. O., Traub, R. D., Kopell, N. J. and Whittington, Miles A. (2012). Rates and rhythms: A synergistic view of frequency and temporal coding in neuronal networks. Neuron **75**, 572-583.

Amagai, S., Friedman, M. A. and Hopkins, C. D. (1998). Time coding in the midbrain of mormyrid electric fish. I. Physiology and anatomy of cells in the nucleus exterolateralis pars anterior. J Comp Physiol A Neuroethol Sens Neural Behav Physiol. **182**, 115-130.

Ashida, G. and Carr, C. E. (2011). Sound localization: Jeffress and beyond. Curr Opin Neurobiol. **21**, 745-751.

Aubie, B., Becker, S. and Faure, P. A. (2009). Computational models of millisecond level duration tuning in neural circuits. J Neurosci. **29**, 9255-9270.

Bathellier, B., Buhl, D. L., Accolla, R. and Carleton, A. (2008). Dynamic ensemble odor coding in the mammalian olfactory bulb: Sensory information at different timescales. Neuron **57**, 586-598.

Batra, R., Kuwada, S. and Fitzpatrick, D. C. (1997). Sensitivity to interaural temporal disparities of low- and high-frequency neurons in the Superior Olivary Complex. I. Heterogeneity of responses. J Neurophysiol. **78**, 1222-1236.

Bell, C. C. and Grant, K. (1989). Corollary discharge inhibition and preservation of temporal information in a sensory nucleus of mormyrid electric fish. J Neurosci. **9**, 1029-1044.

Borst, J. G. G. (2010). The low synaptic release probability in vivo. Trends Neurosci. **33**, 259-266.

Brand, A., Urban, R. and Grothe, B. (2000). Duration tuning in the mouse auditory midbrain. J Neurophysiol. **84**, 1790-1799.

Brand, A., Behrend, O., Marquardt, T., McAlpine, D. and Grothe, B. (2002). Precise inhibition is essential for microsecond interaural time difference coding. Nature **417**, 543-547.

Burger, R. M., Fukui, I., Ohmori, H. and Rubel, E. W. (2011). Inhibition in the balance: binaurally coupled inhibitory feedback in sound localization circuitry. J Neurophysiol **106**, 4-14.

Carlson, B. A. (2012). Diversity matters: The importance of comparative studies and the potential for synergy between neuroscience and evolutionary biology. Arch Neurol. **69**, 987-993.

Carlson, B. A., Hasan, S. M., Hollmann, M., Miller, D. B., Harmon, L. J. and Arnegard, M. E. (2011). Brain Evolution Triggers Increased Diversification of Electric Fishes. Science **332**, 583-586.

Carr, C. E. (1993). Processing of temporal information in the brain. Annu Rev Neurosci **16**, 223-243.

Carr, C. E., Heiligenberg, W. and Rose, G. J. (1986a). A time-comparison circuit in the electric fish midbrain. I. Behavior and physiology. J Neurosci. **6**, 107-119.

Carr, C. E., Maler, L. and Taylor, B. (1986b). A time-comparison circuit in the electric fish midbrain. II. Functional morphology. J Neurosci. **6**, 1372-1383.

Chanda, S. and Xu-Friedman, M. A. (2010). Neuromodulation by GABA Converts a Relay Into a Coincidence Detector. J Neurophysiol. **104**, 2063-2074.

Ferster, D. and Spruston, N. (1995). Cracking the neuronal code. Science. **270**, 756-757.

Fischer, B. J., Steinberg, L. J., Fontaine, B., Brette, R. and Peña, J. L. (2011). Effect of instantaneous frequency glides on interaural time difference processing by auditory coincidence detectors. PNAS **108**, 18138-18143.

Fischl, M. J., Combs, T. D., Klug, A., Grothe, B. and Burger, R. M. (2012). Modulation of synaptic input by GABAB receptors improves coincidence detection for computation of sound location. J Physiol. **590**, 3047-3066.

Friedman, M. A. and Hopkins, C. D. (1998). Neural substrates for species recognition in the time-coding electrosensory pathway of mormyrid electric fish. J Neurosci. **18**, 1171-1185.

George, A. A., Lyons-Warren, A. M., Ma, X. and Carlson, B. A. (2011). A diversity of synaptic filters are created by temporal summation of excitation and inhibition. J Neurosci. **31**, 14721-14734.

Gollisch, T. and Meister, M. (2008). Rapid neural coding in the retina with relative spike latencies. Science **319**, 1108-1111.

Grothe, B. and Klump, G. M. (2000). Temporal processing in sensory systems. Curr Opin Neurobiol. **10**, 467-473.

Grothe, B., Pecka, M. and McAlpine, D. (2010). Mechanisms of Sound Localization in Mammals. Physiol Rev **90**, 983-1012.

Harder, W. (1968). The interrelations between electroreceptors, electric organ, lateral-line organ, and nervous system in Mormyridae (Teleostei, pisces). Zeitschrift für vergleichende Physiologie **59**, 272-318.

Hopkins, C. D. and Bass, A. H. (1981). Temporal coding of species recognition signals in an electric fish. Science **212**, 85-87.

Jen, P. H. S. and Feng, R. B. (1999). Bicuculline application affects discharge pattern and pulse-duration tuning characteristics of bat inferior collicular neurons. J Comp Physiol A Neuroethol Sens Neural Behav Physiol. **184**, 185-194.

Leary, C. J., Edwards, C. J. and Rose, G. J. (2008). Midbrain auditory neurons integrate excitation and inhibition to generate duration selectivity: An in vivo whole-cell patch study in anurans. J Neurosci. **28**, 5481-5493.

Lyons-Warren, A. M., Hollmann, M. and Carlson, B. A. (2012). Sensory receptor diversity establishes a peripheral population code for stimulus duration at low intensities. J Exp Biol. **215**, 2586-600.

Lyons-Warren, A. M., Kohashi, T., Mennerick, S. and Carlson, B. A. (2013). Retrograde fluorescent labeling allows for targeted extracellular single-unit recording from identified neurons in vivo. J. Vis. Exp. **26**:76.

Marsat, G. and Maler, L. (2010). Neural Heterogeneity and Efficient Population Codes for Communication Signals. J Neurophysiol. **104**, 2543-2555.

Michelet, P., Kovačić, D. and Joris, P. X. (2012). Ongoing temporal coding of a stochastic stimulus as a function of intensity: Time-intensity trading. J Neurosci. **32**, 9517-9527.

Montemurro, M. A., Panzeri, S., Maravall, M., Alenda, A., Bale, M. R., Brambilla, M. and Petersen, R. S. (2007). Role of precise spike timing in coding of dynamic vibrissa stimuli in somatosensory thalamus. J Neurophysiol **98**, 1871-1882.

Mori, K. (1997). Across-frequency nonlinear inhibition by GABA in processing of interaural time difference. Hear Res. **111**, 22-30.

Mugnaini, E. and Maler, L. (1987). Cytology and immunocytochemistry of the nucleus extrolateralis anterior of the mormyrid brain: possible role of GABAergic synapses in temporal analysis. Anat Embryol (Berl). **176**, 313-36.

Paintner, S. and Kramer, B. (2003). Electrosensory basis for individual recognition in a weakly electric, mormyrid fish, Pollimyrus adspersus (Günther, 1866). Behav Ecol Sociobiol **55**, 197-208.

Panzeri, S., Brunel, N., Logothetis, N. K. and Kayser, C. (2010). Sensory neural codes using multiplexed temporal scales. Trends Neurosci. **33**, 111-120.

Petersen, R. S., Panzeri, S. and Diamond, M. E. (2001). Population coding of stimulus location in rat somatosensory cortex. Neuron **32**, 503-514.

Rose, G. J. and Fortune, E. S. (1996). New techniques for making whole-cell recording from CNS neurons in vivo. Neurosci Res. **26**, 89-94.

Sayegh, R., Aubie, B. and Faure, P. (2011). Duration tuning in the auditory midbrain of echolocating and non-echolocating vertebrates. J Comp Physiol A Neuroethol Sens Neural Behav Physiol. **197**, 571-583.

Victor, J. D. (2000). How the brain uses time to represent and process visual information. Brain Res. **886**, 33-46.

Xu-Friedman, M. A. and Hopkins, C. D. (1999). Central mechanisms of temporal analysis in the knollenorgan pathway of mormyrid electric fish. J Exp Biol **202**, 1311-1318.

Zakon, H. H. (2003). Insight into the mechanisms of neuronal processing from electric fish. Curr Opin Neurobiol. **13**, 744-750.